PEO-SILANE AMPHIPHILES AS SURFACE-MODIFYING ADDITIVES TO IMPROVE THE PROTEIN RESISTANCE OF SILICONE

A Dissertation

by

MARC ALBERT RUFIN

Submitted to the Office of Graduate and Professional Studies of
Texas A&M University
in partial fulfillment of the requirements for the degree of

DOCTOR OF PHILOSOPHY

Chair of Committee,	Melissa A. Grunlan
Committee Members,	Elizabeth M. Cosgriff-Hernandez
	Duncan J. Maitland
	Victor M. Ugaz
Head of Department,	Gerard L. Coté

December 2015

Major Subject: Biomedical Engineering

ABSTRACT

Silicone materials are commonly used for implantable medical devices because of their favorable bulk properties. Unfortunately, due to their hydrophobicity, silicones have a high affinity for protein adsorption which makes them susceptible to thrombosis. In this work, novel PEO-silane amphiphiles [α-$(EtO)_3Si$-$(CH_2)_2$-$ODMS_m$-*block*-PEO_n-OCH_3] were developed to act as surface-modifying additives (SMAs) for silicone. Based on prior work, the PEO-silane amphiphiles were expected to rapidly migrate to the material surface in response to water exposure and result in a hydrophilic and protein-resistant silicone. These were distinguishable from conventional PEO-silanes due to the hydrophobic oligodimethylsiloxane (ODMS) tether which rendered the SMAs amphiphilic. They were also unique as SMAs due to their diblock structure and crosslinking group (triethoxysilane) to prevent leaching from condensation-cure elastomers.

The PEO-silane amphiphiles were prepared with three PEO lengths (n = 3, 8, and 16) and compared to analogous non-amphiphilic PEO-silanes (PEO-controls). When incorporated into silicone via bulk-modification, the PEO-silane amphiphiles exhibited rapid and extensive water-driven restructuring versus silicones modified with the PEO-controls. Multiple concentrations of each PEO-silane amphiphile were evaluated (5, 10, 25, 50, and 100 μmol per 1 g silicone) in terms of their ability to confer hydrophilicity and protein resistance. From these results, it was determined that PEO length dictates restructuring behavior of PEO-silane amphiphiles. Only n = 8 and 16 were able to

achieve substantial hydrophilicity and reduce protein adsorption, but the n = 8 length was more effective and maximized protein resistance with concentrations as low as 10 μmol per 1 g silicone (1.68 wt%).

Finally, PEO-silane amphiphiles were evaluated in terms of their ability to overcome the limitations associated with SMAs (leaching and poor abrasion recovery). It was found that triethoxysilane did not prevent leaching of PEO-silane amphiphiles (m = 13, n = 8) from silicone in water. However, increasing the ODMS tether length (m = 30) dramatically reduced leaching and water uptake for both the PEO-silane and diblock amphiphiles without impairing restructuring behavior. For all tested SMAs, excellent water-driven surface restructuring behavior persisted on bulk-modified silicones after material abrasion.

DEDICATION

To Miranda

I only came to Texas to earn my PhD and I had no intention of finding love, but I never thought that I would meet such a wonderful person. Now, I can't imagine having made it through grad school without you. Your love and support over the years have been a profound source of encouragement and joy. I can't imagine another person who is more deserving of this dedication.

ACKNOWLEDGEMENTS

I would first like to thank the Sloan Foundation and the National Institute of Health. Without their financial support, this work would not have been possible.

Thanks to my committee members, Dr. Cosgriff-Hernandez, Dr. Maitland, and Dr. Ugaz for their guidance during this project. I would like to specially thank my committee chair, Dr. Melissa Grunlan. Before even visiting Texas A&M University, I knew that I wanted to work on this project, despite having very little knowledge of polymer chemistry and limited research experience. Nonetheless, Dr. Grunlan welcomed me into her research group and has continued to be an incredibly patient and supportive mentor since day one. For that, I will always be grateful.

I'd also like to thank all of the lab mates I have had the privilege to work with over the last five years. Their friendship and help around the lab made my graduate school experience far more enjoyable than I ever expected. Thanks especially to those students who helped directly on this project and without whom, I would still be collecting the data for my second chapter. They include Dr. Melissa Hawkins, John Gruetzner, Matthew Hurley, Paige Adair, and Mikayla Barry. Dr. Jeffery Raymond's support and experience were also invaluable for helping us develop and implement improved methodologies for characterizing our materials.

I'd like to give a big thanks to my friends and family. I have been fortunate to make some very good friends during my time in Texas. Like me, several of them had traveled far from home to attend Texas A&M and were a tremendous source of support

while I was settling in. I also greatly appreciate the Moore and Coufal families that have welcomed me with open arms and made Texas feel like a home away from home. Finally, thanks to my mother and father. All of my life they have been a tremendous source of love and support that has never faltered, even when I moved across the country to embark on this endeavor.

TABLE OF CONTENTS

Page

Page

LIST OF FIGURES

Page

Page

LIST OF TABLES

Page

CHAPTER I

INTRODUCTION

1.1 Overview

Implantable medical devices are often made from materials that are not of biological origin. These include metals, ceramics, glasses, polymers, and composite materials which may be used in a variety of implants ranging from intraocular lenses to artificial joints to heart valves [1]. Such materials can offer several advantages, including more desirable mechanical properties and processability, over materials derived from living tissue. One of the most significant advantages is that synthetic materials lack immunologically recognizable biologic motifs (*i.e.* antigens) that can trigger an immediate or adaptive immune system response [2]. Unfortunately, these materials can still trigger certain innate, nonspecific host responses including inflammation [3-6], foreign body reaction [7-11], and thrombosis [12]. Many implantable medical devices are prone to these reactions which lead to impaired function and adverse consequences for patient health. Of those mentioned, thrombosis is a common and costly complication for implantable medical devices. The focus of this dissertation henceforth is the development of a novel “thromboresistant” biomaterial that addresses this unmet clinical need. The following literature review will describe the mechanisms of thrombosis and its consequences, current methods for prevention, and its clinical significance. The review will also serve as a background before presenting the approach to developing thromboresistant coatings which are the focus of this dissertation.

1.2 Literature Review

1.2.1 Surface-Induced Thrombosis

The hemostatic mechanism of the human body was described thoroughly by Hanson [12]. Briefly, hemostasis is used by the body to arrest bleeding from injured blood vessels by clotting blood at the site of injury. Blood coagulation is directed largely by small, non-nucleated, disk-shaped cells called platelets that are present in the blood. The external surface of the platelet contains membrane bound receptors (*i.e.* integrins) that recognize and interact with damaged tissue. When these receptors are stimulated, they activate the rest of the cell, causing it to become "sticky" and change in shape to an irregular sphere with spiny pseudopods. The platelet then releases the contents of its storage granules that stimulate other nearby platelets, leading to localized platelet aggregation and the formation of a fused platelet thrombus. This process is referred to as "thrombosis" and is highly effective for quickly arresting local blood flow in response to tissue damage. Unfortunately, it can also activate in response to blood-contacting medical implants leading to negative consequences.

As soon as a medical implant makes contact with blood, dissolved proteins in the plasma begin to rapidly deposit on the surface via non-specific adsorption (*e.g.* hydrophobic or electrostatic interactions) and influence the subsequent biological reaction [2, 13]. Once a protein has bound to the surface, it may provide a site for cell attachment, in which case it is referred to as an "adhesion protein". Fibrinogen is one of the best-studied adhesion proteins known to play a major role in platelet adhesion [2, 14-18]. Hu *et al.* found that surface-bound fibrinogen undergoes conformational changes

that expose previously hidden epitopes which are then recognized and bound by cell integrins [19]. Upon binding to adsorbed fibrinogen, platelets become active and spread against the material surface, activating other platelets and thereby advancing thrombosis [12]. Additionally, activated platelets release fibrin which polymerizes dissolved and surface-bound fibrinogen into fibrin [20]. Fibrin formation strengthens the developing thrombus as well as its adhesion to the material [21]. Another important aspect of fibrinogen is that it has a higher affinity for hydrophobic surfaces compared to other proteins [22]. Unfortunately, many biomaterials (*e.g.* silicone, polystyrene, polyvinylchloride, etc.) are hydrophobic and are prone to fibrinogen adsorption. Even if other, less-thrombogenic proteins adsorb to the surface first, they are displaced by fibrinogen over time due to its greater surface affinity (*i.e.* the Vroman effect) [23, 24]. This means that an implanted material will likely induce thrombosis unless it specifically resists fibrinogen adsorption.

Blood-material interactions are complex and the factors that influence thrombosis extend beyond fibrinogen adsorption and platelet adhesion. As discussed in detail by Gorbet and Sefton [20], surface-induced thrombosis may also be heavily influenced or induced by the complement system and leukocyte activation even though these are more generally associated with inflammation (**Figure 1.1**). However, the initiation of all of these mechanisms, and ultimately thrombosis, is still largely dependent on the adsorption of proteins to the material surface.

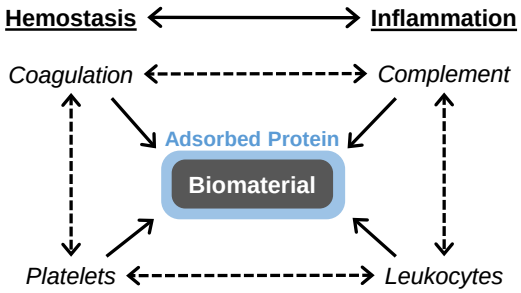

Figure 1.1. Diagram illustrating the relationship of blood-material reactions and their ultimate dependence on adsorbed protein. Adapted from [20].

As discussed by Hanson and Ratner [25], the occurrence of thrombosis on the surface of a blood-contacting implant such as a stent, catheter, or ventricular assist device (VAD) can lead to several adverse consequences. As the thrombus grows, it can obstruct blood flow and cause ischemia of downstream tissue. Segments may break off and float downstream as emboli, occluding blood vessels elsewhere or causing myocardial infarction (heart attack) or ischemic stroke. Furthermore, thrombus formation is believed to provide a substrate that facilitates bacteria adhesion and growth which leads to device infection, a major cause of patient mortality [26-29]. For certain devices, the presence of a thrombus can also impair functionality. For example, it may impede the mechanical motions of a VAD pump, blood flow through a hemodialysis catheter, or gas exchange through oxygenators. As such, most blood-contacting medical devices are only considered safe when antithrombotic drugs are used.

1.2.2 Antithrombotic Therapies and Complications

Currently, the most effective strategies for treating and preventing thrombus formation are antithrombotic therapies, which make use of anticoagulant drugs such as heparin and warfarin. Although the mechanisms by which these drugs work vary, they all ultimately serve to inhibit the hemostatic mechanism of the body, thereby preventing thrombus formation. A number of studies have demonstrated that such drugs effectively reduce the rate of thrombotic complications among patients with blood-contacting medical implants [30-36]. Unfortunately, the hemostatic mechanism serves a vital role for the body, and impairing it for any length of time puts the patient at risk for other serious complications.

The major complication of any antithrombotic therapy is bleeding. When the body is unable to arrest blood flow at the site of injured blood vessels, what otherwise may have been a minor or manageable injury can become life-threatening due to excessive loss of blood. Levine *et al.* reviewed a number of studies monitoring the occurrences of bleeding complications in patients who had received prosthetic heart valves and were treated with various anticoagulant therapies over multiple years [37]. Major bleeding complications occurred in as many as 19% of patients with fatalities reaching as high as 3%. Higher dosage therapies were associated with higher rates of bleeding complications. Rogacka *et al.* studied the safety of an antithrombotic therapy (*i.e.* aspirin, warfarin, and thienopyridines) for patients with implanted coronary stents [38]. During the therapy, six of the 128 patients (5%) developed major bleeding complications, four of which occurred in the first month of treatment. Three of the six

patients died, indicating the dangers of bleeding complications. This was confirmed in a more recent retrospective review where Guerrouij *et al.* determined the case-fatality rate of 142 patients who suffered warfarin-associated bleeding complications [39]. Of the bleeding episodes, 72 (50%) were classified as major bleeds and seven (10%) of those patients died. Anticoagulant dosages can be reduced to treat or prevent bleeding, but thromboembolic complications are likely to occur if the therapy is not sufficiently aggressive [40]. Also, it has been reported that elderly patients are more susceptible to thromboembolic complications, which poses a dilemma for physicians considering that the risk of bleeding complications from anticoagulants increases with age [41, 42]. Clearly, antithrombotic therapies are far from ideal.

In addition to bleeding risks, anticoagulants are associated with comorbidities. For example, it is well-known that heparin usage can result in a condition called heparin-induced thrombocytopenia (HIT) where platelets become hyperactive and risk of thrombosis actually increases [43]. This can lead to occurrences of deep vein thrombosis. Other complications resulting from anticoagulants have only recently been discovered, as is the case with warfarin. Patients with end-stage renal disease (ESRD) undergoing dialysis have a 10-20 times greater risk of mortality from cardiovascular events attributed to an increase in vascular calcification versus healthy, age-matched individuals [44]. It was also shown in a retrospective study of ESRD patients by Dua *et al.* that warfarin use was associated with significantly higher occurrences of pathologies rooted to vascular calcification [45]. Although vascular calcification was originally considered a passive process, more recent reports suggest that it’s actually caused by an

upregulation of bone matrix proteins and calcium-regulatory hormones [46]. It is possible that this upregulation results from an active vitamin K deficiency caused by long-term warfarin use [45, 47].

1.2.3 Thrombotic Complications

Despite antithrombotic therapies, thrombotic complications still persist in patients with blood-contacting medical devices. For example, a recent clinical study of the HeartWare® VAD found that 3 of 34 patients (8%) suffered device failure due to thrombosis [48]. Similar thrombosis rates have been observed in other VADs. A larger-scale study (414 patients total) of the HeartMate II® (HMII) VAD found that pump thrombosis occurred with 4-6% of patients while 8% suffered ischemic stroke [49]. Kirklin *et al.* examined the cause of HMII failures in the U.S. between 2006 and 2013 and of 6,910 patients, 659 (10%) suffered device failure [50]. Thrombosis was believed to have caused 382 (58%) of those cases which required device replacement (334 patients [51%]) or resulted in death (45 patients [7%]). According to this study, thrombosis should be considered the leading cause of VAD failure.

Thrombosis is generally less common in coronary stents compared to VADs but is still recognized as a major limitation. Stents are typically designed with an antiproliferative-drug-eluting coating to help prevent restenosis (not thrombosis). Restenosis is an ingrowth of endothelial tissue that may occur around the struts which would cause stent narrowing or obstruction and require device replacement [51]. Many clinical studies have reported low thrombotic complication rates (< 2%) for up to one

year in patients with drug-eluting stents (DESs) while undergoing antithrombotic therapy [51-54]. A large-scale study of 15,147 patients undergoing dual antiplatelet therapy after stent implantation found that only 1.0% suffered stent thrombosis within one year of the surgery [55]. Unfortunately, by preventing restenosis, the struts of the DES are left exposed to blood so that despite the seemingly low day-to-day risk of surface-induced thrombosis, that risk persists for many years after implantation [56-62]. This represents a significant issue considering the lethal implications of stent thrombosis [63-68]. Notably, it is believed that stent thrombosis may lead to heart attack and/or death in as many as 90% of cases [69].

Hemodialysis catheters represent a blood-contacting implant that is highly susceptible to thrombosis and they will be the focus of the remainder of this review. Catheters are heavily relied upon for hemodialysis of patients with ESRD [70] and for cancer patient chemotherapy [71] despite the fact that thrombosis remains a common complication [72-75]. Thrombosis can occur within hours of device insertion or after long periods of successful usage [76]. Studies have reported thrombotic occlusion in 30 – 40% of catheter patients which causes dysfunction by preventing adequate blood flow [76, 77]. In addition to dysfunction and the associated healthcare costs [78], catheter thrombosis may have lethal consequences for dialysis patients. As mentioned earlier, it can lead to embolic complications including ischemic stroke and heart attack [79, 80]. Catheter thrombosis is also believed to facilitate infection, the leading cause of patient mortality [26-29]. This is particularly alarming considering that infection-attributable

deaths of dialysis patients are 100 times more common than that of the general population [81].

Thrombosis may occur on the intraluminal or extraluminal surfaces of catheters. Extraluminal thrombosis is the most common, with incidence on nearly all implanted catheters [27, 82]. It typically begins near where the catheter enters the vein and facilitates the formation of a “fibrin sheath” that can grow to close off the tip [83]. Fibrin sheath formation begins within hours of device insertion and may cover as much as 80 to 100% of the catheter length within 7 days [83, 84]. In addition to preventing blood flow through the catheter, fibrin sheath formation can also reduce blood flow around the catheter by as much as 60%, which also increases platelet adhesion [85]. This reduced blood flow causes a complication known as deep vein thrombosis which is associated with swelling and tenderness of tissue along the affected vein [71]. It occurs in 1 to 5% of patients with catheters [86-89], and can be dangerous if left untreated. Despite its high incidence, the presence of a fibrin sheath often goes unnoticed prior to removal as it can only otherwise be detected when adverse symptoms occur.

Intraluminal catheter thrombosis is much more likely to impair function and is combatted with use of locking solutions. Typically, this involves the insertion of a concentrated heparin solution (or “lock”) into the lumens up to the very tip of the catheter after dialysis and is intended to prevent intraluminal clot formation between dialysis sessions [74, 90-92]. It has been found that these solutions leak from the lumen tip [93-95], administering heparin systemically which results in HIT and bleeding complications [96-98]. Another anticoagulant, trisodium citrate (often referred to as

"sodium citrate") has been used for locks instead of heparin because it has a lower risk of producing this systemic effect [95, 99]. While trisodium citrate is generally not as effective at inhibiting hemostasis compared to heparin [100, 101], the two anticoagulants have been shown to preserve catheter efficacy equally well in clinical studies [92, 99-101]. However, regardless of the locking solution, leaking will occur and most catheters eventually become dysfunctional [102]. With leaking, the catheter tip becomes particularly susceptible to thrombosis and may produce thromboemboli after resuming hemodialysis [80, 95].

1.2.4 Improving Material Thromboresistance

The persistence of thrombotic complications despite antithrombotic therapies has motivated the development of alternative materials for improving the safety of catheters and other medical implants. As thrombosis is largely induced by biological interactions with the device surface, one solution is to use materials with surface properties that resist or inhibit thrombosis (thromboresistance). Unfortunately, material selection for medical devices such as catheters is largely based on bulk properties rather than surface properties. Silicones and polyurethanes are widely used for catheters because of their favorable mechanical strength and flexibility [103, 104], despite inherent hydrophobicity which makes them susceptible to surface-induced thrombosis [105, 106]. Ideally, thromboresistance could be achieved through surface modification that would preserve the bulk properties [107]. In addition, a clinically and commercially feasible approach must achieve complete and uniform surface modification, be stable under *in vivo*

conditions, be broadly applicable to medical device materials, and consist of a process that is facile and reproducible [108]. To date, no such strategy has met all of these requirements, but some of the more successful surface modification strategies to achieve thromboresistance will now be reviewed.

1.2.4.1 Heparin Coatings

A well-established approach to reduce material thrombogenicity has been to apply heparin coatings to blood-contacting medical devices [108]. Although the coating methods vary, they each aim to prevent thrombosis through active inhibition of hemostatic mechanisms at the material surface [109, 110]. Because this effect is localized to the implant site, it theoretically permits the use of the anticoagulant without typical risks associated with systemic therapy. Over 200 heparin-coated medical devices have received FDA approval [111], but there are serious concerns regarding the efficacy and safety of heparin coatings. It has been demonstrated that heparin-coated surfaces exhibit leaching, non-uniform distribution, and reduced anti-coagulant activity versus unbound heparin [112]. It has also been found that surface-bound heparin chains, due to their inherent negative charge, may in fact promote protein adsorption and subsequent thrombosis [113]. This may explain the current lack of evidence demonstrating that the patency of blood-contacting catheters is statistically improved with heparin-coatings.

In the case of pediatric central venous catheters, no study has conclusively shown that heparin-coatings reduce catheter-related thrombosis or improve patency [114]. Also, a number of clinical studies have compared hemodialysis catheters with and without

heparin coatings and observed no statistical difference in dysfunction rates [115-117]. Furthermore, heparin coatings are known to likewise cause HIT [118-120]. The use of heparin coatings to prevent surface-induced thrombosis is therefore difficult to justify, especially considering the complexity and cost of heparin coating application [109, 110].

1.2.4.2 Passive Coatings

An attractive alternative to “bioactive” heparin coatings are materials that resist biological interactions. As discussed earlier, the first stage of surface-induced thrombosis occurs with the adsorption of plasma proteins. Thus a surface that resists protein adsorption should minimize thrombosis. “Passivation” refers to a strategy which achieves thromboresistance through protein resistance.

An early passivation strategy was based on pre-adsorbing a non-adhesion protein to a surface before implantation. Albumin, the most abundant protein in blood, doesn’t present any epitopes recognized by platelets when bound to a surface [121]. Thus, it was hypothesized that a device surface preadsorbed with albumin before implantation should block underlying adsorption sites and prevent subsequent platelet interactions [122]. Albumin coatings have been evaluated to improve the thromboresistance of devices such as artificial kidneys and blood oxygenators [122, 123]. Unfortunately, their efficacy was only temporary and they lost the ability to prevent thrombosis within hours of implantation. This is attributed to the Vroman effect in which physically adsorbed albumin is gradually displaced by proteins with higher surface affinity including fibrinogen [2]. Chemical modifications have been used to prevent albumin displacement

[121], but this does not prevent the protein from denaturing over time. Denatured albumin forms a substrate to which adhesion proteins can adsorb [124]. Therefore, regardless of the immobilization technique for albumin coatings, adsorption of adhesion proteins will eventually occur followed by thrombosis.

As with fibrinogen and albumin, plasma proteins generally have a strong affinity for hydrophobic materials [125]. Non-polar regions on protein are attracted to the material and the interaction is thermodynamically favorable as adsorption reduces the high interfacial energy between the hydrophobic surface and aqueous (biological) environment [126, 127]. Therefore, enhancing surface hydrophilicity (*i.e.* wettability) can also passively improve biomaterial thromboresistance. A popular method to achieve hydrophilicity is the creation of a hydrogel at the surface. Hydrogel coatings are comprised of water-soluble, crosslinked polymers which are able to retain large amounts of water without dissolving [121]. Under aqueous (biological) conditions, they minimize interfacial energy which makes them highly resistant to protein adsorption and cell adhesion [128]. A number of studies confirmed this by demonstrating a decrease in thrombus formation on hydrogel surfaces that decreased with higher water content [129, 130]. Despite their resistance to protein adsorption, hydrogel coatings can still have adverse consequences. Although the mechanism is unclear, hydrogels have also been associated with platelet activation. It has been observed that surfaces with high water content can cause destruction of circulating platelets which results in platelet microemboli [131] and the associated medical complications [132]. Furthermore, it has

been shown that hydroxyl (-OH) or amine ($-NH_3$) polar groups commonly present in hydrogels can induce complement activation and inflammation [4].

1.2.4.3 PEO Coatings

One of the most popular hydrophilic polymers for surface passivation, and largely considered as a gold standard, is poly(ethylene oxide) (PEO) [or poly(ethylene glycol) (PEG) depending on the polymerization method]. PEO has been incorporated onto surfaces by physical adsorption [133-138] or chemical grafting techniques [139-153] and has been shown to dramatically reduce protein adsorption and thrombogenicity *in vitro*. The mechanisms of PEO's exceptional protein resistance have been widely studied. In addition to the aforementioned low interfacial energy associated with water-soluble polymers, theoretical models have demonstrated that extended and highly flexible PEO chains sterically repel protein from the surface [154-157]. This effect largely results from a resistance to the thermodynamically unfavorable loss in configurational entropy that occurs as PEO chains are compressed by approaching protein. PEO coatings on hydrophobic materials can also prevent protein adsorption simply by blocking underlying binding sites [158]. More advanced molecular simulations have also revealed that via hydrogen bonding, grafted PEO chains tightly associate with local water molecules and create a "hydration layer" that physically excludes protein and other macromolecules [159].

In order to be effective, the PEO must be present at the surface in an extended "brush" conformation [144] so as to provide the most surface coverage. The brush

regime is achieved when the distance between neighboring chains (D) is less than the sum of their Flory radii ($D < 2R_f$) (**Figure 1.2**) and is indicative of high graft density (σ, $\sigma = 4\pi/D^2$) [160]. Efficacy is therefore largely dependent on PEO chain spacing (D) and molecular weight (MW $\propto R_f$). With less efficient PEO incorporation strategies, high MW chains (MW >> 3,500 g mol^{-1}) can be used to optimize material protein resistance [149, 150, 161-163]. However, Prime and Whitesides were also able to attain excellent protein resistance with PEO oligomers (MW ≈ 50 – 750 g mol^{-1}) [142]. They attributed the results to their use of a highly efficient self-assembled monolayers (SAMs) grafting strategy that resulted in closely packed PEO chains (low D, high σ). The importance of graft density in dictating PEO protein resistance has since been confirmed in additional studies [144, 164, 165]. Interestingly, with PEO SAMs it has been observed that the graft density can become too high, at which point the protein resistance is reduced [166-168]. It is believed that when neighboring PEO chains are packed too tightly, water is excluded which impairs formation of an effective hydration layer [159].

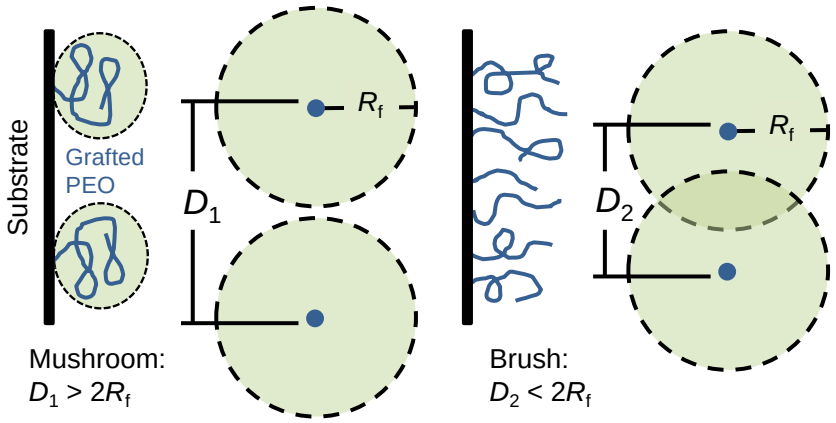

Figure 1.2. Grafted PEO chains will be in a brush conformation if the distance between neighboring chains (*D*) is less than the sum of their Flory radii ($2R_f$), otherwise they will be in a "mushroom" regime (Reprinted with permission from [160], Copyright 2015 by John Wiley and Sons).

Despite promising *in vitro* evaluations of PEO coatings, their performance *in vivo* has been disappointing or inconsistent [169-171]. For example, Park and coworkers evaluated a variety of common biomaterials on cardiovascular devices *in vivo* and obtained mixed results [169]. They found that grafting PEO onto nitinol stents reduced thrombus formation by more than 85% in porcine shunt experiments. However, PEO on vascular grafts of silicone, polyethylene, and Teflon in canine shunts only reduced platelet adhesion by 35% versus uncoated controls. They also implanted heart valves made with PEO-coated and uncoated Dacron into pigs and observed no improvement of thromboresistance *in vivo*.

While the reason for the poor success of PEO coatings remains unclear, several groups have attributed this to the postulated oxidative degradation of PEO under biological conditions [172-176]. However, Browning *et al.* recently examined the stability of PEO-diacrylamide hydrogels implanted in rats for three months and observed

no significant loss in mechanical strength [177]. This indicated that contrary to popular claim, little to no PEO degradation actually occurred *in vivo*. A more likely explanation for poor PEO coating performance is their inability to reduce fibrinogen adsorption sufficiently to prevent platelet adhesion. It has been reported that adsorption levels must be less than 5 ng/cm^2 [178]. When PEO is grafted at the surface of polymeric biomaterials, it will also be prone to thermodynamically-driven migration into the bulk of the material (*i.e.* hydrophobic recovery) [107], particularly during storage in air [179]. This effectively would reduce graft density and efficacy over time. Therefore, despite their proven efficacy in improving material thromboresistance [176], PEO coatings do have significant shortcomings that limit their potential.

1.2.4.4 Zwitterionic Coatings

Another passive approach to improving material thromboresistance has been to design coatings that mimic the inert surface chemistries of the natural vascular endothelium [180]. Taken into consideration is the fact that mammalian cell membranes are largely comprised of a phospholipid bilayer. The polar head group of the phospholipid, which is presented at the membrane surface, contains a closely associated positively charged phosphate and negatively charged choline, resulting in an overall neutral charge and referred to as a zwitterion. Researchers have attempted to mimic this with polymeric coatings containing zwitterions such as phosphobetaine, sulfobetaine, carboxybetaine (**Figure 1.3**), and amino acids [174].

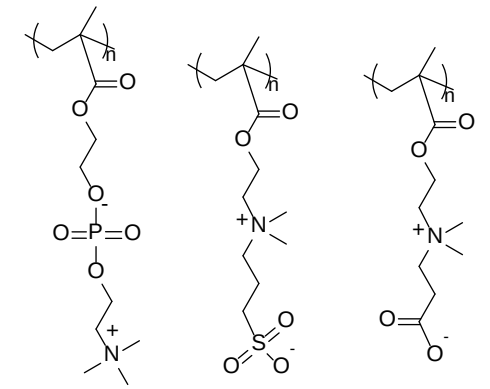

Figure 1.3. Examples of methacrylate-based polymers with zwitterionic side chains used for thromboresistant coatings.

Zwitterionic coatings have been incorporated onto a variety of materials to dramatically reduce protein adsorption and cell adhesion [181-197]. Similar to PEO, grafted zwitterionic polymers are density-dependent [194] and prevent protein adsorption through formation of a hydration layer. For zwitterions, the hydration layer is more tightly bound by electrostatic interactions as opposed to hydrogen bonding with PEO [159, 198]. It could therefore be inferred from this that zwitterions are more repellant towards protein than PEO. However, in comparing the two at similar graft chain length and density, Feng and coworkers demonstrated that PEO and zwitterionic coatings achieved similar protein resistance [195, 196]. As with PEO, there is a lack of evidence supporting the efficacy of zwitterionic coatings' ability to prevent thrombosis *in vivo* [176, 199, 200].

1.2.4.5 Limitations of Material Modification Strategies

The limitations of passive coatings using direct surface modification strategies are largely related to the chosen application technique. Physical adsorption techniques are generally simple (*e.g.* dip-coating), but the attractive forces of the secondary interactions are weak and immobilized polymers may be removed from the surface over time [201]. Thus, such coatings are not appropriate for blood-contacting implants intended for long-term use. Surface-grafting techniques result in polymers covalently attached to the substrate thereby improving potential long-term stability. These polymers can either be synthesized before attachment ("graft-to") or formed by polymerizing monomers directly from the substrate ("graft-from") [160]. However, both of these techniques can be quite complex. For example, a graftable substrate must contain functional groups or initiators to which the polymers can covalently attach or grow from, respectively. Many biomaterials lack these, so the surface must be pre-treated accordingly with additional steps. High grafting efficiency may also be difficult to achieve with "graft-to" techniques. Substrate attachment by free chains is inhibited due to steric blocking of attachment sites by other chains [121]. This can result in low-graft-density coatings with poor protein resistance. Thermodynamically poor solvents may diminish this effect by reducing the grafting chains' R_f [121], but this approach may result in dissolution or swelling of polymer substrates.

PEO and zwitterionic polymers have been mostly studied when surface-grafted on model substrates (*e.g.* glass [145, 146, 184], silicon [151-153, 194, 195], and gold [140-142, 186-192]). On model substrates, surface-grafted PEO and zwitterionic

polymers are highly protein resistant. However, their efficacy may change considerably when incorporated into polymeric materials. As discussed earlier, surface-grafted polymeric materials can undergo hydrophobic recovery which reduces graft-chain density over time [107]. Alternatively, PEO has been incorporated via bulk covalent attachment [161, 163, 201-205] or physical blending [162, 206-209] strategies. In order to reduce protein adsorption, bulk-modified systems must undergo microphase restructuring to create a surface that is sufficiently dense in PEO. An inability to properly "surface restructure" could explain the poor performance of PEO in some bulk-modified biomaterials [161, 202, 205].

1.2.4.6 Surface-Modifying Additives

Toward the goal of optimizing PEO surface restructuring in bulk-modified systems, surface-modifying additives (SMAs) have been studied [210]. In this approach, a small concentration (< 5 wt%) of SMA is mixed into a base polymer and high PEO surface coverage can be achieved without any adverse effects to the bulk-properties [108]. Most frequently, SMAs are designed as amphiphilic tribock copolymers (A-B-A), the centers of which are a hydrophobic chain (B) capped on both ends by identical, hydrophilic chains (A). When blended into a base polymer, SMAs migrate to the material surface driven by the minimization of interfacial energy during or after fabrication. The hydrophilic component of the SMA improves surface wettability to reduce protein adsorption. The hydrophobic component physically anchors the additive into the base polymer to prevent leaching.

Tsai *et al.* tested the thromboresistance of polyvinylchloride (PVC) modified with a SMA (1 wt%) composed of hydrophobic polydimethylsiloxane (PDMS; $MW_{PDMS} \approx 2{,}000$ g mol^{-1}) and hydrophilic polycaprolactone (PCL; $MW_{PCL} \approx 2{,}000$ g mol^{-1}) (PCL-PDMS-PCL) [211]. When compared to unmodified PVC, they observed that the thrombogenicity of PVC with SMA was significantly reduced. To improve the protein resistance of polyurethane (PU), Tan and coworkers recently developed a PEO-PU-PEO ($MW_{PEO} \approx 550$ g mol^{-1}; $MW_{PU} \approx 4750$ g mol^{-1}) SMA that was found to be more effective than surface-grafted PEO ("graft-to" approach) [176, 209]. They hypothesized that migration of the SMA to the surface created a denser PEO layer than what was attainable by surface grafting. Commercially available triblock copolymers consisting of poly(propylene oxide) (PPO) and PEO (PEO-PPO-PEO, Pluronics®) have also been shown to be effective as additives for improving material thromboresistance [207, 208]. Zwitterionic SMA oligomers have been reported [212, 213], but their poor solubility in aprotic solvents makes blending difficult and has limited their commercial use [214]. In clinical trials, SMAs have successfully reduced thrombotic complications on several blood-contacting medical devices including catheters [215, 216], vascular grafts [217], and cardiopulmonary bypass circuits [218, 219].

Despite its success, current SMA technology has some significant shortcomings that have been a source of criticism [108]. Restructuring of SMAs to the surface can be very slow or may not occur after fabrication. Thus, accidental abrasion of the device can remove surface-present SMAs and compromise protein resistance. Also, leaching of SMAs may occur, particularly with low molecular weight chains. Similar to physically

adsorbed polymers, SMAs are not covalently attached to the base polymer and can be removed during implantation. Safe usage of SMA-modified materials therefore requires additional processing steps to remove the leachable additive species. Otherwise, leaching could adversely affect patient health and reduce protein resistance as SMAs are gradually lost.

1.3 Innovation

Surface passivation strategies, including those based on PEO, have failed to produce thromboresistant materials. As noted earlier (1.2.4), silicones are widely utilized for blood-contacting medical devices (*e.g.* catheters) despite their exceptional hydrophobicity which causes thrombosis. In previous work by Grunlan and coworkers, new PEO-silane amphiphiles were evaluated as SMAs for silicones [220]. As shown in **Figure 1.4**, these PEO-silane amphiphiles consist of three main components: (1) a hydrophilic PEO segment of length *n*, (2) a crosslinkable triethoxysilane group, and (3) a hydrophobic oligodimethylsiloxane (ODMS) tether of length *m*. Their efficacy as SMAs in a medical-grade silicone was shown to be dependent on siloxane tether length. Specifically, it was demonstrated that silicone wettability increased and protein resistance improved when it was modified with PEO-silane amphiphiles ($n = 8$) consisting of longer siloxane tethers ($m = 0 < m = 4 < m = 13$). A subsequent study verified that concentrations as low as 1 and 5 wt% of PEO-silane amphiphile ($m = 13$, $n = 8$) were effective in reducing protein adsorption [221]. Furthermore, it was demonstrated that the SMAs underwent water-driven restructuring which resulted in a

PEO-rich silicone surface in response to aqueous exposure [222]. In the present work, towards improving their efficacy as SMAs, key changes were systematically evaluated: (1) PEO-segment length (*n*), (2) SMA concentration, (3) siloxane tether length (*m*), (4) omission of the crosslinkable group, and (5) a triblock architecture (*i.e.* PEO_n-$ODMS_m$-PEO_n). The corresponding changes in water-driven surface restructuring and protein resistance were likewise evaluated.

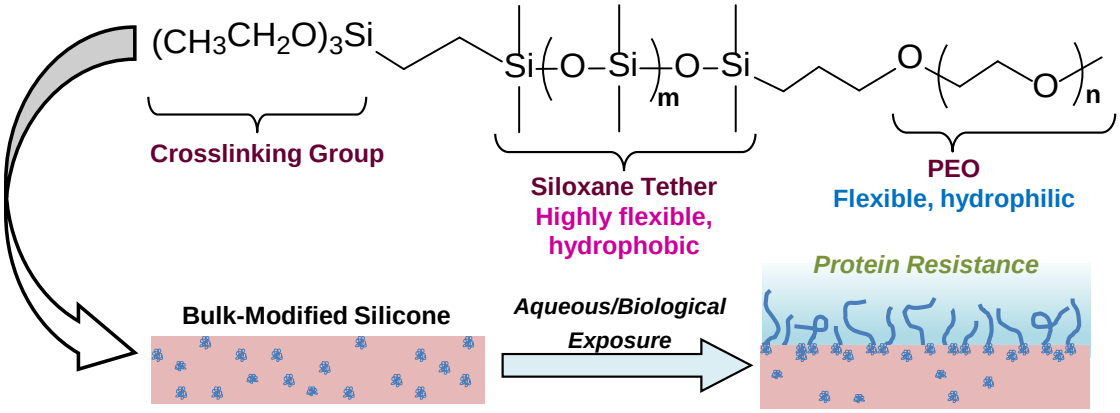

Figure 1.4. PEO-silane amphiphile structure and illustration of water-driven surface restructuring mechanism on bulk-modified silicone.

PEO-silanes have been reported by Chen and coworkers for use as additives to improve silicone protein resistance [201, 202]. In their work, PEO was complexed directly with triethoxysilane so that the polymer would chemically crosslink within a condensation-cure silicone elastomer and prevent leaching. However, these PEO-silanes were not explicitly designed to be SMAs and it is hypothesized that they did not rapidly migrate to the material surface due to their poor mobility within the hydrophobic silicone network. The PEO-silane amphiphiles described in this work differ from those non-amphiphilic PEO-silanes in that the PEO is separated from the triethoxysilane by a

flexible, hydrophobic siloxane tether. The siloxane tether serves to improve the miscibility and mobility of PEO within the silicone so it can more effectively migrate to the surface as a SMA. PEO-silane amphiphiles are also innovative because they are a diblock (A-B) structure, not triblock (A-B-A) like most SMAs. It is hypothesized that this reduces solubility and subsequent leaching in aqueous environments as only one (rather than two) water-soluble component (A) is present.

More recent findings have demonstrated that increasing the length of the siloxane tether beyond m = 13 does not impair PEO-silane amphiphile restructuring [223] and it could foreseeably benefit the SMAs for two reasons. Firstly, a larger hydrophobic segment should prevent leaching of uncrosslinked SMAs by simultaneously increasing chain affinity for the base silicone and reducing solubility in water. Secondly, it could obviate the need for a crosslinking group (triethoxysilane) if leaching is sufficiently reduced. This would simplify synthesis considerably and could permit use of the amphiphiles in a greater variety of silicone elastomers regardless of crosslinking chemistry.

As SMAs, the PEO-silane amphiphiles address many of the shortcomings associated with passive coating strategies (described in 1.2.4.5**)**. However, they also overcome the limitations historically associated with SMAs [108]. As demonstrated in the presented work, PEO-silane amphiphiles achieve rapid water-driven migration to the surface of silicone. This makes them highly effective in reducing protein adsorption and in the case of material abrasion, ensures that the PEO-silane amphiphiles can quickly migrate from the bulk to replenish PEO surface coverage. By incorporating

triethoxysilane or increasing the siloxane tether length, undesirable leaching of PEO-silane amphiphiles is also reduced.

1.4 Approach

As previously discussed (1.2.4.3), the MW of surface-grafted PEO can significantly influence its protein resistance by affecting chain conformation. However, its size may also affect the efficacy of PEO SMAs [208, 209]. As the length of PEO is increased, it becomes increasingly immiscible in silicone and is faced with a greater steric challenge in reaching the material surface. However, short lengths may not be able to achieve the high PEO surface coverage necessary for effective protein resistance. In attempt to optimize their performance, PEO-silane amphiphiles were prepared with multiple PEO-segment lengths (n = 3, 8, and 16) while the siloxane length was kept constant (m = 13).

As mentioned earlier (1.2.4.5), novel passive coatings are typically screened on model substrates such as gold, glass, and silicon before they are applied to polymeric biomaterials. Model substrates are planar and absent surface restructuring effects which permits excellent coating characterization and use of highly sensitive protein adsorption measurement techniques (*e.g.* quartz crystal microbalance [QCM] and surface plasmon resonance [SPR]). PEO-silane amphiphiles were similarly evaluated by grafting onto silicon wafers. Analogous non-amphiphilic PEO-silanes were also prepared where the PEO was separated from the grafting group by a short propyl spacer (**Figure 1.5**). This permitted evaluation of the siloxane tether's effect on the inherent protein resistance of

PEO absent surface restructuring effects. Next, PEO-silane amphiphiles and their non-amphiphilic analogues were incorporated into a medical-grade, condensation-cure silicone via bulk-modification as illustrated in Figure 1.4. Water-driven surface restructuring and protein resistance were then evaluated. As the silicone is used for actual blood-contacting medical devices, these results were considered more significant than those of the surface-grafted silicon wafers. By comparing the results, the prudence of using a model substrate to screen SMAs for protein resistance was also evaluated.

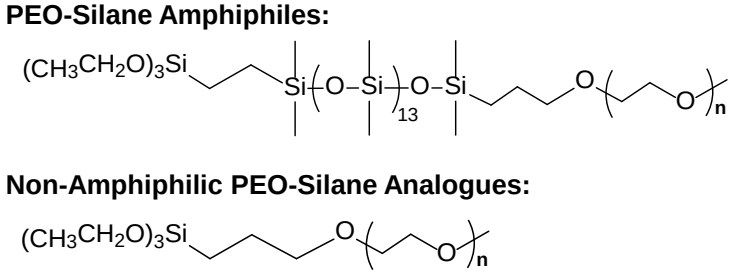

Figure 1.5. Structures of PEO-silane amphiphiles and non-amphiphilic analogues evaluated on silicon wafers. Lengths of PEO included *n* = 3, 8, and 16.

In a subsequent study, multiple molar concentrations of the PEO-silane amphiphiles in silicone were prepared. Again, water-driven surface restructuring and protein resistance were evaluated at each PEO-segment length and concentration. This distinguished whether observed differences in additive performance were due to PEO chain length or rather differences in PEO weight content. Furthermore, these results helped to estimate the minimum concentration of PEO-silane amphiphile required to improve silicone protein resistance. In this study, bacterial growth was also measured on the bulk-modified silicones to evaluate their ability to resist infection.

Finally, the PEO-silane amphiphiles were compared to analogous diblock amphiphiles (PEO_n-$ODMS_m$) in an effort to understand how covalent crosslinking or lack-thereof influences their performance. Triblock amphiphiles were also prepared that were representative of more traditional SMA structure for comparison. The structures of these amphiphiles are illustrated in **Figure 1.6**. In order to estimate their propensity for leaching, bulk-modified silicone films were conditioned in water and evaluated for resulting mass loss, surface restructuring, and water-uptake. A longer siloxane tether (*m* = 30) was also tested with each amphiphile to determine if it could reduce SMA leaching in water. The results of this study were used to determine which structure of PEO-ODMS block copolymers was best-suited for use as a silicone SMA.

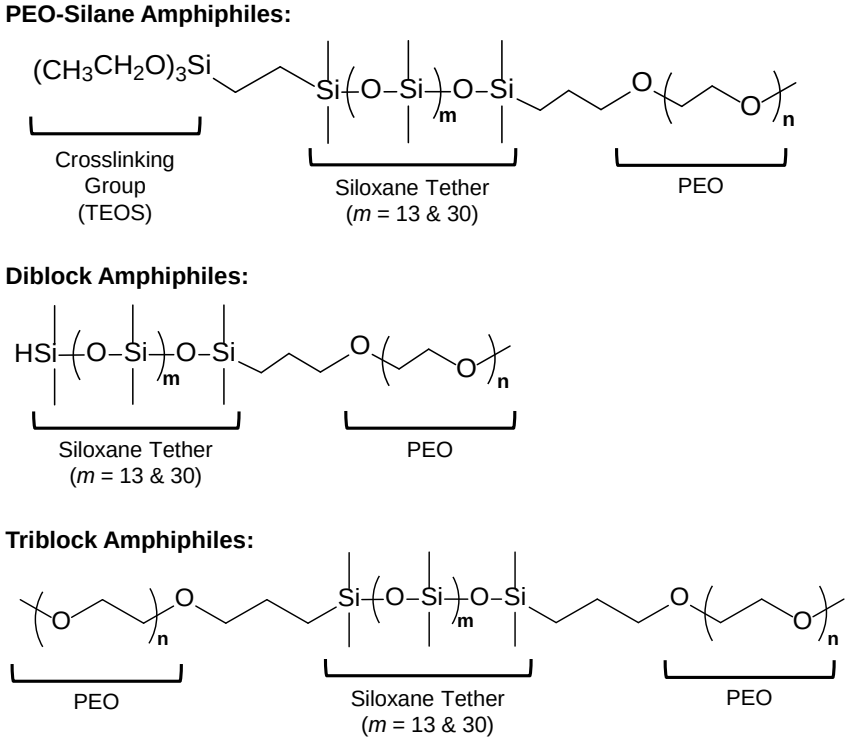

Figure 1.6. Structures of amphiphiles evaluated as potential SMAs for silicone.

CHAPTER II

ENHANCING THE PROTEIN RESISTANCE OF SILICONE *VIA* SURFACE-RESTRUCTURING PEO-SILANE AMPHIPHILES WITH VARIABLE PEO LENGTH*

2.1 Overview

Silicones with superior protein resistance were produced by bulk-modification with poly(ethylene oxide) (PEO)-silane amphiphiles that demonstrated a higher capacity to restructure to the surface-water interface versus conventional non-amphiphilic PEO-silanes. The PEO-silane amphiphiles were prepared with a single siloxane tether length but variable PEO segment lengths: α-$(EtO)_3Si(CH_2)_2$-oligodimethylsiloxane$_{13}$-*block*-poly(ethylene oxide)$_n$-OCH_3 (n = 3, 8, and 16). Conventional PEO-silane analogues (n = 3, 8, and 16) as well as a siloxane tether-silane (*i.e.* no PEO segment) were prepared as controls. When surface-grafted onto silicon wafer, PEO-silane amphiphiles produced surfaces that were more hydrophobic and thus more adherent towards fibrinogen versus the corresponding PEO-silane. However, when blended into a silicone, PEO-silane amphiphiles exhibited rapid restructuring to the surface-water interface and excellent protein resistance whereas the PEO-silanes did not. Silicones modified with PEO-silane amphiphiles of PEO segment lengths n = 8 and 16 achieved the highest protein resistance.

---

*Reprinted with permission from "Enhancing the protein resistance of silicone via surface-restructuring PEO-silane amphiphiles with variable PEO length" by Rufin, M.A., et al., 2015. *J Mater Chem B*. 3(14), p. 2816-2825, Copyright 2015 by The Royal Society of Chemistry.

2.2 Introduction

Silicones, particularly silica-reinforced, crosslinked polydimethylsiloxane (PDMS), are widely used for medical, marine and industrial applications. These include blood-contacting devices (*e.g.* hemodialysis catheters, catheter balloons and cardiac pacing leads) [224-226] and marine coatings [227]. Unfortunately, as a result of their extreme hydrophobicity, the performance of silicones is severely limited by poor resistance to biomolecules such as proteins [228, 229]. For example, in the case of blood-contacting devices, the non-specific adsorption of plasma proteins is considered the first step of thrombosis and even infection [12, 26, 27]. Various modifications have been utilized to hydrophilize silicones in order to reduce protein adsorption, including physical, chemical and combined approaches [230-234].

Modification with poly(ethylene oxide) (PEO; or poly[ethylene glycol] [PEG]) represents arguably the most widely utilized method for enhancing hydrophilicity and protein resistance [147, 208, 235-238]. The exceptional protein resistance of PEO is attributed to its hydrophilicity and hydration, as well as its configurational mobility [154-157]. The biocompatibility [239] and recently demonstrated in vivo oxidative stability [177] of PEO contributes to its widespread use. Notably, the protein resistance of PEO has largely been assessed for chains surface-grafted onto physically stable substrates such as gold [140-142], silicon [151-153], and glass [145, 146]. For these "model PEO surfaces," PEO chains are maintained at the surface irrespective of the environment (*i.e.* air versus water). In contrast, PEO chains incorporated into silicones are subject to surface reorganization upon exposure to a different environment [240].

This process has been studied mainly in terms of hydrophobic recovery (*i.e.* loss of hydrophilicity with exposure to air) such as that observed for plasma treated silicones [241]. This behavior is attributed to the low surface energy of silicones [242, 243], coupled with their high chain flexibility [244, 245]. For example, hydrophobic recovery has been observed for PEO-modified silicones formed by bulk crosslinking with triethoxysilylpropyl PEO monomethyl ether [$(EtO)_3Si(CH_2)_3$-$(OCH_2CH_2)_x$-OCH_3] [201, 202] as well as allyl PEO monomethyl ether [CH_2=$CHCH_2$-$(OCH_2CH_2)_x$-OCH_3] [246]. Hydrophobic recovery is also observed for surface-grafted PEO chains such as those prepared with allyl PEO monomethyl ether [147, 246]. However, since biofouling events such as protein adsorption occur in an aqueous environment, the rapid and substantial surface restructuring of PEO to the surface-water interface is of critical importance.

Towards the goal of enhancing the protein resistance of silicones, we sought to improve the capacity of PEO to migrate to the surface-water interface by altering its molecular structure. Previously, we reported PEO-silane amphiphiles prepared with a siloxane tether of varying lengths (m) separating the PEO segment from the crosslinkable ethoxy silane groups [$\alpha(EtO)_3$-$Si(CH_2)_2$-oligodimethylsiloxane$_m$-$(OCH_2CH_2)_8$-OCH_3; m = 0, 4, and 13] [220]. The siloxane tether distinguishes the PEO-silane amphiphiles from the analogous conventional PEO-silanes noted above which contain a short alkane (*e.g.* propyl) spacer [147, 201, 202, 246]. The siloxane tether is characterized by high flexibility resulting from the wide bond angle (~145°) and low barrier to linearization (~0.3 kcal mol^{-1}) of Si-O-Si dimethylsiloxane bonds, features that give rise to low glass transition temperatures (*e.g.* PDMS, T_g = -125 °C) [244, 245]. Like

a silicone elastomer, the siloxane tether is also hydrophobic, imparting an amphiphilic character to these PEO-silanes. We anticipated that the flexibility and similarly hydrophobic nature of the siloxane tether would facilitate water-driven migration to the surface of a bulk-modified silicone thereby reducing protein adsorption. Indeed, when the PEO-silane amphiphiles (m = 0, 4, and 13) were bulk-crosslinked with α,ω-bis(Si-OH) PDMS (M_n = 3000 g mol^{-1}), protein resistance [220], as well as bacteria and diatom resistance [247], increased with siloxane tether length. Furthermore, extensive atomic force microscopy (AFM) analysis has confirmed the water-driven migration of PEO to these silicone coating surfaces to form nanocomplex surfaces [222]. Herein, we evaluated the impact of PEO segment length by bulk crosslinking a medical grade RTV silicone with three PEO-silane amphiphiles of different PEO segment lengths (n = 3, 8, and 16) and a single siloxane tether length (m = 13) (**Figure 2.1**).

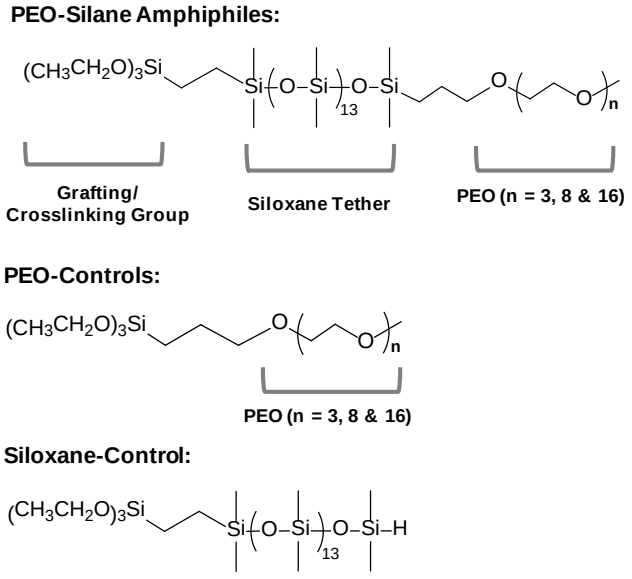

Figure 2.1. Structures of PEO-silane amphiphiles, PEO-controls, and siloxane-control.

Given the protein resistance of PEO oligomers when surface-grafted onto a model substrate [142], the PEO-silane amphiphile (n = 8) was selected for our previous work to enhance the protein resistance of bulk-modified silicones [220-222, 247-249]. Thus, for this study, values of "n" (3, 8, and 16) were chosen as they are "substantially" different from one another (by a factor of approximately two) and thus were predicted to have different restructuring potentials. Analogous conventional PEO-silanes or "PEO-controls" (*i.e.* no siloxane tether, n = 3, 8, and 16) as well as a "siloxane-control" (*i.e.* no PEO segment, m = 13) were likewise evaluated to highlight the effect of the siloxane tether. Water-driven surface restructuring was quantified by temporal static contact angle analysis of water droplets, and resistance to fibrinogen was also measured. In addition, PEO-silane amphiphiles, PEO-controls and the siloxane-control were each surface-grafted onto silicon wafers in order to evaluate their protein resistance in the absence of surface restructuring. This study therefore represents an effort to better understand the influence of the siloxane tether and PEO segment length on the protein resistance and surface restructuring of PEO-silanes through systematic comparisons versus controls.

2.3 Materials and Methods

2.3.1 Materials

Vinyltriethoxysilane (VTEOS), triethoxysilane, α,ω-bis-(SiH)oligodimethyl-siloxane [M_n = 1000–1100 g mol^{-1} per manufacturer's specifications; M_n = 1096 g mol^{-1} per ^{1}H NMR end group analysis; ^{1}H NMR (δ, ppm): 0.05–0.10 (m, 78H, SiCH_3), 0.19 (d, J = 2.7 Hz, 12H, OSi[CH_3]$_2$H) and 4.67–4.73 (m, 2H, SiH)] and allyl methyl PEO$_3$

[M_n = 204 g mol^{-1} per manufacturer's specifications; M_n = 204 g mol^{-1} per ^{1}H NMR end group analysis; ^{1}H NMR (δ, ppm): 3.35 (s, 3H, OCH_3), 3.50–3.67 (m, 12H, OCH_2CH_2), 4.00 (dt, J = 6.0 and 1.5 Hz, 2H, CH_2=CHCH_2O), 5.13–5.28 (m, 2H, CH_2=CHCH_2O) and 5.82–5.96 (m, 1H, CH_2=CHCH_2O)] were purchased from Gelest. Allyl methyl PEO [Polyglykol AM 450, M_n = 292–644 g mol^{-1} per manufacturer's specifications; M_n = 424 g mol^{-1} per ^{1}H NMR end group analysis; ^{1}H NMR (δ, ppm): 3.35 (s, 3H, OCH_3), 3.51–3.66 (m, 32H, OCH_2CH_2), 4.00 (d, J = 5.4 Hz, 2H, CH_2=CHCH_2O), 5.13–5.28 (m, 2H, CH_2=CHCH_2O) and 5.82–5.96 (m, 1H, CH_2=CHCH_2O)] was graciously provided by Clariant. Anhydrous magnesium sulfate ($MgSO_4$), hydrogen peroxide (H_2O_2) solution (30%), glass microscope slides (75 mm x 25 mm x 1 mm), and phosphate buffer solution (PBS, without calcium and magnesium, pH = 7.4) were purchased from Fisher. Sulfuric acid (H_2SO_4, 95–98%), PEO methyl ether [M_n = 750 g mol^{-1} per manufacturer's specifications, M_n = 736 g mol^{-1} per ^{1}H NMR end group analysis; ^{1}H NMR (δ, ppm): 3.37 (s, 3H, OCH_3) and 3.53–3.73 (m, 64H, OCH_2CH_2)], sodium hydride (NaH; 60 wt% dispersion in mineral oil), allyl bromide, $RhCl(Ph_3P)_3$ (Wilkinson's catalyst), Pt-divinyl-tetramethyl-disiloxane complex (Karstedt's catalyst), and human fibrinogen (HF; M_w = 340 kDa; lyophilized powder; ≥90% clottable protein) were purchased from Sigma-Aldrich and were used as received. Organic solvents were also purchased from Sigma-Aldrich and were dried over 4 Å molecular sieves prior to use. Silicon wafers (111) were obtained from University Wafer, Inc. Silica-coated QCM-D sensor crystals (QSX-303) were purchased from Q-Sense. Medical-grade RTV silicone (MED-1137) was purchased from NuSil. Per manufacturer specifications, MED-1137 is comprised of α,ω-bis(Si-

OH)PDMS, silica (11–21%), methyltriacetoxysilane (<5%), ethyltriacetoxysilane (<5%), and trace amounts of acetic acid. The Alexa Fluor 546-dye conjugate of HF (AF-546 HF; M_w = 340 kDa; lyophilized) was obtained from Invitrogen.

2.3.2 Synthetic Approach

All reactions were run under a N_2 atmosphere with a Teflon-covered stir bar to agitate the reaction mixture. Chemical structures were confirmed with nuclear magnetic resonance (NMR) spectroscopy using a Mercury 300 MHz spectrometer operating in the Fourier transform mode and with $CDCl_3$ as the standard.

2.3.2.1 Synthesis of Allyl Methyl PEO_{16}

Allyl methyl PEO_{16} was prepared using a procedure adapted from literature [250, 251]. PEO methyl ether (M_n = 736 g mol^{-1}, 13.98 g, 19 mmol) was dissolved in 90 mL tetrahydrofuran (THF) and added dropwise to a chilled (0 °C) NaH dispersion (6.24 g, 156 mmol) in 120 mL THF. The reaction was then warmed to room temperature (RT) and stirred for 6 h. Next, the PEO solution was chilled, allyl bromide (19.32 g, 160 mmol) in 120 mL THF was added dropwise, and the mixture was warmed to RT and stirred for 16 h. The reaction was then filtered to remove precipitates and volatiles removed under reduced pressure. The resulting orange oil was dissolved in 75 mL de-ionized (DI) water and washed three times with 75 mL toluene. The product was extracted three times with 50 mL chloroform. The chloroform solution was then dried with anhydrous $MgSO_4$, filtered, and volatiles removed under reduced pressure to yield

the final product (8.32 g, 56% yield) as a white, waxy solid. ^{1}H NMR (δ, ppm): 3.36 (s, 3H, OCH_3), 3.51–3.68 (m, 64H, OCH_2CH_2), 4.00 (dt, J = 5.7 and 1.5 Hz, 2H, CH_2=CH-CH_2O), 5.14–5.28 (m, 2H, CH_2=CHCH_2O) and 5.83–5.96 (m, 1H, CH_2=CHCH_2O).

2.3.2.2 Synthesis of PEO-Silane Amphiphiles (n = 3, 8, and 16)

PEO-silane amphiphiles (**Figure 2.1**) were prepared as previously reported for n = 8 [220]. Wilkinson's-catalyzed regioselective hydrosilylation of VTEOS and α,ω-bis-(SiH)oligodimethylsiloxane$_{13}$ produced "**1**" which was then subjected to Karstedt's-catalyzed hydrosilylation with the designated allyl methyl PEO$_n$.

PEO-silane amphiphile (n = 3). ***1*** (22.11 g, 17.2 mmol), allyl methyl PEO$_3$ (3.50 g, 17.2 mmol) and Karstedt's catalyst were reacted together. In this way, the product (25.76 g, 94% yield) was obtained. ^{1}H NMR (δ, ppm): 0.00–0.15 (m, 90H, SiCH_3), 0.48–0.55 (m, 2H, SiCH_2CH_2CH_2), 0.56 (s, 3H, SiCH_2CH_2), 1.09 (d, J = 7.8 Hz, 1H, SiCH_2CH_2), 1.22 (t, J = 7.1 Hz, 9H, SiOCH_2CH_3), 1.54–1.66 (m, 2H, SiCH_2CH_2CH_2), 3.38 (s, 3H, OCH_3), 3.41 (t, J = 7.2 Hz, 2H, SiCH_2CH_2CH_2), 3.52–3.69 (m, 12H, CH_2CH_2O) and 3.82 (q, J = 7.0 Hz, 6H, SiOCH_2CH_3).

PEO-silane amphiphile (n = 8). **1** (20.02 g, 15.57 mmol), allyl methyl PEO$_8$ (6.60 g, 15.57 mmol) and Karstedt's catalyst were reacted together [220]. In this way, the product (22.68 g, 85% yield) was obtained. ^{1}H NMR (δ, ppm): -0.02–0.14 (m, 90H, SiCH_3), 0.47–0.53 (m, 2H, SiCH_2CH_2CH_2), 0.55 (s, 3H, SiCH_2CH_2), 1.08 (d, J = 7.5 Hz,

1H, SiCH_2CH_2), 1.22 (t, J = 7.1 Hz, 9H, SiOCH_2CH_3), 1.52–1.66 (m, 2H, SiCH_2CH_2CH_2), 3.37 (s, 3H, OCH_3), 3.40 (t, J = 7.2 Hz, 2H, SiCH_2CH_2CH_2), 3.51–3.68 (m, 32H, CH_2CH_2O) and 3.81 (q, J = 7.0 Hz, 6H, SiOCH_2CH_3).

PEO-silane amphiphile (n = 16). **1** (17.98 g, 13.98 mmol), allyl methyl PEO_{16} (10.85 g, 13.98 mmol) and Karstedt's catalyst were reacted together. In this way, the product (23.55 g, 82% yield) was obtained. ^{1}H NMR (δ, ppm): -0.01–0.15 (m, 90H, SiCH_3), 0.47–0.54 (m, 2H, SiCH_2CH_2CH_2), 0.55 (s, 3H, SiCH_2CH_2), 1.09 (d, J = 7.5 Hz, 1H, SiCH_2CH_2), 1.22 (t, J = 6.9 Hz, 9H, SiOCH_2CH_3), 1.52–1.66 (m, 2H, SiCH_2CH_2CH_2), 3.37 (s, 3H, OCH_3), 3.41 (t, J = 7.2 Hz, 2H, SiCH_2CH_2CH_2), 3.52–3.72 (m, 64H, CH_2CH_2O) and 3.82 (q, J = 6.9 Hz, 6H, SiOCH_2CH_3).

2.3.2.3 Synthesis of Siloxane- and PEO-Controls (n = 3, 8, and 16)

PEO-controls (*i.e.* no siloxane tethers) (**Figure 2.1**) were prepared as previously reported for n = 8 by the Karstedt's-catalyzed hydrosilylation of triethoxysilane and the designated allyl methyl PEO_n (1.1 : 1.0 molar ratio) [220].

PEO-control (n = 3). Triethoxysilane (5.43 g, 33.1 mmol), allyl methyl PEO_3 (6.14 g, 30.1 mmol) and Karstedt's catalyst were reacted together. In this way, the product (7.53 g, 65% yield) was obtained. ^{1}H NMR (δ, ppm): 0.57–0.65 (m, 2H, SiCH_2CH_2CH_2), 1.20 (t, J = 6.9 Hz, 9H, SiOCH_2CH_3), 1.62–1.74 (m, 2H,

$SiCH_2CH_2CH_2$), 3.36 (s, 3H, OCH_3), 3.41 (t, J = 6.9 Hz, 2H, $SiCH_2CH_2CH_2$), 3.51–3.68 (m, 12H, CH_2CH_2O) and 3.80 (q, J = 7.1 Hz, 6H, $SiOCH_2CH_3$).

PEO-control (n = 8). Triethoxysilane (4.24 g, 25.8 mmol), allyl methyl PEO_8 (9.94 g, 23.4 mmol) and Karstedt's catalyst were reacted together [220]. In this way, the product (9.32 g, 68% yield) was obtained. ^{1}H NMR (δ, ppm): 0.57–0.64 (m, 2H, $SiCH_2CH_2CH_2$), 1.20 (t, J = 7.1 Hz, 9H, $SiOCH_2CH_3$), 1.62–1.74 (m, 2H, $SiCH_2CH_2CH_2$), 3.36 (s, 3H, OCH_3), 3.41 (t, J = 6.8 Hz, 2H, $SiCH_2CH_2CH_2$), 3.50–3.66 (m, 32H, CH_2CH_2O) and 3.79 (q, J = 7.0 Hz, 6H, $SiOCH_2CH_3$).

PEO-control (n = 16). Triethoxysilane (1.57 g, 9.57 mmol), allyl methyl PEO_{16} (6.74 g, 8.69 mmol) and Karstedt's catalyst were reacted together. In this way, the product (4.17 g, 50% yield) was obtained. ^{1}H NMR (δ, ppm): 0.57–0.65 (m, 2H, $SiCH_2CH_2CH_2$), 1.20 (t, J = 6.9 Hz, 9H, $SiOCH_2CH_3$), 1.62–1.74 (m, 2H, $SiCH_2CH_2CH_2$), 3.36 (s, 3H, OCH_3), 3.41 (t, J = 6.9 Hz, 2H, $SiCH_2CH_2CH_2$), 3.50–3.71 (m, 64H, CH_2CH_2O) and 3.80 (q, J = 7.0 Hz, 6H, $SiOCH_2CH_3$).

*Siloxane-control (**1**).* **1** served as the siloxane-control and was prepared as noted above for the first step of the synthesis of the PEO-silane amphiphiles. VTEOS (3.53 g, 18.6 mmol) and α,ω-bis-(SiH)oligodimethylsiloxane (20.37 g, 18.6 mmol) were reacted together [220]. In this way, the product (23.65 g, 99% yield) was obtained. ^{1}H NMR (δ, ppm): 0.003–0.177 (m, 84H, $SiCH_3$), 0.19 (d, J = 2.7 Hz, 6H, $OSi[CH_3]_2H$), 0.56 (s, 3H,

SiC*H*$_2$C*H*$_2$), 1.09 (d, *J* = 7.5 Hz, 1H, SiC*H*$_2$C*H*$_2$), 1.23 (t, *J* = 7.1 Hz, 9H, SiOCH$_2$C*H*$_3$), 3.83 (q, *J* = 7.0 Hz, 6H, SiOC*H*$_2$CH$_3$) and 4.67–4.73 (m, 1H, Si*H*).

2.3.3 Coating Preparation

2.3.3.1 Preparation of Surface-Grafted Coatings on Silicon Wafers

Silicon wafers (1" x 1") were cleaned by sequentially sonicating in (10 min) and rinsing with acetone, repeating with DI water, and then drying in a 120 °C oven overnight. Next, the surfaces of the wafers were oxidized by submerging in a 7 : 3 v/v concentrated H_2SO_4/30% H_2O_2 (Piranha) solution for 30 min (warning: Piranha solution must be handled with extreme caution), removed, rinsed thoroughly with DI water and dried under a stream of air. In a typical procedure, grafting solutions comprised of each of the PEO-silane amphiphiles, PEO-controls and the siloxane-control were prepared at a concentration of 0.012 M in isopropanol (IPA) (30 mL). Following the addition of 1 drop of DI water, the grafting solutions were mixed in sealed jars for 1 h on a shaker table. Next, an oxidized wafer was placed into a jar and remained on a shaker table for 12 h. Afterwards, the wafers were removed, air dried, and cured under vacuum (36 mm Hg) at 150 °C for 12 h. To remove unbound chains, the wafers were sequentially soaked (1 h), sonicated (3 min) and rinsed with ethanol, the sequence repeated with DI water and then lastly dried under a stream of air.

2.3.3.2 Preparation of Modified Silicone Coatings

Glass microscope slides were sequentially rinsed with dichloromethane (DCM) and acetone followed by drying in a 120 °C oven overnight. Casting solutions were prepared by combining 2.0 g MED-1137 silicone in 6 g (9 mL) hexane and mixing with a vortexer until a homogenous solution was obtained. The PEO-silane amphiphiles, PEO-controls and siloxane-control were each added to individual casting solutions at 50 µmol of silane per 1.0 g silicone and mixed thoroughly. Solutions were solvent-cast onto leveled glass microscope slides (1.5 mL per slide) and a polystyrene Petri dish cover placed on top of each so as to slow solvent evaporation and prevent bubble formation. The films were allowed to cure for one week at RT and immediately used for designated analyses.

2.3.4 Surface Characterization

2.3.4.1 X-Ray Photoelectron Spectroscopy (XPS)

Surface composition analysis of surface-grafted coatings on silicon wafers was performed with a KRATO AXIS Ultra Imaging X-ray Photoelectron Spectrometer with a monochromatized Mg K_α source and operating at a base pressure of ~2% x 10^{-9} mbar. The area of analysis was 7 x 3 mm. Elemental atomic percent compositions were determined from three survey spectra sweeps performed from 0 to 1100 eV. High resolution (HR) analyses with a pass energy of 40 eV were performed with a take-off angle of 90°. HR scans (180 s sweeps) were performed at 526 to 536 eV for O 1s, 280 to

295 eV for C 1s, and 96 to 106 eV for Si 2p. Raw data was quantified and analyzed using XPS Peak Processing software.

2.3.4.2 Ellipsometry

The thickness of surface-grafted coatings on silicon wafers was measured via ellipsometry (Alpha-SE, J.A. Woollam) with an incident angle of 70° in the spectral range of 380–900 nm and in the high-precision mode (30 s data acquisition time). The average thickness of the oxide layer of an oxidized silicon wafer was determined at three regions of a wafer specimen (taken from a wafer designated for grafting with a particular composition) using a standard two-layer (silica-silicon) optical model included in the manufacturer's software. To measure the thickness of the grafted chains, the previously determined oxide layer thickness was utilized in a second optical model that included the third “Cauchy layer” (polymer-silica-silicon). The index of refraction (n) was set to 1.450 which is that of crystalline PEO [248, 252]. The average thickness (h) of the grafted layers was based on four individual wafers, each measured at three different regions.

2.3.4.3 Water Contact Angle Analysis

Static contact angles (θ_{static}) of DI water droplets were measured at RT using a CAM-200 goniometer (KSV Instruments) equipped with an autodispenser, video camera, and drop-shape analysis software (Attension Theta). Following deposition, a 5 μL sessile drop of water was iteratively measured over a 2 min (surface-grafted wafers)

and 3 min (silicone-based coatings) period. The reported θ_{static} values of the surface-grafted wafers were based on four individual wafers, each measured at three different areas (12 measurements total). The θ_{static} for the silicone-based coatings was an average of three measurements from different areas of the same film surface.

2.3.4.4 Protein Adsorption

Protein adsorption onto surface-grafted coatings was measured by QCM-D (Q-Sense E4). Silicon dioxide coated sensors (50 nm thickness; Q-Sense) were ultrasonically cleaned with acetone and DI water as described above for silicon wafers. Following exposure to oxygen plasma for 2 min (Harrick Plasma, PDC-001), the sensors were surface-grafted with the designated PEO-silane amphiphile, PEO-control or siloxane-control as described above for silicon wafers. Contact angle analysis was used to verify grafting. Grafted sensors were subjected to the following sequence: (1) 150 µL min^{-1} flow of PBS until the frequency and dissipation values remained constant for >5 min, (2) 150 µL min^{-1} flow of 100 µg mL^{-1} HF in PBS for 20 min and (3) 150 µL min^{-1} flow of PBS for 5 min to remove loosely bound protein. The manufacturer's software was used to process the raw data and determine the mass of HF adsorbed to each sensor.

The adsorption of AF-546 HF onto silicone coatings was measured via fluorescence microscopy. A silicone isolator well (20 mm well diameter, 2 mm depth; McMaster-Carr) was pressed against silicone films thereby creating a seal which prevented leakage of solution from the well. Fibrinogen solution (100 µg mL^{-1} in PBS, 0.7 mL) was added to each well. (Note: per manufacturer specifications, the AF-546 was

first dissolved in 0.1 M $NaHCO_3$ to obtain a 1.5 mg mL^{-1} solution and was further diluted in PBS to obtain a final concentration of 0.1 μg mL^{-1}) After 3 h at RT (protected from light), the solution was removed and 0.7 mL of fresh PBS was then added to each well and removed after 5 min. This process was repeated five times with fresh PBS and lastly one time with DI water. The samples were dried under a stream of air and protected from light until imaged. For each coating, an additional specimen was prepared and likewise rinsed with PBS and DI water, but without exposure to AF-546 (*i.e.* soaked 3 h in PBS) in order to correct for the background intensity.

A FV1000 (Olympus) laser scanning confocal microscope was used for quantification of protein adsorption onto all films. Imaging conditions, both in excitation and collection, were identical for all samples: objective (SPLSAPO 10x objective, NA 0.40), laser excitation type and intensity (HeNe 543 nm source), field of view and resolution (256 x 256 pixels, 317 x 317 micron field of view), depth (40 slices at 1 mm per slice), slice averaging, and collection (150 mm pinhole, 560 nm long-pass filter followed by a 560–660 nm band-pass filter, identical photomultiplier voltages/ sensitivities). Data analysis was performed on the FV10-ASW v3.1 software suite (Olympus). Each surface was imaged in three locations and aggregate intensities computed. These were compared to three images obtained from the analogous surface that had similar treatment without protein exposure. Changes in intensity from exposure to protein were then obtained and compared, with errors reported as the standard deviation of three measurements.

2.4 Results and Discussion

2.4.1 Surface-Grafted Coatings on Silicon Wafers

The protein resistance of PEO-silane amphiphiles (*n* = 3, 8, and 16) in the absence of water-driven restructuring to the surface was evaluated with surface-grafted coatings prepared on silicon wafers. PEO-controls (*n* = 3, 8, and 16) and the siloxane-control were likewise evaluated to elucidate the impact of the siloxane tether.

2.4.1.1 X-Ray Photoelectron Spectroscopy (XPS)

The surface-grafting of conventional PEO-silanes onto silicon wafers has been widely reported [151-153]. Likewise, the successful surface-grafting of PEO-silane amphiphiles (*n* = 3, 8, and 16) was confirmed via XPS with the PEO-control (*n* = 8) and siloxane-control serving as controls. Surface elemental atomic percent compositions are reported in **Table 2.1**. For the oxidized silicon wafer, the O 1s and Si 2p peaks correspond to the wafer composition whereas the carbon (C 1s) is attributed to adsorbed contaminants [253, 254]. Following surface-grafting, a decrease in Si 2p and increase in C 1s content was observed as expected.

Table 2.1. Surface atomic % compositions by XPS.

	C 1s	*C-Si/C-C*	*C-O*	O 1s	Si 2p
Surface	**Total**	***284.5 eV***	***286.4 eV***		
Oxidized silica	**5**			**34**	**61**
Siloxane-control	**34**	94	6	**29**	**38**
n = 3	**24**	82	18	**29**	**47**
n = 8	**22**	71	29	**34**	**44**
n = 16	**26**	48	52	**33**	**42**
PEO-control (n = 8)	**26**	*38*	*62*	**35**	**38**

To further confirm surface-grafting, the C 1s peak was deconvoluted into two peaks of different binding energies and normalized to the peak centered at 284.5 eV (**Figure 2.2**). These peaks correspond to the C-C/C-Si (at 284.5 eV) and C-O (at 286.4 eV) of PEO [147]. The areas of the C-C/C-Si and C-O peaks are reported in **Table 2.1**. When surfaces were grafted with PEO–silane amphiphiles, C-O content increased with PEO segment length (*n*) and a concomitant decrease in C-C/C-Si content was also observed. As expected, the relative quantity of C-O on the surface grafted with the PEO-control was greatest due to the absence of C-Si associated with the siloxane tether that was present on all other samples. Finally, for the surface-grafted siloxane-control, C-O content was very low and may be attributed to residual unreacted ethoxy groups. Together, these results confirm the successful grafting of PEO-silane amphiphiles to silicon wafers.

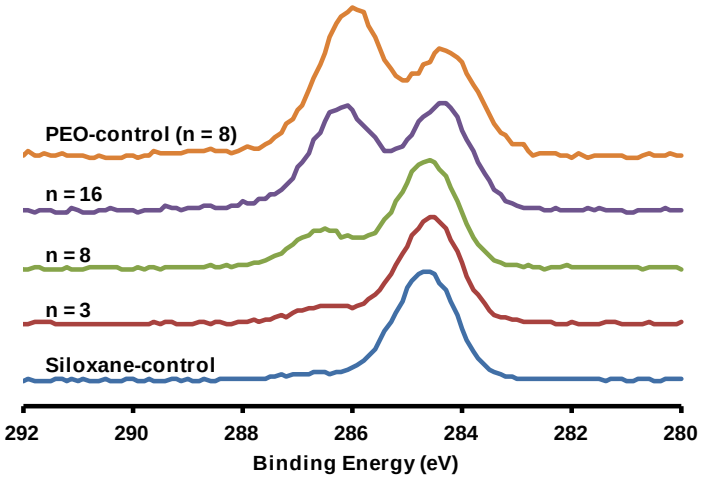

Figure 2.2. HR C 1s XPS spectra of silicon wafers grafted with PEO-silane amphiphiles (*n* = 3, 8, and 16) as well as the PEO-control (*n* = 8) and siloxane-control.

2.4.1.2 Ellipsometry

As chain spacing is known to influence the protein resistance of grafted PEO coatings [144, 252], it was important to ensure that the graft density was similar for all samples using ellipsometry. Dry thickness values (h) of grafted PEO-silane amphiphiles, PEO-controls, and siloxane-control were measured and the obtained values of h were then used to estimate the chain density (σ) (**Table 2.2**) [194, 255, 256]:

$$\sigma = (h \rho N_A) / M_n \qquad \textbf{(Equation 2.1)}$$

where ρ is the density of the dry grafted layer, N_A is Avogadro's number and M_n is the number average molecular weight of the chain. The chain distance or "spacing" (D, nm) (*i.e.* distance between grafting sites) was also calculated (**Table 2.2**) [256]:

$$D = (4 / \pi \sigma)^{1/2} \qquad \textbf{(Equation 2.2)}$$

Utilizing the described grafting conditions, all grafted layers were found to have similar chain spacing (D) (1.0–1.5 nm) except for the PEO-control (n = 8). Initially, this particular composition yielded high values of h (~4.3 nm) which are significantly higher than the fully extended chain length of the PEO segment (~2.8 nm) [257], indicative of substantial multilayer formation. To prevent multilayer formation and increase D, the grafting conditions for the PEO-control (n = 8) were adjusted as follows: grafting solution concentration = 0.006 M, exclusion of water droplet from grafting solution, and cure under vacuum at RT.

Table 2.2. Ellipsometry data for grafted surfaces.

Surface	M_n (g/mol)	Density ρ (g/mL)	Measured Thickness h (nm)	Chain Density $\sigma = (h\rho/M_n) \times N_A$ (chains/nm^2)	Chain Spacing $D = (4/\pi\sigma)^{1/2}$ (nm)	PEO Flory Spacing $2R_f = 2aN^{3/5}$ (nm)	Siloxane Flory Spacing $2R_f = 2aN^{1/3}$ (nm)
Siloxane-control	1286	1.01	2.5 ± 0.9	1.2 ± 0.4	**1.1 ± 0.2**	*n/a*	**2.4**
PEO-control (n = 3)	368	1.04	0.6 ± 0.1	1.0 ± 0.2	**1.1 ± 0.1**	**1.4**	*n/a*
PEO-control (n = 8)	588	1.13	2.3 ± 0.2	2.6 ± 0.2	**0.70 ± 0.03**	**2.4**	*n/a*
PEO-control (n = 16)	940	1.16	1.2 ± 0.2	0.9 ± 0.2	**1.2 ± 0.1**	**3.7**	*n/a*
Amphiphile (n = 3)	1490	1.04	2.1 ± 0.2	0.9 ± 0.1	**1.2 ± 0.1**	**1.4**	**2.4**
Amphiphile (n = 8)	1710	1.13	1.7 ± 0.2	0.6 ± 0.1	**1.4 ± 0.1**	**2.4**	**2.4**
Amphiphile (n = 16)	2062	1.04	3.1 ± 0.8	0.9 ± 0.2	**1.2 ± 0.1**	**3.7**	**2.4**

For all compositions of surface-grafted chains to be in the brush regime, D must be less than twice the Flory radius ($2R_f$) [252]. For each chain composition, R_f was calculated on the basis of the length of one monomer (a) and the degree of polymerization (N) as follows [252, 258, 259]: (i) for the siloxane-control in a poor solvent (water): $R_f = aN^{1/3}$, where a = 0.5 nm and N = 13 and (ii) for the PEO-controls in a good solvent (water): $R_f = aN^{3/5}$, where a = 0.35 nm and $N = n$. For all of these controls, $D < 2R_f$. Calculation of R_f for the PEO-silane amphiphiles is complicated by the fact that these contain two "blocks" (*i.e.* siloxane tether and PEO segment) of differing solubility in water. Thus, R_f was individually calculated on the basis of both the siloxane tether and the PEO segment [248] using the aforementioned equations. For all grafted PEO-silane amphiphiles, $D < 2R_f$, even when considering the lower of the two calculated R_f values. Thus, for all grafted chains, a brush regime was obtained.

2.4.1.3 Water Contact Angle Analysis

An oxidized silicon wafer provides a physically stable surface such that the concentration of grafted chains is maintained at the surface, irrespective of an air or water environment. Thus, the impact of PEO-silane amphiphile structure, including PEO segment length, on surface wettability (*i.e.* θ_{static}) may be elucidated by comparing these grafted surfaces to those prepared with the PEO-controls and the siloxane-control. θ_{static} was measured immediately after water droplet deposition (0 s) and at 2 min (**Figure 2.3**). For all grafted surfaces, θ_{static} (0 s) was very similar to θ_{static} (2 min) due to the expected lack of surface restructuring. For the siloxane-control grafted surface, the hydrophobicity of the siloxane tether (and the absence of a hydrophilic PEO segment) led to a hydrophobic surface as characterized by $\theta_{static} > 90°$ [260]. In the case of PEO-control grafted surfaces, surface hydrophilicity increased (*i.e.* θ_{static} decreased) with increased PEO segment length (n). This trend was likewise observed for PEO-silane amphiphile grafted surfaces. However, due to the contributions of the PEO–silane amphiphiles' hydrophobic siloxane tethers, these surfaces were substantially more hydrophobic versus the corresponding PEO-controls (*i.e.* same n).

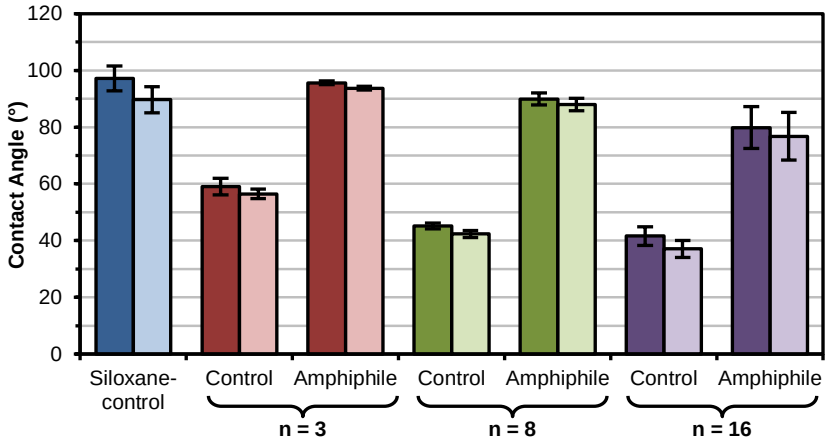

Figure 2.3. Static contact angle (θ_{static}) of surface-grafted silicon wafers at 0 s (dark) and 2 min (light) following placement of water droplet. Each bar represents the average and standard deviation of measurements performed in triplicate on four identically prepared samples.

2.4.1.4 Protein Adsorption

Human fibrinogen (HF) was chosen as the protein for these adsorption studies due to its well-established influence in surface-induced thrombosis by causing platelet adhesion and activation [14-19]. Its use in evaluating the thromboresistance of materials *in vitro* has also been well established [16, 136, 142, 169, 189, 194, 201, 221, 247-249, 252, 261, 262]. Adsorption of HF onto surface-grafted silicon wafers was measured by quartz crystal microbalance with dissipation monitoring (QCM-D) (**Figure 2.4**). QCM-D has been widely used for measuring adsorption of proteins on low-fouling grafted monolayers and thin films [262-265]. The Sauerbrey model was used to approximate the mass of fibrinogen due to the relatively low dissipation of the adsorbed protein [261]. Furthermore, the changes in frequency and dissipation for the most protein-resistant surfaces were too small for the software to accurately calculate the mass using a viscoelastic (Voigt) model. Mass was calculated from the seventh overtone of frequency.

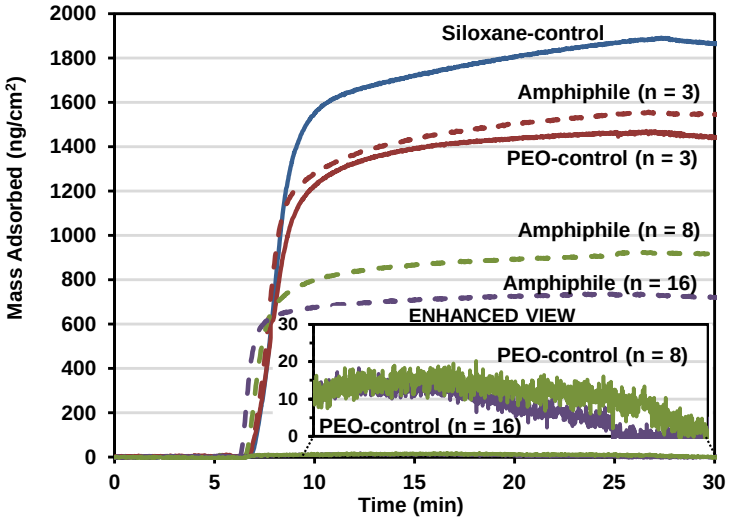

Figure 2.4. QCM-D-measured adsorption of human fibrinogen (HF) onto silica-coated sensors grafted with the siloxane-control [blue solid line], PEO-silane amphiphiles (*n* = 3, 8, and 16) [dashed lines] and PEO-controls (*n* = 3, 8, and 16) [solid lines]. After equilibration for 5 min with PBS, the sensors were exposed to HF for 20 min and then to PBS for 5 min.

Proteins, including HF, are known to adsorb more onto hydrophobic versus hydrophilic surfaces [22, 125]. Indeed, the degree of hydrophobicity of the grafted surfaces (as indicated by θ_{static} reported in **Figure 2.3**) correlates well with the observed amounts of HF adsorbed (**Figure 2.4**). For instance, the siloxane-control produced the most hydrophobic grafted surface which led to the highest level of HF adsorption. Due to increasing hydrophilicity, the protein resistance of grafted surfaces with PEO-silane amphiphiles as well as PEO-controls increased with PEO segment length (*n*). Notably, for a given PEO segment length (*n*), the PEO-silane amphiphile adsorbed more HF than the PEO-control which is consistent with the higher hydrophobicity of the former. These results agree with the exceptionally low fouling nature observed for PEO chains grafted onto stable surfaces [140, 142, 145, 146, 151, 153].

2.4.2 Bulk-Modified Silicone Coatings

In order to evaluate the capacity of the silanes to undergo water-driven surface reorganization and reduce protein adsorption, a medical-grade RTV silicone was bulk-modified with PEO-silane amphiphiles (n = 3, 8, and 16), PEO-controls (n = 3, 8, and 16) and the siloxane-control. Each silane was introduced at a constant level (50 μmol of silane per 1.0 g silicone) and the solvent-cast films were cured on glass slides (**Figure 2.5**). The thicknesses of all films were measured by an electronic caliper and found to be 0.14 ± 0.01 mm. When modified with the hydrophobic siloxane-control, the coating appearance resembled that of the unmodified silicone. The lack of increased opacity of these films was attributed to the solubility of the siloxane-control in the silicone matrix. In contrast, silicones modified with PEO-controls were substantially more opaque and notably so when compared to those prepared with the corresponding PEO-silane amphiphiles. Opacity increased, particularly for the PEO-controls, as the PEO segment length (n) increased. The lesser increase in opacity of silicones modified with PEO-silane amphiphiles may be attributed to reduced phase separation stemming from the solubility of the hydrophobic siloxane tether in the silicone matrix.

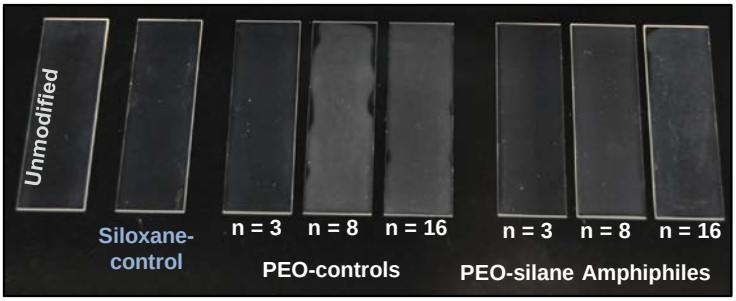

Figure 2.5. Unmodified silicone and silicones bulk-modified with PEO-silane amphiphiles (*n* = 3, 8, and 16), PEO-controls (*n* = 3, 8, and 16), and the siloxane-control.

2.4.2.1 Water Contact Angle Analysis

As noted, AFM was previously used to confirm the water-driven formation of a PEO-enriched surface for silicone modified with the PEO-silane amphiphile (*n* = 8) [222]. Water-driven surface restructuring of bulk-modified silicones was evaluated by temporally measuring θ_{static} of a water droplet placed on the surface over a 3 min period (**Figure 2.6**).

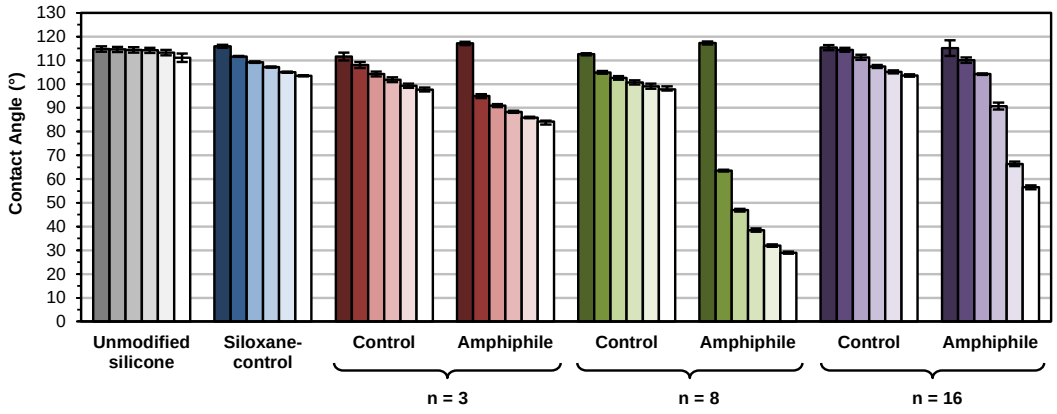

Figure 2.6. Static water contact angles measured over three minutes on bulk-modified silicone films. Bars are organized as the time after initial drop placement from dark color to light as follows: 0 s, 15 s, 30 s, 1 min, 2 min and 3 min. Each bar represents the average of three contact angles measured at the same time point on the same sample and the error bar is the standard deviation.

As expected, the unmodified silicone was very hydrophobic and the θ_{static} value did not change significantly during the 3 min measurement. The siloxane-control produced a modified silicone that was also very hydrophobic but displayed a slight decrease in θ_{static} over 3 min (Δ = ~12°). However, at 3 min, θ_{static} was still >90° and therefore hydrophobic [260]. Notably, silicones modified with PEO-controls also remained hydrophobic after 3 min ($\theta_{static,3min}$ > 90°), similarly exhibiting only a moderate decrease in θ_{static} 3 min after droplet deposition (n = 3, Δ = ~19°; n = 8, Δ = ~15°; n = 16, Δ = ~12°). Thus, the PEO-controls demonstrated a limited capacity to migrate to the surface-water interface and hydrophobicity was only slightly diminished with decreased PEO length. In contrast, when modified with PEO-silane amphiphiles, silicone surfaces underwent extensive and rapid water-driven surface reorganization as noted by large decreases in θ_{static} over a 3 min period (n = 3, Δ = ~33°; n = 8, Δ = ~88°; n = 16, Δ = ~59°). Thus, the siloxane tether critically facilitates the migration of PEO segments to the surface-water interface. Due to this enhanced surface reorganization, initially hydrophobic surfaces quickly became more hydrophilic, with hydrophilicity increasing in the order: n = 3 ($\theta_{static,3min}$ = ~84°) < n = 16 ($\theta_{static,3min}$ = ~57°) < n = 8 ($\theta_{static,3min}$ = ~29°). Thus, the PEO segment length of PEO–silane amphiphiles produced an obvious impact. For n = 8, modified silicones displayed the greatest decrease in θ_{static} over 3 min (i.e. Δ) and also achieved the highest hydrophilicity (*i.e.* $\theta_{static,3min}$). For n = 16, the longer PEO segment length likely imparts a greater steric challenge for water-driven surface reorganization. In contrast, for n = 3, while short PEO segments may more readily move

to the surface-water interface, the reduced number of PEO repeating units diminishes the relative potential to increase hydrophilicity.

2.4.2.2 Protein Adsorption

Protein resistance of the bulk-modified silicone "thick" films was determined via confocal microscopy [220-222, 249]. Adsorption of fluorescently-labeled HF (100 µg mL^{-1}) was measured on silicone in terms of absolute fluorescence intensity and that normalized to unmodified silicone (**Figure 2.7**).

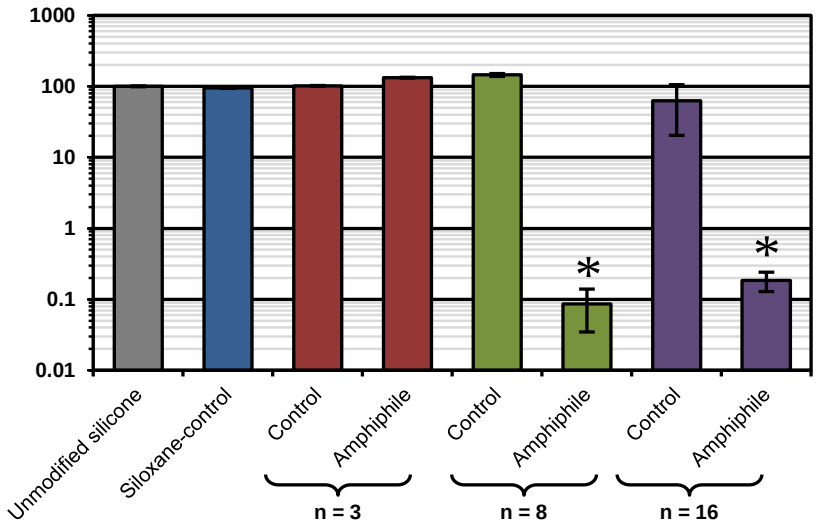

Figure 2.7. Fibrinogen adsorption on bulk-modified silicones as measured by fluorescence intensity with confocal microscopy. Each bar represents the average and standard deviation of pixel intensity for three images normalized to unmodified silicone. Statistical significance was determined for low-fouling samples by one-way analysis of variance (Holm-Sidak method where * indicates $p < 0.05$).

The unmodified silicone, due to its high hydrophobicity, resulted in characteristically high protein adsorption. Due to its hydrophobic nature, the siloxane-

tether produced modified silicones with similarly high protein adsorption. Despite modification of silicones with PEO-controls (n = 3, 8, and 16), protein adsorption was also high. This is notably contrary to the high protein repellency of PEO-controls when grafted onto silicon wafers (**Figure 2.4**). This can be explained by the contact angle analysis that demonstrates that the PEO segments comprising the PEO-controls are severely inhibited in their migration to the surface-water interface where protein adsorption occurs (**Figure 2.6**). The PEO-silane amphiphile (n = 3), due to its short PEO segment length and corresponding inability to effectively hydrophilize the surface-water interface (**Figure 2.6**), also produced modified silicones that adsorbed high levels of protein. However, distinctively low protein adsorption was observed for silicones modified with PEO–silane amphiphiles (n = 8 and 16), with the PEO–silane amphiphile (n = 8) yielding the lowest of the two. This agrees with the contact angle analysis that shows the rapid transition from a hydrophobic to hydrophilic surface, indicative of highly efficient water-driven PEO surface migration (**Figure 2.6**). Thus, while these PEO-silane amphiphiles demonstrated reduced protein repellency versus the corresponding PEO-controls when surface-grafted onto silicon wafers (**Figure 2.4**), they are superior and highly effective in reducing protein adsorption onto bulk-modified silicones.

2.5 Conclusions

While the exceptional protein resistance of PEO (*e.g.* conventional PEO-silanes) is well described, these observations have largely been made when PEO is grafted to a

physically stable substrate (*e.g.* silicon wafer). In this way, migration of the PEO to the surface-water interface (where protein and other biological adhesion occurs) is not required. However, when PEO is used to bulk-modify a silicone elastomer, rapid water-driven restructuring is essential in order to affect protein resistance. In this work, both surface-grafted silicon and bulk-modified silicones were prepared with PEO-silane amphiphiles comprised of a siloxane tether (m = 13) and a PEO segment of variable lengths (n = 3, 8, and 16) as well as the corresponding PEO-controls (*i.e.* no siloxane tether). Surface-grafted PEO-controls, due to their greater hydrophilicity, demonstrated superior resistance to fibrinogen versus the PEO-silane amphiphiles. However, when used to bulk-modify a silicone, PEO-controls produced surfaces that remained hydrophobic after 3 min of exposure to water. As a result, these surfaces exhibited poor resistance to protein adsorption. In contrast, PEO-silane amphiphiles (n = 8 and 16) demonstrated dramatic and rapid water-driven surface restructuring, becoming extremely hydrophilic after exposure to water for only 3 min. As a result, these surfaces displayed exceptionally high resistance to fibrinogen. While the PEO-silane amphiphile (n = 3) also exhibited water-driven restructuring, the achieved hydrophilicity and resistance to protein was diminished by its low PEO content. The enhanced potential of PEO-silane amphiphiles to migrate to the surface-water interface and reduce protein adsorption may be attributed to the hydrophobic nature as well as flexibility of the siloxane tether which allows movement of the tether and attached PEO segment through the silicone network. Furthermore, these results point to the limitations of predicting PEO's protein resistance using model substrates.

CHAPTER III

PROTEIN RESISTANCE EFFICACY OF PEO-SILANE AMPHIPHILES: DEPENDENCE ON PEO-SEGMENT LENGTH AND CONCENTRATION IN SILICONE

3.1 Overview

In contrast to modification with conventional PEO-silanes (*i.e.* no siloxane tether), silicones with dramatically enhanced protein resistance have been previously achieved via bulk-modification with poly(ethylene oxide) (PEO)-silane amphiphiles α-$(EtO)_3Si(CH_2)_2$-oligodimethylsiloxane$_{13}$-*block*-PEO_n-OCH_3 when n = 8 and 16 but not when n = 3. In this work, their efficacy was evaluated in terms of optimal PEO-segment length and minimum concentration required in silicone. For each PEO-silane amphiphile (n = 3, 8, and 16), five concentrations (5, 10, 25, 50, and 100 μmol per 1 g silicone) were evaluated. Efficacy was quantified in terms of the modified silicones' abilities to undergo rapid, water-driven surface restructuring to form hydrophilic surfaces as well as resistance to fibrinogen adsorption. Only n = 8 and 16 were effective, with a lower minimum concentration in silicone required for n = 8 (10 μmol per 1 g silicone) versus n = 16 (25 μmol per 1 g silicone).

3.2 Introduction

Silicone is a widely used material for blood-contacting medical devices such as hemodialysis catheters, catheter balloons, and cardiac pacing leads [224-226]. Silicone materials strike an excellent balance of durability, flexibility, and processability that makes them well-suited for such applications. Unfortunately, due to their hydrophobic nature, silicones suffer from poor resistance to protein adsorption which causes subsequent thrombus formation [228, 229]. This surface-induced thrombosis may lead to a variety of device complications including obstruction of blood flow [76], thromboemboli [49, 69, 79, 80], and infection [26-29], all of which result in diminished device efficacy or failure, ultimately jeopardizing patient health. Antithrombotic drugs can reduce such complications [30-36] but put the patient at risk for major bleeding events [37-41]. Therefore, silicone materials that are inherently resistant to protein adsorption and thrombosis, thereby reducing the need for antithrombotic drugs, would dramatically improve the efficacy and safety of blood-contacting medical devices.

Perhaps the most popular strategy to achieve protein resistance is the introduction of poly(ethylene oxide) [PEO or poly(ethylene glycol) (PEG)] to model substrates (*e.g.* gold and silicon) [140-142, 144, 151-153] as well as to various biomaterials [133-136, 139, 149, 150, 163, 169, 203-209] including silicone [138, 147, 161, 201, 202]. PEO inhibits protein adsorption by a number of mechanisms including steric repulsion [155, 156], blockage of underlying adsorption sites [158], and formation of a repulsive "hydration layer" [159]. Furthermore, in addition to its biocompatibility [239], PEO's excellent oxidative stability under biological conditions has been demonstrated [177].

Despite the promising performance of PEO coatings *in vitro*, their performance *in vivo* has been disappointing and inconsistent [169-171].

In order for PEO to effectively diminish protein adsorption, its surface concentration must be sufficiently high [142, 144, 164, 165]. Thus, for the modification of silicones, it is critical that a PEO-enriched surface is formed at the aqueous (*i.e.* biological) interface where protein adsorption occurs. Due to the low surface energy [242, 243] and high chain flexibility [244, 245] of silicones, surface reorganization occurs depending on the environment (*e.g.* in air or underwater) [240]. For example, silicone can be plasma-treated to improve surface hydrophilicity, but unless maintained in water, it will undergo hydrophobic recovery [241]. Both bulk- and surface-modification strategies used to introduce PEO into silicone have been shown to similarly undergo hydrophobic recovery. These include silicones bulk-crosslinked with conventional PEO-silanes such as triethoxysilylpropyl PEO monomethyl ether [$(EtO)_3Si\text{-}(CH_2)_3\text{-}PEO_n\text{-}OCH_3$] [201, 202] and allyl PEO monomethyl ether [$CH_2{=}CHCH_2\text{-}PEO_n\text{-}OCH_3$] [246] as well as silicones surface-grafted with allyl PEO monomethyl ether [147, 246]. We recently demonstrated that for silicones bulk-modified with PEO-silanes (n = 3, 8, and 16), poor surface restructuring of PEO was observed [266]. In this way, the surfaces remained hydrophobic, even after exposure to water, and exhibited high protein adsorption similar to that of unmodified silicone. The inability of conventional PEO-silanes to undergo water-driven surface restructuring could explain the poor protein resistance of other bulk-modified polymers [161, 202, 205].

We have reported silicones with enhanced protein resistance prepared via bulk-modification with PEO-silane amphiphiles bearing an oligodimethylsiloxane (ODMS) tether [α-$(EtO)_3$-$(CH_2)_3$-$ODMS_m$-*block*-PEO_n-OCH_3] [220-222, 266]. Silicones bulk-modified with these PEO-silane amphiphiles were observed to undergo substantial, rapid, water-driven surface restructuring to form a PEO-enriched surface (by atomic force microscopy [AFM]) [222] with high resistance to proteins [220-222, 266] and other biofoulers [247]. Their ability to function as an effective "surface-modifying additive" (SMA) can be attributed to the ODMS tether's flexibility [244, 245] as well as similar composition and thus compatibility with the silicone matrix. The extent of water-driven surface restructuring and protein resistance has been shown to be dependent on ODMS tether length and PEO-segment length. For instance, for PEO-silane amphiphiles of constant PEO-segment length (m = 0, 4, and 13; n = 8), protein resistance of bulk-modified silicones increased with siloxane tether length [220]. More recently, silicones were modified using PEO-silane amphiphiles with a variable PEO-segment length (m = 13; n = 3, 8, and 16) (**Figure 3.1**) [266]. Water-driven change from a hydrophobic to hydrophilic (*i.e.* PEO-enriched) surface was evaluated by temporally measuring the static contact angle (θ_{static}) of a deposited water droplet. While initially hydrophobic ($\theta_{static,\ 0\ s} \approx 115°$), a rapid and substantial decrease of θ_{static} was observed when silicone was modified with n = 8 ($\theta_{static,\ 3\ min} \approx 29°$) and n = 16 ($\theta_{static,\ 3\ min} \approx 57°$), but less so with n = 3 ($\theta_{static,\ 3\ min} \approx 84°$). Thus, the most hydrophilic PEO-modified silicone surface was achieved with n = 8. In contrast, silicone modified with analogous conventional PEO-

silanes (n = 3, 8, and 16) remained hydrophobic with minimal decrease in θ_{static} as a result of their limited surface-restructuring potential.

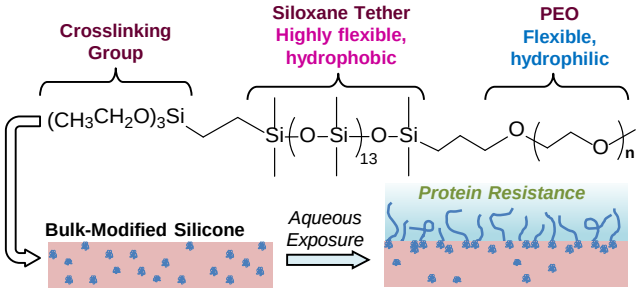

Figure 3.1. PEO-silane amphiphile chemical structure (n = 3, 8, and 16) and illustration of water-driven surface restructuring of bulk-modified silicone.

In the previous study, PEO-silane amphiphiles (m = 13; n = 3, 8, and 16) were incorporated into silicone at a single molar concentration of 50 µmol (per 1 gram of silicone). Due to their different respective molecular weights of the PEO segment (*i.e.* the n value), at this single molar concentration, the "wt% of PEO" was variable: $n = 3 < n = 8 < n = 16$ (**Table 3.1**). In this study, the efficacy of these PEO-silane amphiphiles to undergo water-driven restructuring and subsequently reduce protein adsorption was similarly evaluated. However, five concentrations (5, 10, 25, 50, and 100 µmol per 1 g silicone) were evaluated to determine the minimum concentration necessary. Furthermore, this series permitted determination as to whether it was PEO length (n) or PEO concentration (irrespective of length) that impacted protein resistance efficacy.

Table 3.1. Total wt% of PEO-silane amphiphile (*i.e.* surface-modifying additive, SMA) and corresponding wt% of PEO in a modified silicone for each total molar concentration of SMA. [wt% PEO calculated as the wt% SMA multiplied by the ratio of PEO M_n (n x 44 g/mol) to SMA M_n]

Molar Concentration (per 1 g silicone)	n = 3		n = 8		n = 16	
	wt% SMA	wt% PEO	wt% SMA	wt% PEO	wt% SMA	wt% PEO
5 µmol	0.74	0.07	0.85	0.17	1.02	0.35
10 µmol	1.47	0.13	1.68	0.35	2.02	0.69
25 µmol	3.59	0.32	4.10	0.84	4.90	1.67
50 µmol	6.93	0.61	7.88	1.62	9.35	3.19
100 µmol	12.97	1.15	14.60	3.01	17.10	5.84

3.3 Materials and Methods

3.3.1 Materials

Vinyltriethoxysilane, α,ω-bis-(SiH)oligodimethylsiloxane [M_n = 1000 – 1100 g/mol per manufacturer's specifications; M_n = 1096 g/mol per ^{1}H NMR end group analysis; ^{1}H NMR (300 MHz, $CDCl_3$, δ): 0.05 – 0.10 (m, 78H, SiCH_3), 0.185 (d, J = 2.7 Hz, 12H, SiCH_3), and 4.67 – 4.73 (m, 2H, SiH)], and allyloxy(triethylene oxide) methyl ether [M_n = 204 g/mol per manufacturer's specifications; M_n = 204 g/mol per ^{1}H NMR end group analysis; ^{1}H NMR (300 MHz, $CDCl_3$, δ): 3.35 (s, 3H, OCH_3), 3.50 – 3.67 (m, 12H, OCH_2CH_2), 4.00 (dt, J = 6.0 and 1.5 Hz, 2H, CH_2=CHCH_2O), 5.13 – 5.28 (m, 2H, CH_2=CHCH_2O), and 5.82 – 5.96 (m, 1H, CH_2=CHCH_2O)] were purchased from Gelest. Allyl methyl PEO [Polyglykol AM 450, M_n = 292 – 644 g/mol per manufacturer's specifications; M_n = 424 g/mol per ^{1}H NMR end group analysis; ^{1}H NMR (300 MHz, $CDCl_3$, δ): 3.35 (s, 3H, OCH_3), 3.51 – 3.66 (m, 32H, OCH_2CH_2), 4.00 (d, J = 5.4 Hz, 2H, CH_2=CHCH_2O), 5.13 – 5.28 (m, 2H, CH_2=CHCH_2O), and 5.82 – 5.96 (m, 1H,

CH_2=C*H*CH_2O)] was provided by Clariant. Anhydrous magnesium sulfate ($MgSO_4$) and glass microscope slides (75 mm x 25 mm x 1 mm) were purchased from Fisher. PEO mono methyl ether [M_n = 750 g/mol per manufacturer's specifications, M_n = 736 g/mol per ^{1}H NMR end group analysis; ^{1}H NMR (300 MHz, $CDCl_3$, δ): 3.37 (s, 3H, OCH_3) and 3.53 – 3.73 (m, 64H, OCH_2CH_2)], sodium hydride (NaH; 60 wt% in mineral oil), allyl bromide, $RhCl(Ph_3P)_3$ (Wilkinson's catalyst), and Pt-divinyltetramethyldisiloxane complex (Karstedt's catalyst) were purchased from Sigma-Aldrich and were used as received. Organic solvents were also purchased from Sigma-Aldrich and were dried over 4 Å molecular sieves prior to use. Medical-grade RTV silicone (MED-1137) was purchased from Nusil. Per manufacturer's specifications, MED-1137 is comprised of α,ω-bis(Si–OH)PDMS, silica (11–21%), methyltriacetoxysilane (<5%), ethyltriacetoxysilane (<5%), and trace amounts of acetic acid. The Alexa Fluor 546-dye conjugate of human fibrinogen (AF-546 HF; M_w = 340 kDa; lyophilized) was obtained from Invitrogen. Phosphate buffered saline (PBS, without calcium and magnesium, pH = 7.4) was purchased from Cellgro.

3.3.2 Synthesis

PEO-silane amphiphiles (*m* = 13; *n* = 3, 8, and 16) were prepared and characterized as previously reported using a two-step hydrosilylation procedure [266]. Briefly, α,ω-bis-(SiH)$ODMS_{13}$ was reacted with vinyltriethoxysilane in a regioselective reaction using Wilkinson's catalyst. Next, the product and each allyl methyl PEO (*n* = 3, 8, and 16) were reacted with Karstedt's catalyst to afford the corresponding PEO-silane

amphiphiles. Allyl methyl PEO (n = 16) was synthesized using established methods [266].

3.3.3 Film Preparation

Glass microscope slides were sequentially rinsed with dichloromethane (DCM) and acetone followed by drying in a 120 °C oven overnight. Silicone films were prepared by solvent-casting onto glass microscope slides. Each casting solution consisted of 2.0 g of uncured MED-1137 dissolved in 9 mL hexane (25 wt%). Each PEO-silane amphiphile was thoroughly mixed into the casting solution with a vortexer at the following molar concentrations: 5, 10, 25, 50, and 100 µmol (per 1 g MED-1137). Solutions were solvent-cast onto leveled glass microscope slides (1.5 mL per slide) and a polystyrene Petri dish cover placed on top to reduce the rate of solvent evaporation and prevent bubble formation. Films were allowed to cure one week at room temperature (RT) before analysis. Unmodified silicone films (*i.e.* containing no PEO-silane amphiphile) were likewise prepared as controls.

3.3.4 Water Contact Angle Analysis

Static contact angles (θ_{static}) of distilled/DI water droplets on silicone films were measured at RT using a CAM-200 goniometer (KSV Instruments) equipped with an autodispenser, video camera, and drop-shape analysis software (Attension Theta). Following deposition of a 5 µL sessile drop of water, the contact angle was iteratively measured every 15 seconds over a 5 min period. The reported values at each time point

are the averages and standard deviations of three measurements on different regions of the same film.

3.3.5 Protein Adsorption

AF-546 HF adsorption onto films was measured *via* fluorescence microscopy. On each film, a silicone isolator well (20 mm well diameter, 2 mm depth; McMaster-Carr) was pressed against the surface, thereby creating a seal which prevented leakage of solution from the well. HF solution (100 μg mL^{-1} in PBS, 0.7 mL) was added to each well. (Note: Per manufacturer's specifications, the AF-546 HF was first dissolved in 0.1 M $NaHCO_3$ to obtain a 1.5 mg mL^{-1} solution that was further diluted in PBS to obtain the final concentration of 100 μg mL^{-1}.) After 3 h at RT and protected from light, the solution was removed and 0.7 mL of fresh PBS was added to each well and then removed after 5 min. This process was repeated five times with fresh PBS and lastly once with DI water. The protein-exposed films were dried under a stream of air and protected from light until imaged. For each film composition, an additional film was prepared and likewise rinsed with PBS and DI water, but without exposure to HF solution (*i.e.* soaked 3 h in PBS) in order to correct for the background intensity.

A FV1000 (Olympus) laser scanning confocal microscope was used for quantification of HF adsorption on all silicone films. Imaging conditions (both in excitation and collection) were identical for all samples: objective (SPLSAPO 10x objective, NA 0.40), laser excitation type and intensity (HeNe 543 nm source), field of view and resolution (256 x 256 pixels, 317 x 317 μm field of view), depth (40 slices at 1

μm per slice), slice averaging, and collection (150 μm pinhole, 560 nm long-pass filter followed by a 560–660 nm band-pass filter, identical photo-multiplier voltages/sensitivities). Data analysis was performed on the FV10-ASW v3.1 software suite (Olympus). Each HF-exposed film was imaged in three randomly-selected locations within the region of HF solution exposure and aggregate intensities computed. These were compared to three images obtained from the analogous surface that had similar treatment without HF exposure. Changes in intensity from exposure to HF were then obtained and compared, with errors reported as the standard deviation of the three measurements.

3.4 Results and Discussion

3.4.1 Surface Restructuring

The efficacy of PEO-silane amphiphiles (n = 3, 8, and 16) as SMAs to produce protein-resistant silicones was evaluated first in terms of their capacity to undergo water-driven surface reorganization to form a hydrophilic, PEO-enriched surface. The water-driven restructuring of PEO to the surface of such bulk-modified silicones has been directly observed [222]. In addition, temporally measuring the θ_{static} of a deposited water droplet has been shown to effectively monitor reorganization of PEO to the surface-water interface [220, 221, 247, 249, 266]. Therefore, the 15 bulk-modified silicones and unmodified silicone control (0.14 ± 0.01 mm thick by electronic caliper) were evaluated by measuring θ_{static} of water droplets over a 5 min period. In this way, the rate of migration of PEO to the surface-water interface was characterized by how quickly θ_{static}

decreased (*i.e.* the rate of increase in surface hydrophilicity). The final value of θ_{static} (*i.e.* at 5 min) reflected the hydrophilicity achieved through PEO migration. Therefore, lower θ_{static} values were indicative of higher PEO surface coverage which was expected to better resist protein adsorption [267].

For each PEO-silane amphiphile, the molar concentration had a distinct impact on the rate and extent of water-driven surface restructuring of bulk-modified silicones and the final hydrophilicity achieved **(Figure 3.2)**. For all concentrations, the bulk-modified silicones are initially similarly hydrophobic when compared to the unmodified silicone (*i.e.* high $\theta_{static,\ 0\ s}$), reflecting a lack of PEO at the surface. At the lowest concentration (5 µmol), minimal restructuring was observed and the modified silicone surfaces remained quite hydrophobic, even at the 5 min time point. At higher concentrations, restructuring behavior varied with the PEO-segment length (*n*). For *n* = 3, increasing the concentration from 10 to 100 µmol produced a somewhat small change in the achieved hydrophilicity (*i.e.* $\theta_{static,\ 5\ min}$ = 93 and 76°, respectively). Moreover, at each concentration, the majority of the water-driven restructuring occurred by 15 s. Despite rapid reorganization, the low number of PEO repeat units limited its capacity to increase surface hydrophilicity, even at high concentrations. In stark contrast, *n* = 8 restructured at a rapid rate to form hydrophilic surfaces, even at a low concentration of 10 µmol ($\theta_{static,\ 5\ min}$ = 72°). At higher concentrations, surfaces ultimately became exceptionally hydrophilic as characterized by very low $\theta_{static,\ 5\ min}$ values: 25 µmol (38°), 50 µmol (30°), and 100 µmol (25°). In the case of *n* = 16, substantial restructuring, resulting in a notable increase in surface hydrophilicity, did not occur until the

concentration was 25 µmol or higher. At these concentrations, $\theta_{\text{static, 5 min}}$ values were higher for n = 16 versus for n = 8, but were lower than for n = 3. Also, the total wt% of PEO-silane amphiphile corresponding to the minimum effective molar concentration is much less for n = 8 (10 µmol; 1.68 wt%) versus n = 16 (25 µmol; 4.90 wt%) (**Table 3.1**). Thus, on the basis of molar concentration and total wt% incorporated into silicone, the PEO-silane amphiphile with the intermediate length (n = 8) was the most efficient SMA.

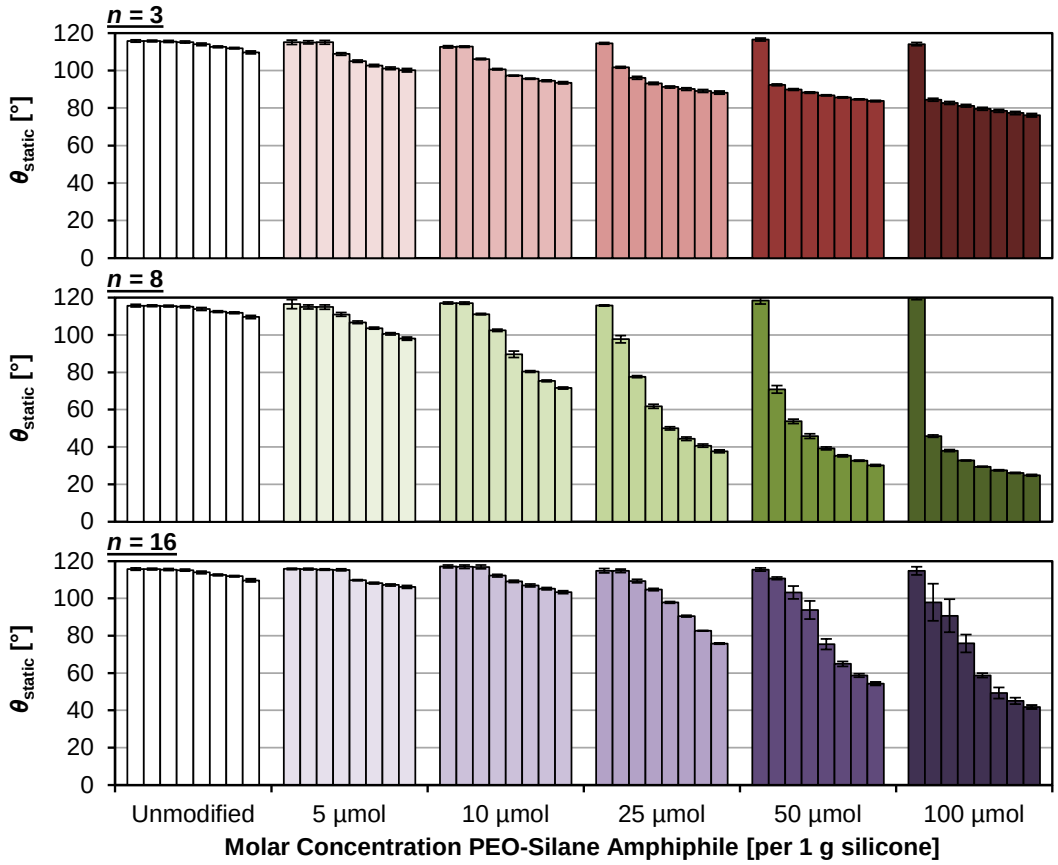

Figure 3.2. Static water contact angle (θ_{static}) measured over a 5 min period on bulk-modified silicone films. For each sample, bars are organized as the time after initial drop placement from left to right as follows: 0 s, 15 s, 30 s, 1 min, 2 min, 3 min, 4 min, and 5 min. Each bar represents the average of measurements made on three water droplets on the same sample at the same time point and the error bar is the standard deviation.

In addition to the "total molar concentration," the efficacy of PEO-silane amphiphiles as SMAs was also considered in terms of the "PEO concentration" expressed in terms of "wt% PEO" (**Table 3.1**). This permits validation as to whether it is the PEO *length* that gives rise to differences in water-driven surface restructuring (**Figure 3.2**) rather than PEO *concentration* (independent of length). Because of the different molecular weights of the PEO segments (n = 3, 8, and 16) for a given molar concentration, the contribution from PEO increases with segment length. For instance, at 10 µmol PEO-silane amphiphile, the wt% PEO increases in the order: 0.13 (n = 3) < 0.35 (n = 8) < 0.69 (n = 16). To determine the impact of PEO length versus PEO concentration (*i.e.* wt% PEO), one series of modified silicones is particularly illustrative. Silicones prepared with n = 3 (25 µmol), n = 8 (10 µmol), and n = 16 (5 µmol) contain the same PEO concentration (0.32 – 0.35 wt%). However, their surface-restructuring profiles are quite different and $\theta_{\text{static, 5 min}}$ = 88°, 72°, and 106°, respectively. Thus, this confirms that PEO length (n) dictates surface restructuring and hydrophilicity, rather than simply concentration independent of length.

Having confirmed the significance of PEO length for surface reorganization, the observed results can be explained on the basis of PEO-silane amphiphile steric effects as well as solubility in the silicone matrix. For longer PEO segments, steric hindrance may reduce surface restructuring potential. Also, in prior work [266], the transparency of modified silicones was observed to decrease with PEO length: n = 3 > n = 8 > n = 16. Thus, longer PEO segments were more prone to phase separation which would be expected to reduce their affinity for water and thus their tendency to migrate to the

surface-water interface. Given the low molecular weight of n = 3, the rapid restructuring can be attributed to its low steric hindrance and greater solubility in silicone. However, the low number of PEO repeat units reduces its ability to give rise to substantial hydrophilicity. For n = 16, its restructuring is relatively inhibited by the chain length as well as phase separation within the silicone, requiring higher concentrations (≥ 25 μmol) to achieve substantial water-driven hydrophilicity. Thus, n = 8 represents the most efficient PEO length, striking a balance between these two effects to achieve hydrophilicity at the surface-water interface at only 10 μmol.

3.4.2 Protein Resistance

Adsorbed fibrinogen plays a well-established role in the initiation of surface-induced thrombosis [2, 12, 15-17] and is commonly used to evaluate material thrombogenicity *in vitro* [16, 136, 142, 147, 169, 189, 194, 221, 222, 248, 249, 252, 261, 262]. Oeveren *et al.* concluded that fibrinogen adsorption was one of the most reliable methods to predict thrombogenicity for many materials [268]. Furthermore, silicone was found to adsorb the most fibrinogen of all the materials tested, which could explain silicone's high susceptibility to thrombosis. Therefore, fibrinogen adsorption was utilized in this study to evaluate the thromboresistance of bulk-modified silicone films.

Resistance of bulk-modified silicone films to HF adsorption was determined using confocal microscopy [220-222, 249, 266]. Following exposure to a solution of fluorescently labeled HF (100 μg mL^{-1}; 3 h), the resulting fluorescence intensity of each film was measured and normalized to that of the unmodified silicone (**Figure 3.3**). As

expected, HF adsorption was relatively high for the unmodified silicone. The efficacy of the PEO-silane amphiphiles (n = 3, 8, and 16) to reduce protein adsorption onto surfaces was impacted by PEO-segment length as well as molar concentration, with protein resistance corresponding to their ability to undergo water-driven restructuring to achieve hydrophilicity (per **Figure 3.2**). At all molar concentrations, silicone modified with n = 3 adsorbed high levels of HF similar to unmodified silicone. This agrees with the observed lack of hydrophilicity, even at higher concentrations. Modification of silicone with n = 8 dramatically reduced HF adsorption at molar concentrations as low as 10 μmol. As the concentration was increased, protein adsorption levels remained very low but did not substantially change. While increasing the molar concentration beyond 10 μmol led to surfaces with greater water-induced hydrophilicity, it did not additionally benefit protein resistance. This indicates that the surface presents a sufficient amount of PEO (n = 8) at 10 μmol. In the case of n = 16, the minimum molar concentration required was 25 μmol, with higher concentrations not leading to an improvement in protein resistance. Again, this parallels the observation that a 25 μmol concentration is required to achieve water-induced hydrophilicity. Although hydrophilicity increases somewhat at higher concentrations (50 and 100 μmol), they are not necessary for high protein resistance.

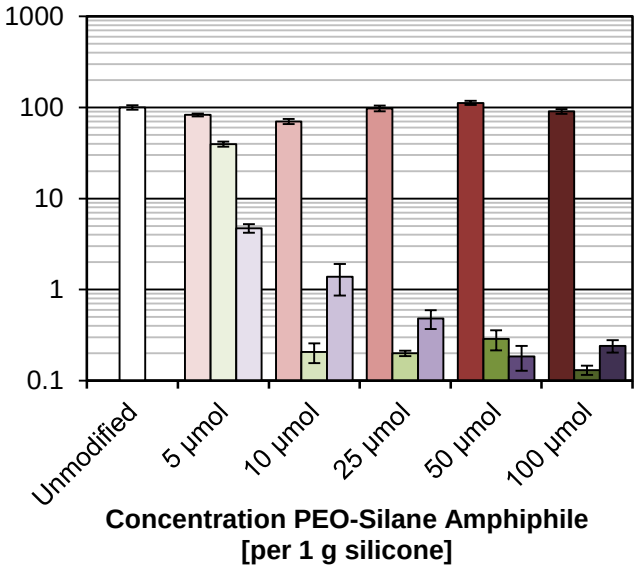

Figure 3.3. HF adsorption on bulk-modified silicone films as measured by fluorescence intensity with confocal microscopy. Each bar represents the average and standard deviation of pixel intensity for three images of the sample normalized to that of unmodified silicone. Each set of three bars indicates sample fluorescence at the given concentration for *n* = 3 (left), *n* = 8 (middle), and *n* = 16 (right).

3.5 Conclusions

To achieve protein resistance and subsequent thromboresistance, a SMA is required that can be incorporated into silicones so as to effectively induce water-driven PEO-enrichment and hydrophilicity at the surface. PEO-silane amphiphiles comprised of a siloxane tether (*m*) and a PEO segment (*n*) represent a new class of SMAs with the potential to do so. When evaluated previously at a constant molar concentration (50 µmol per 1 g silicone), PEO-silane amphiphiles (*m* = 13) dramatically improved protein resistance of silicones when *n* = 8 and 16 but not when *n* = 3. In this work, the efficacy of these PEO-silane amphiphiles (*m* = 13; *n* = 3, 8, and 16) was explored in terms of the minimum molar concentration required as well as the significance of the PEO-segment

length. Each PEO-silane amphiphile was incorporated into a silicone at 5, 10, 25, 50, and 100 μmol (per 1 g silicone). Even at higher concentrations, while n = 3 produced rapid, water-driven restructuring of modified silicones, it did not achieve appreciable hydrophilicity nor protein resistance. In contrast, at a concentration of only 10 μmol, n = 8 achieved high protein resistance. This represents a total weight concentration of n = 8 of only 1.68%. While increasing the molar concentration further enhanced water-induced hydrophilicity, it did not lead to further substantial reductions in protein adsorption. Finally, for n = 16, the minimum concentration required for protein resistance was found to be higher (25 μmol; 4.90 wt%). When compared on the basis of "wt% PEO", it was determined that PEO length did in fact influence surface restructuring and protein resistance, with n = 8 being the most effective. The efficacy of n = 8 to undergo water-driven surface migration and induce subsequent protein resistance may be attributed to the balance of steric effects and solubility in the silicone matrix. Given the low concentration (10 μmol; 1.68 wt%) necessary to invoke a substantial reduction in protein adsorption, the n = 8 PEO-silane amphiphile is considered to be a potent SMA for silicones.

CHAPTER IV

PEO-SILANE AMPHIPHILES ADDRESS THE LIMITATIONS ASSOCIATED WITH TRADITIONAL SURFACE-MODIFYING ADDITIVES

4.1 Overview

Poly(ethylene oxide) (PEO)-silane amphiphiles are promising as surface-modifying additives (SMAs) to improve the protein resistance of silicone for medical applications. SMAs have traditionally been associated with significant limitations, namely leaching and an inability to adequately repopulate at the surface after material abrasion due to poor surface restructuring ability. In this work, key structural features of PEO-silane amphiphiles were probed to address those limitations. PEO-silane amphiphiles with two oligodimethylsiloxane (ODMS) tether lengths (PEO_8-$ODMS_m$-triethoxysilane, m = 13 and 30) were evaluated and compared to analogous diblock (PEO_8-$ODMS_m$) and triblock (PEO_8-$ODMS_m$-PEO_8) SMA controls. For all SMA formulations, bulk-modified silicones were found to undergo excellent water-driven surface restructuring that persisted even after material abrasion. Leaching from bulk-modified silicones left in water for two weeks was minimized by using the m = 30 PEO-silane amphiphile and diblock SMAs. Those two SMAs also caused the smallest increase in silicone water uptake. These results indicate that the crosslinking group (triethoxysilane) does not impart a significant benefit if the ODMS length is sufficiently long. Also, the triblock SMA structures did not improve silicone wettability substantially despite having twice the PEO content of respective analogues.

4.2 Introduction

Despite favorable mechanical and chemical properties [103, 104], a major limitation of silicone for implantable medical devices is its poor blood compatibility [106]. Due to its hydrophobic nature [228, 229], when silicone is brought into contact with blood, it rapidly fouls with plasma proteins (*e.g.* fibrinogen [268]) that induce platelet adhesion and activation [2, 13]. This leads to thrombus formation that, for devices such as dialysis catheters, can cause dysfunction, obstruct blood flow, and facilitate infection [25-29]. Therefore, silicone modification strategies that can prevent protein adsorption and subsequent thrombosis are of significant interest.

Coatings comprised of poly(ethylene oxide) (PEO) [or poly(ethylene glycol) (PEG)] [138, 147, 148] or zwitterionic polymers [183, 185, 193, 197] have been proposed to improve silicone protein resistance. It is theorized that these polymers effectively prevent biomolecule adsorption via minimization of interfacial free energy [128] and formation of a repulsive hydration layer [159]. The excellent protein resistance of PEO and zwitterionic coatings has been thoroughly demonstrated *in vitro* when coated onto model substrates such as gold [140-142, 186-192], glass [145, 146, 184], and silicon wafer [151-153, 194, 195]. Unfortunately, evidence of their efficacy on polymer substrates *in vivo* is limited and a number of studies have observed poor or inconsistent efficacy [169-171, 176, 199, 200]. This may be attributed to the limitations of coating techniques.

Physical adsorption techniques, while quite simple (*e.g.* dip-coating), result in coatings with poor adhesive stability that are prone to removal during implantation

[201]. Surface-grafting techniques result in more stable coatings via covalent attachment to the substrate. However, such techniques can be quite complex which limits their utility. For example, a “graftable” substrate must contain functional groups or initiators to which polymers can covalently attach (“graft-to”) or grow from (“graft-from”) [160]. Many biomaterials lack these and must be modified accordingly with additional pre-treatment steps. Also, the efficacy of these coatings is dependent on high graft density [144, 164, 165] which can be difficult to establish, particularly with “graft-to” methods. Substrate attachment by free chains may be inhibited due to steric blocking of attachment sites by other grafted chains [121]. High graft density can also be difficult to maintain. For example, on silicone, surface grafted PEO chains can migrate into the bulk during storage in air (*i.e.* hydrophobic recovery) which reduces PEO surface coverage over time [179].

To avoid the complexities associated with surface grafting, PEO has been incorporated into silicone via bulk-modification [201, 202]. Bulk-modification with zwitterionic polymers may also be possible, but their poor solubility in aprotic solvents has limited such efforts [214]. In order to be effective, silicone bulk-modified with PEO must undergo microphase separation to achieve the high PEO surface coverage necessary prevent protein adsorption. Surface modifying additives (SMAs) have proven particularly effective for the bulk-modification of other polymeric biomaterials [210, 214]. SMAs are typically designed as triblock copolymers (A-B-A) where the end blocks (A) are hydrophilic (*e.g.* PEO) and migrate to the material surface where they confer protein resistance while the center block (B) is hydrophobic with affinity for the base

polymer network to improve SMA solubility in the network while also preventing leaching. When blended in small quantity with the base polymer, SMAs undergo migration either during or after fabrication to the material surface [108]. Despite their successful use in a variety of biomaterials [214], there is limited literature describing SMAs for improving the protein resistance of silicone. Also, SMAs are associated with two major shortcomings [108]. First, low molecular weight SMAs can leach from the material under aqueous conditions. Also, due to poor restructuring ability, migration of SMAs to the surface may be slow or not occur after fabrication. This means that in the event of SMA removal caused by surface abrasion, SMAs from the bulk may be incapable of repopulating the material surface in time to prevent protein adsorption.

Our group has designed a SMA (PEO-silane amphiphile; **Figure 4.1**) intended to specifically improve the protein resistance of a medical-grade, condensation-cure silicone elastomer (MED-1137, NuSil). This SMA is a diblock structure (A-B) with PEO as the hydrophilic segment (A) and oligodimethylsiloxane (ODMS) as the hydrophobic segment (B). This particular SMA includes a triethoxysilane (TEOS) functional group – attached to ODMS, opposite PEO (PEO-*block*-ODMS-TEOS) – that can undergo condensation reactions to covalently crosslink with the silicone network to prevent leaching. Prior work demonstrated that when the PEO-silane amphiphiles were blended into silicone in small quantities (less than 10 wt%) prior to curing, they dramatically improved the elastomer's resistance to fibrinogen adsorption (Chapter III). This was attributed to the ability of the PEO-silane amphiphile to undergo rapid migration and achieve high PEO surface-coverage when bulk-modified silicone was exposed to

aqueous conditions. The speed and extent of surface restructuring was largely dependent on PEO length. An oligomeric length of 8 repeat units was found to achieve the best protein resistance with minimal concentration (1.7 wt%). It was also confirmed that the ODMS segment (m = 13) dramatically enhanced the ability of PEO to migrate to the surface when compared to non-amphiphilic PEO-silane controls (PEO-TEOS) [266].

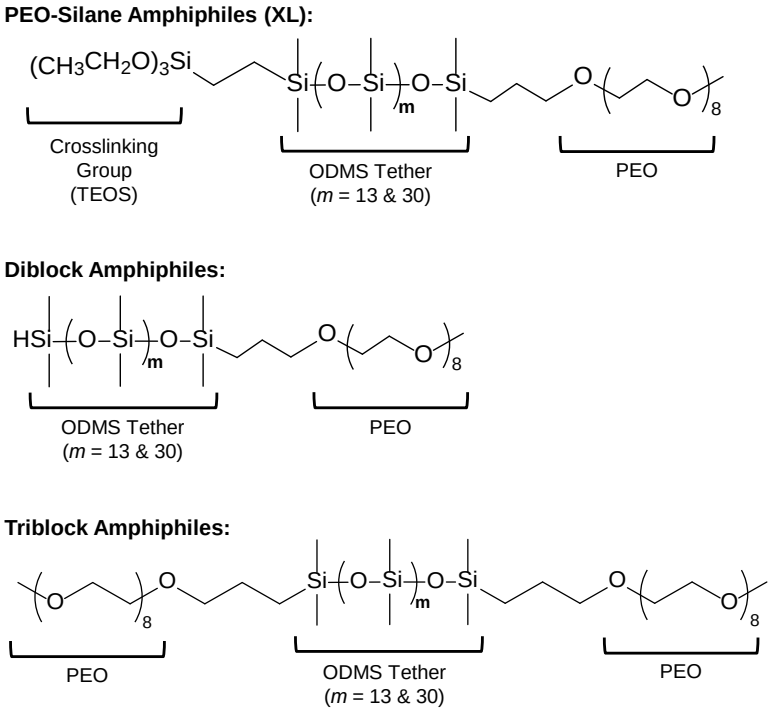

Figure 4.1. Structures of SMA amphiphiles evaluated in this study.

In this work, PEO-silane amphiphiles were evaluated in terms of their ability to overcome the limitations associated with SMAs (*i.e.* leaching and inadequate abrasion recovery). The abilities of the SMAs to efficiently replenish PEO at the silicone surface after abrasion were evaluated. Key structural features of the PEO-silane amphiphiles were also probed. In order to determine the efficacy of the crosslinker, diblock analogues

(A-B) without TEOS were prepared (**Figure 4.1**). To determine if there was a benefit to the non-crosslinkable, triblock structure (A-B-A) that is most commonly used for SMAs [207-211], PEO-ODMS-PEO analogues were also prepared and evaluated. As these contain twice the quantity of PEO, these could foreseeably improve silicone wettability more effectively. Without the ability to crosslink, both analogues were expected to be more susceptible to leaching. As an alternative to crosslinking, a longer ODMS segment (m = 30) was also tested for each SMA architecture. This was hypothesized to physically reduce leaching of SMAs by decreasing the additive's solubility in water while simultaneously increasing its affinity for the silicone base network. If sufficiently effective, the longer tether could obviate the need for chemical crosslinking (TEOS) entirely. It has also been shown in previous work that PEO-silane amphiphiles of this ODMS length achieve excellent silicone hydrophilicity and protein resistance similar to those of m = 13 [223].

4.3 Materials and Methods

4.3.1 Materials

Allyl methyl PEO [Polyglykol AM 450, M_n = 292–644 g mol^{-1} per manufacturer's specifications; M_n = 424 g mol^{-1} per ^{1}H NMR end group analysis; ^{1}H NMR (δ, ppm): 3.35 (s, 3H, OCH_3), 3.51–3.66 (m, 32H, OCH_2CH_2), 4.00 (d, J = 5.4 Hz, 2H, CH_2=CHCH_2O), 5.13–5.28 (m, 2H, CH_2=CHCH_2O) and 5.82–5.96 (m, 1H, CH_2=CHCH_2O)] was kindly provided by Clariant. Octamethylcyclotetrasiloxane, vinyltriethoxysilane (VTEOS), Pt-divinyltetramethyldisiloxane complex (Kastedt's

catalyst) in xylene, and α,ω-bis-(SiH)oligodimethylsiloxane [$ODMS_{13}$; M_n = 1000–1100 g mol^{-1} per manufacturer's specifications; M_n = 1096 g mol^{-1} per ^1H NMR end group analysis; ^1H NMR (δ, ppm): 0.05–0.10 (m, 78H, $SiCH_3$), 0.19 (d, J = 2.7 Hz, 12H, $OSi[CH_3]_2H$) and 4.67–4.73 (m, 2H, Si*H*)] were purchased from Gelest. Triflic acid, $RhCl(Ph_3P)_3$ (Wilkinson's catalyst), hexamethyldisilazane (HMDS), and solvents were obtained from Sigma-Aldrich. All solvents were dried over 4Å molecular sieves prior to use for hydrosilylation reactions and film casting. Glass microscope slides (3" x 1") were purchased from Fisher Scientific. Medical-grade condensation-cure room-temperature-vulcanizing (RTV) silicone elastomer (MED-1137) was purchased from NuSil Technology.

4.3.2 Synthetic Approach

Reactions were all run under a N_2 atmosphere with a Teflon-covered stir bar to agitate the mixture. Chemical structures were confirmed with nuclear magnetic resonance (NMR) spectroscopy using a Mercury 300 MHz spectrometer operating in the Fourier transform mode and using $CDCl_3$ as the standard. Syntheses of α,ω-bis-(SiH)oligodimethylsiloxane [$ODMS_{30}$; M_n = 2338 g mol^{-1} per ^1H NMR end group analysis) and PEO-silane amphiphiles (m = 13 and 30) were carried out following previously-established procedures [223, 266].

4.3.2.1 Synthesis of Diblock Amphiphiles

Diblock amphiphiles were prepared using a Wilkinson's-catalyzed regioselective hydrosilylation procedure. Allyl methyl PEO_8 (M_n = 424 g mol^{-1}) and $ODMS_m$ (1:1 molar ratio) were dissolved in toluene in a sealed round bottom flask with 10 mg Wilkinson's catalyst and heated to 80 °C. After 16 h, the catalyst was removed from the reaction mixture by adding activated charcoal and heating at 90 °C for 2 h. The mixture was then cooled to room temperature (RT) and filtered to remove the charcoal. After filtration, the volatiles were removed under reduced pressure to yield colorless polymer liquid.

Diblock Amphiphile (m = 13). Allyl methyl PEO_8 (3.09 g, 7.29 mmol) and $ODMS_{13}$ (8.00 g, 7.30 mmol) and Wilkinson's catalyst were reacted in 50 mL toluene. The product (8.98 g, 81% yield) was obtained using the described procedure. ^{1}H NMR (δ, ppm): 0.03–0.10 (m, 84H, SiCH_3), 0.18 (d, J = 2.7 Hz, 6H, OSi[CH_3]$_2$H), 0.46–0.55 (m, 2H, SiCH_2CH$_2$CH$_2$), 1.51–1.67 (m, 2H, SiCH$_2$CH_2-CH$_2$), 3.38 (s, 3H, OCH_3), 3.41 (t, J = 7.1 Hz, 2H, SiCH$_2$CH$_2$CH_2), 3.50–3.73 (m, 32H, CH_2CH_2O), and 4.67–4.73 (m, 1H, SiH).

Diblock Amphiphile (m = 30). Allyl methyl PEO_8 (2.48 g, 5.85 mmol) and $ODMS_{30}$ (13.79 g, 5.86 mmol) and Wilkinson's catalyst were reacted in 50 mL toluene. The product (13.00 g, 80% yield) was obtained using the described procedure. ^{1}H NMR (δ, ppm): -0.08–0.15 (m, 186H, SiCH_3), 0.18 (d, J = 2.7 Hz, 6H, OSi[CH_3]$_2$H), 0.47–

0.55 (m, 2H, SiCH_2CH$_2$CH$_2$), 1.52–1.66 (m, 2H, SiCH$_2$CH_2-CH$_2$), 3.38 (s, 3H, OCH_3), 3.41 (t, J = 7.4 Hz, 2H, SiCH$_2$CH$_2$CH_2), 3.52–3.69 (m, 32H, CH_2CH_2O), and 4.68–4.72 (m, 1H, SiH).

4.3.2.2 Synthesis of Triblock Amphiphiles

Triblock amphiphiles were prepared using a Karstedt's-catalyzed hydrosilylation procedure. Allyl methyl PEO (M_n = 424 g mol^{-1}) and ODMS$_m$ (2:1 molar ratio) were dissolved in toluene in a sealed round bottom flask with Karstedt's catalyst and heated to 80 °C. After 16 h, the catalyst was removed by adding activated charcoal to the reaction mixture and heating at 90 °C for 2 h. The mixture was then cooled to RT and filtered. The volatiles were then removed under reduced pressure to yield the colorless polymer product.

Triblock Amphiphile (m = 13). Allyl methyl PEO$_8$ (3.21 g, 7.57 mmol) and ODMS$_{13}$ (4.15 g, 3.79 mmol) and Karstedt's catalyst (25 µL) were reacted in 30 mL toluene. The product (3.35 g, 46% yield) was obtained using the described procedure. ^{1}H NMR (δ, ppm): 0.05–0.09 (m, 90H, SiCH_3), 0.47–0.54 (m, 4H, SiCH_2CH$_2$CH$_2$), 1.54–1.66 (m, 4H, SiCH$_2$CH_2-CH$_2$), 3.37 (s, 6H, OCH_3), 3.41 (t, J = 7.2 Hz, 4H, SiCH$_2$CH$_2$CH_2), and 3.52–3.68 (m, 64H, CH_2CH_2O).

Triblock Amphiphile (m = 30). Allyl methyl PEO$_8$ (1.49 g, 3.51 mmol) and ODMS$_{30}$ (4.12 g, 1.75 mmol) and Karstedt's catalyst (25 µL) were reacted in 30 mL

toluene. The product (3.67 g, 65% yield) was obtained using the described procedure. ^{1}H NMR (δ, ppm): -0.02–0.17 (m, 192H, SiCH_3), 0.46–0.55 (m, 4H, SiCH_2CH$_2$CH$_2$), 1.52–1.65 (m, 4H, SiCH$_2$CH_2-CH$_2$), 3.37 (s, 6H, OCH_3), 3.41 (t, J = 7.2 Hz, 4H, SiCH$_2$CH$_2$CH_2), and 3.52–3.68 (m, 64H, CH_2CH_2O).

4.3.3 Silicone Film Preparation

Glass microscope slides were sequentially rinsed with DCM and acetone followed by drying in a 120 °C oven overnight. Casting solutions were prepared by mixing 2 g uncured MED-1137 with 6 g (9 mL) hexane and mixing with a vortexer until a homogenous solution was obtained. For modification of silicone, the PEO-silane, diblock, and triblock amphiphiles were added to individual casting solutions at 50 µmol of SMA per 1 g silicone and mixed thoroughly. Solutions were solvent-cast onto leveled glass slides (1.5 mL per slide [2.0 mL for leaching study]) in a covered polystyrene Petri dish. The films were allowed to cure for one week at RT and then promptly used for designated analyses.

4.3.4 Characterization

4.3.4.1 Water-Driven Surface Restructuring

Water-driven surface restructuring of bulk-modified silicone was characterized with static water contact angle (θ_{static}) using a CAM-200 goniometer (KSV Instruments) equipped with an autodispenser, video camera, and drop-shape analysis software (Attension Theta). For each measurement, a 5 µL DI water droplet was placed on the

film and θ_{static} was iteratively measured over a 5 min period. Afterwards, the film was dried under a stream of air. The reported θ_{static} values are an average and standard deviation of three measurements each made on different areas of the same film.

Water-driven surface restructuring of bulk-modified silicone was also evaluated immediately after abrasion. A razor blade was used to cut away a thin layer from the surface of the film. θ_{static} was then measured on the freshly exposed surface. This process was repeated on three different regions of each film to yield an average and standard deviation as reported.

Changes in water-driven surface restructuring of bulk-modified silicone were measured during and after water and air equilibration. Two of each film type were prepared and one week after casting, θ_{static} was measured on both. Next, one film was submerged in ~30 mL DI water (water-equilibrated) while the other was left in air (air-equilibrated), both in a polystyrene Petri dish. The film in water was removed after 2 h and briefly dried under stream of air before measuring θ_{static}. After making three 5-min θ_{static} measurements, the film was resubmerged in fresh DI water. This process was repeated at 6 h, 24 h, 48 h, 72 h, 6 days, 10 days, and 14 days after the initial water submersion. At the 14^{th} day, each film was dried under reduced pressure at 50 °C overnight and a final θ_{static} was measured. The film left in air was measured again 7 and 14 days after the initial measurement.

4.3.4.2 Leaching

For leaching studies, six of each film type were prepared. Using a razor, silicone films were removed from the glass slide and uniquely marked for identification purposes. The mass of each film was then measured and recorded. For each film type, three films were submerged in 30 mL DCM and three were submerged in 30 mL DI water, both in sealed glass jars. After one week, the solution in each jar was replaced with 30 mL fresh solvent. One week later, the films were removed and dried overnight under reduced pressure. The final mass of each film was then measured and was used to calculate the mass loss ratio of bulk-modified films as follows:

$$Mass\ Loss\ Ratio = (FML - UML) / MA \qquad \textbf{(Equation 4.1)}$$

where FML is the bulk-modified film percent mass loss, UML is the unmodified film percent mass loss, and MA is the percent mass of additive. Percent mass loss was calculated using established methods [208]. The mass loss ratio was useful in estimating what portion of the mass loss was attributable to the additive of bulk-modified films by accounting for differences in additive weight concentrations and the mass loss that occurs in silicone without the SMAs.

4.3.4.3 Water Uptake

Three of each film type on glass slides were submerged in ~30 mL DI water in individual polystyrene Petri dishes. After 24 h, the films were removed from water and

dried with stream of air and dabbed dry with a paper towel. The water content of the film was then measured by thermal gravimetric analysis (TGA). A 20 ± 2 mg segment of film was removed from the glass slide by razor blade and placed in a platinum TGA pan. Using a TA Instruments Q50, weight loss was measured as the sample was heated from RT to 150 °C at a rate of 10 °C min^{-1}. Water loss was observed as a peak in the mass loss derivative curve that occurred between RT and approximately 100 °C. Water content of each film was then determined by measuring the percent mass loss over the bounds of that peak. After each measurement, the films were resubmerged in fresh DI water. TGA measurements were repeated again 7 and 14 days after initial submersion in water. The reported values are the average water contents and standard deviation of three identically-prepared films at the same submersion time. This technique provided accurate and reproducible measurements that were not influenced by leaching-caused changes in mass as may occur with other techniques [208].

4.4 Results and Discussion

4.4.1 Water-Driven Surface Restructuring

Water-driven restructuring of PEO to the surface of bulk-modified silicone films was characterized with static water contact angle measurements. Significant decreases in contact angle (*i.e.* increasing hydrophilicity) were attributed to increasing PEO chain density at the surface as the migrating hydrophilic polymer enhanced surface wettability. **Figure 4.2** shows the five-minute θ_{static} profiles for water droplets left on each of the silicone films. As expected, the unmodified silicone remained hydrophobic [260] and the

contact angle changed only slightly during the measurement period, indicating minimal surface restructuring. All of the bulk-modified films achieved rapid and substantial water-induced hydrophilicity, but some of the profiles were distinct based on the structure of the SMA. Pronounced differences were observed between SMAs of siloxane length, m = 13. For those SMAs, the diblock structure achieved the greatest hydrophilicity ($\theta_{\text{static, 5min}}$ = 6°) and the speed and extent of PEO migration was reduced when SMAs were crosslinked or changed to a triblock architecture ($\theta_{\text{static, 5min}}$ = 27° & 21°, respectively). Crosslinking essentially anchors the PEO-silane amphiphiles to the silicone network, so it stands to reason that this would reduce its ability to migrate to the surface. However, considering that the triblock-modified silicone contained twice the quantity of PEO and the SMA was uncrosslinked, it was remarkable that the hydrophilicity was reduced compared to the diblock structure. This could be due to the short ODMS which is insufficient for improving the solubility of that amount of PEO within silicone. In agreement, the triblock architecture became more effective when the ODMS length was increased to m = 30 ($\theta_{\text{static, 5min}}$ = 17°). Regardless of crosslinking, the m = 30 diblock SMA structures exhibited restructuring behavior and hydrophilicity that were similar to each other ($\theta_{\text{static, 5min}}$ = 26° [uncrosslinked] & 30° [crosslinked]) and to that of the m = 13 PEO-silane amphiphile. These results indicate that increasing the length of ODMS to m = 30 has a similar effect on restructuring as chemically crosslinking with TEOS. Therefore, at the longer ODMS length (m = 30), TEOS had little effect on restructuring.

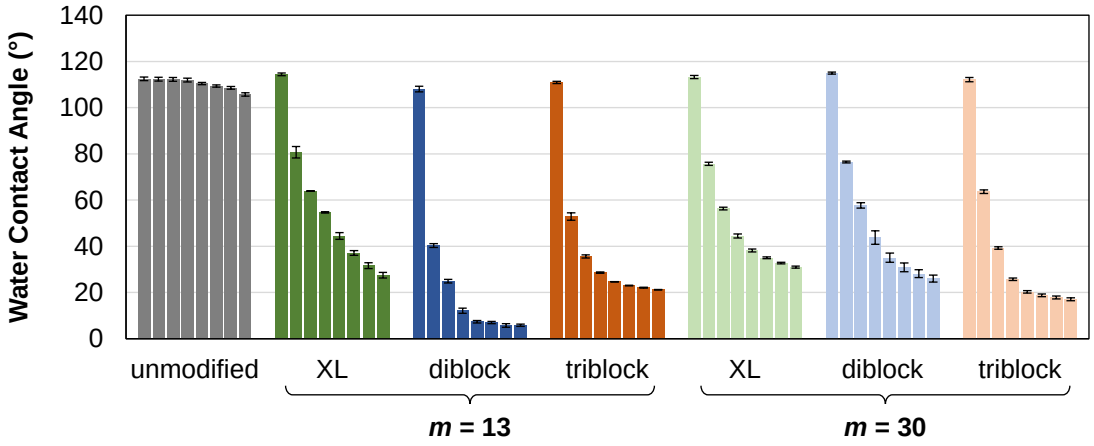

Figure 4.2. θ_{static} measured over a five minute period on bulk-modified silicone films one week after casting. Bars are organized as the time after initial drop placement from left to right as follows: 0 s, 15 s, 30 s, 1 min, 2 min 3 min, 4 min, and 5 min. (XL: 'crosslinked' PEO-silane amphiphile)

Water-driven surface restructuring was also evaluated immediately after inflicting abrasion with a razor. **Figure 4.3** shows the five-minute θ_{static} profiles measured on the freshly exposed surfaces of each film. The film that changed the most after abrasion was the unmodified silicone control which became more hydrophilic ($\Delta\theta_{static,\ 5min} \approx -18°$). All of the bulk-modified silicone films maintained the ability to become hydrophilic and were nearly indistinguishable in restructuring behavior versus their original profiles. The only exception was the m = 30 triblock SMA film which restructured faster and became more hydrophilic ($\Delta\theta_{static,\ 5min} \approx -12°$). This seems to imply that there's a higher concentration of that SMA in the bulk than near the surface which would enhance the apparent water-driven restructuring when the film surface is removed. However, this would not be expected to adversely affect protein resistance.

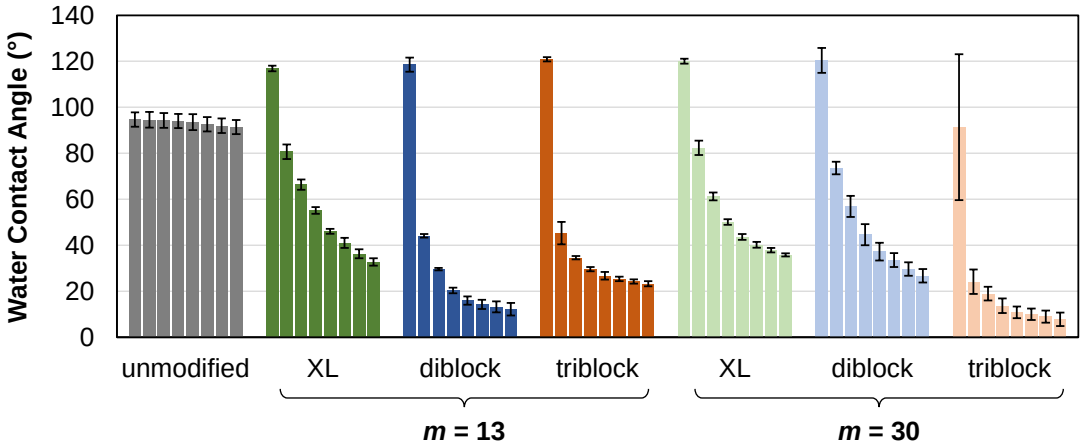

Figure 4.3. θ_{static} measured over a five minute period on freshly exposed surface of bulk-modified silicone films after cutting away top layer with a razor. Bars are organized as the time after initial drop placement from left to right as follows: 0 s, 15 s, 30 s, 1 min, 2 min 3 min, 4 min, and 5 min. (XL: 'crosslinked' PEO-silane amphiphile)

While equilibrating bulk-modified silicone films in water for two weeks, they were periodically removed and quickly dried under a stream of air to make θ_{static} measurements. By the second week, all of the water-soaked films achieved reduced hydrophilicity with contact angles ranging between 35 and 45° (**Figure 4.4**). The $\theta_{static, 5min}$ was at least 15° greater than the initial measurements for all films except that modified with the m = 30 PEO-silane amphiphile ($\Delta\theta_{static, 5min} \approx 8°$). The two SMAs that best improved silicone hydrophilicity initially were most adversely affected by water conditioning: $\theta_{static, 5min}$ for m = 13 diblock and m = 30 triblock amphiphile films increased by approximately 30° and 20° respectively. The apparent loss in SMA restructuring ability was hypothesized to be caused by two factors: (1) leaching of the SMAs under aqueous conditions which would reduce their concentration in the silicone bulk and diminish hydrophilicity accordingly (Chapter III) and (2) water uptake by the

films which would inhibit SMA surface migration by reducing the driving force of PEO for the surface-water interface. Of these two explanations, SMA leaching would be expected to cause a permanent change in restructuring behavior whereas changes caused by water uptake could be reversed by drying the films.

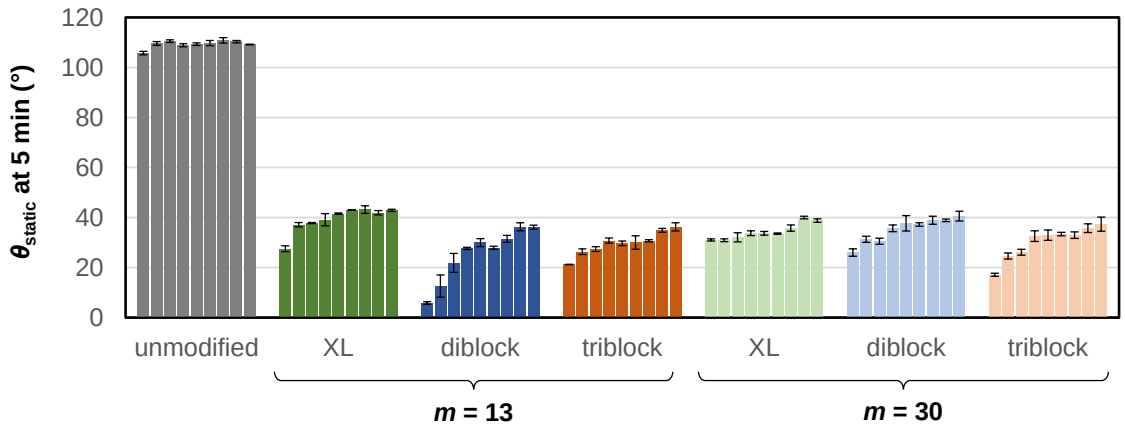

Figure 4.4. θ_{static} measured at "5 min" time point after drop placement on bulk-modified silicone films during two-week water equilibration study. (XL: 'crosslinked' PEO-silane amphiphile)

To determine if the observed hydrophilicity loss was due to water uptake, films were dried under vacuum at 50°C overnight and θ_{static} measurements were made afterwards. Surface restructuring profiles were compared for each film after curing (initial), after two weeks in water (water equilibrated), and after drying (dried) (**Figure 4.5**). It was observed on most of the films that after drying, the water-driven restructuring behavior was very similar to initial measurements. The recovery of hydrophilicity indicated that water uptake was the primary cause of changes that occurred with water conditioning. The only exception was silicone modified with the *m* = 13 diblock amphiphile on which $\theta_{static,\ 5min}$ reached 20° after drying compared to 7°

before water conditioning. This irreversible change in restructuring was considered indicative of substantial SMA leaching compared to the other bulk-modified films. The water-driven restructuring profile of the m = 30 triblock amphiphile film also changed after drying. Similar to the abrasion results, it restructured faster than the original film. These results are not indicative of leaching. It is hypothesized instead that there is a permanently higher concentration of SMA near the surface than before water-equilibration.

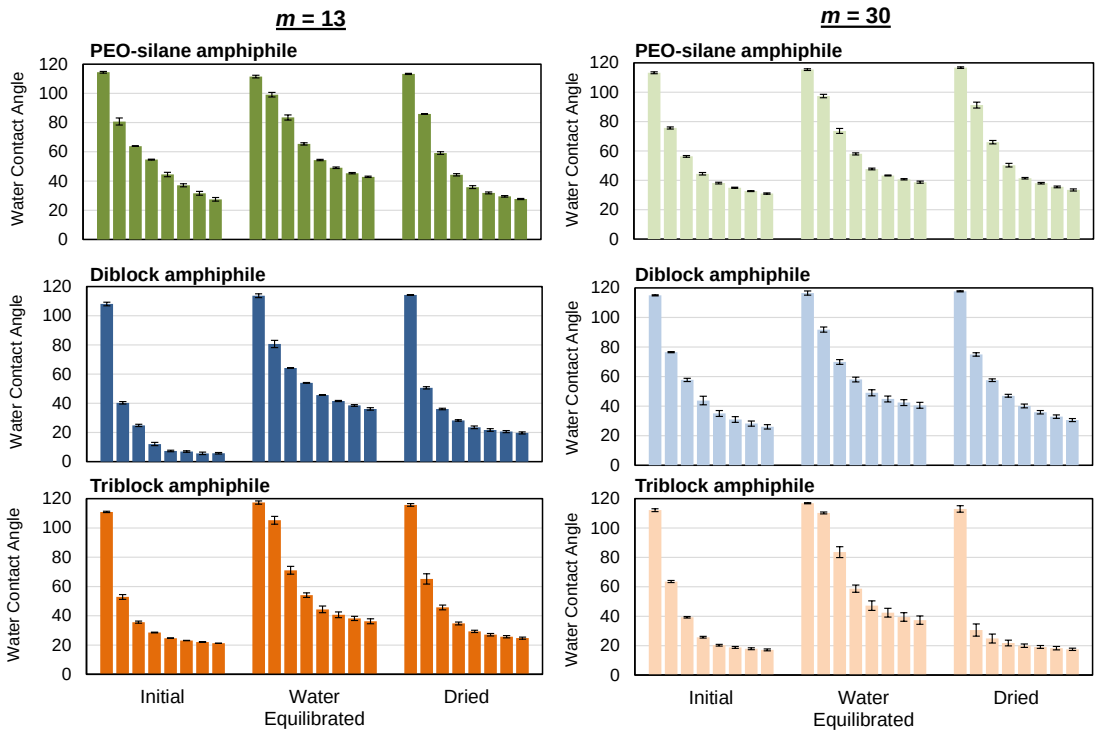

Figure 4.5. θ_{static} measured over a five minute period on bulk-modified silicone films after one week curing in air (Initial), two weeks soaked in water (Water Equilibrated), and drying under vacuum and elevated temperature (Dried). Bars are organized as the time after initial drop placement from left to right as follows: 0 s, 15 s, 30 s, 1 min, 2 min 3 min, 4 min, and 5 min.

4.4.2 Leaching

To detect SMA leaching, bulk-modified silicone films were soaked in DI water and DCM for two weeks and the resulting changes in mass were measured. The percent mass loss of each film is reported in **Figure 4.6** as well as the mass loss ratios of bulk-modified films. It can be seen that the unmodified silicone films did undergo measureable mass loss, even in water. Therefore, for any bulk-modified films that underwent similar mass loss, the corresponding SMA was considered resistant to leaching. The mass loss ratio equation accounts for this by subtracting the measured mass loss of unmodified silicone from the mass loss of each bulk-modified film. The equation then divides by the percent mass of SMA in the given film to account for differing weight concentrations of the various structures. In water, films modified with m = 13 SMAs experienced the most mass loss, greatest of which was the non-crosslinkable diblock structure. It therefore appears that because of the diblock structure, small tether length, and inability to crosslink, that particular SMA is the least stable within silicone under aqueous conditions. These results explain the permanent change in water-driven restructuring behavior observed on silicone modified with the m = 13 diblock SMA. It can be seen by comparing the mass loss ratio values that the m = 30 amphiphiles were the most resistant to leaching in water. As PEO-silane amphiphile synthesis is more complex, the uncrosslinkable m = 30 diblock SMA appears to be the best structure for use in silicone.

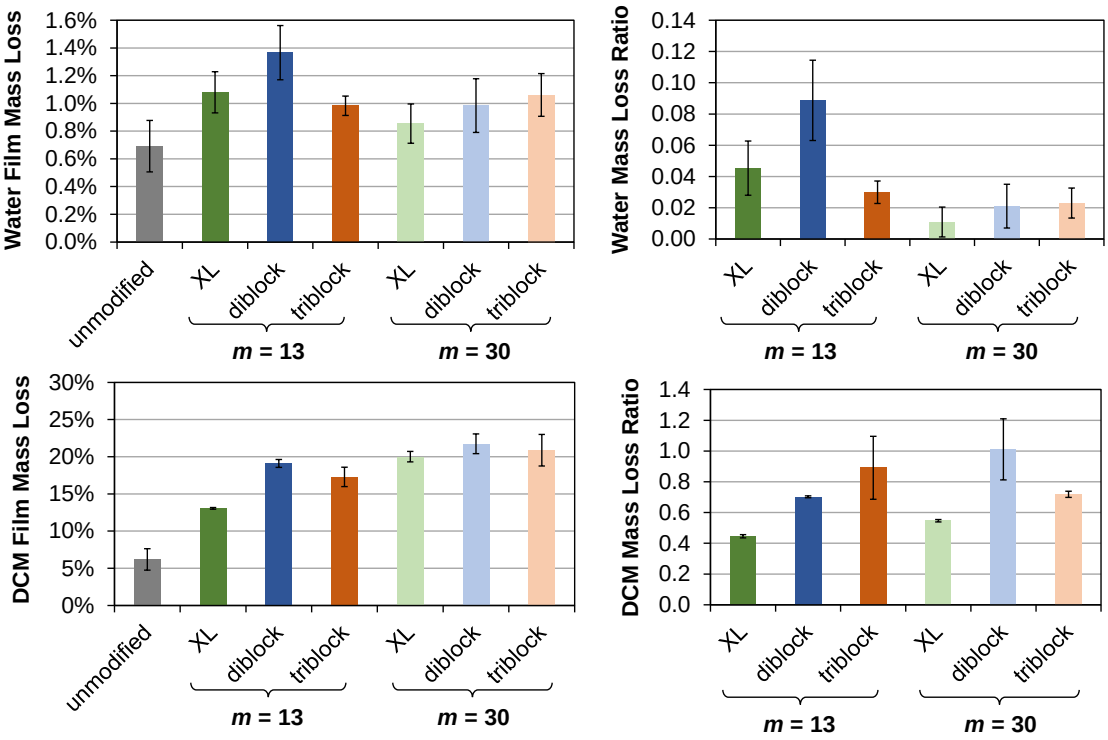

Figure 4.6. Film mass loss (left) and mass loss ratio (right) of bulk-modified silicone films after soaking in water (above) and DCM (below) for two weeks. Each bar represents the average percent mass loss of three identically-prepared films and the error bar is the standard deviation. (XL: 'crosslinked' PEO-silane amphiphile)

Also shown in **Figure 4.6** are the mass loss results for silicone films soaked in DCM. As this is a good solvent for silicone as well as the SMAs, it caused film swelling and extraction of high quantities of uncrosslinked material. The mass losses for all bulk-modified films were significantly greater than that of unmodified silicone. The PEO-silane amphiphiles were found to undergo less mass loss than their respective uncrosslinkable diblock analogues, but still increased the sol content of silicone. Therefore, TEOS may not effectively form covalent bonds with the silicone network to ensure complete crosslinking of PEO-silane amphiphiles. The TEOS could also interfere

with the elastomer crosslinking which would cause mass loss consisting of uncrosslinked silicone.

4.4.3 Water Uptake

The water contents of water-conditioned films were measured by TGA during and after a two-week soaking period (**Figure 4.7**). It can be seen that all of the bulk-modified films absorbed significantly more water than unmodified silicone films within 24 h. It is hypothesized that SMAs within the hydrophobic silicone network undergo phase separation, forming micelle-like structures with a hydrophilic PEO core that can store water [269]. Therefore, it was expected that the quantity of water uptake would be related to the amount of PEO and the ability of the SMAs to form stable hydrophilic domains. After two weeks, all m = 13 SMAs caused relatively large increases to silicone water uptake (>3 wt%). At that tether length, the PEO-silane amphiphile took up the least water, perhaps due to an inability of the immobilized SMA to effectively transport water from the silicone surface to the bulk. Despite a higher PEO content, the m = 13 triblock-modified silicone took up less water than silicone modified with the diblock amphiphile. This is likely due to the higher portion of PEO to ODMS in each chain which could impair micelle formation. Furthermore, this would explain why the triblock amphiphile SMAs caused greater water uptake when the ODMS length was increased to m = 30. The m = 30 PEO-silane and diblock amphiphiles both caused the lowest silicone water uptake (1 wt%). This may be explained by the improved solubility of those SMAs

in silicone due to the longer ODMS tether which would reduce their tendency to phase separate and hydrophilic domains for water storage.

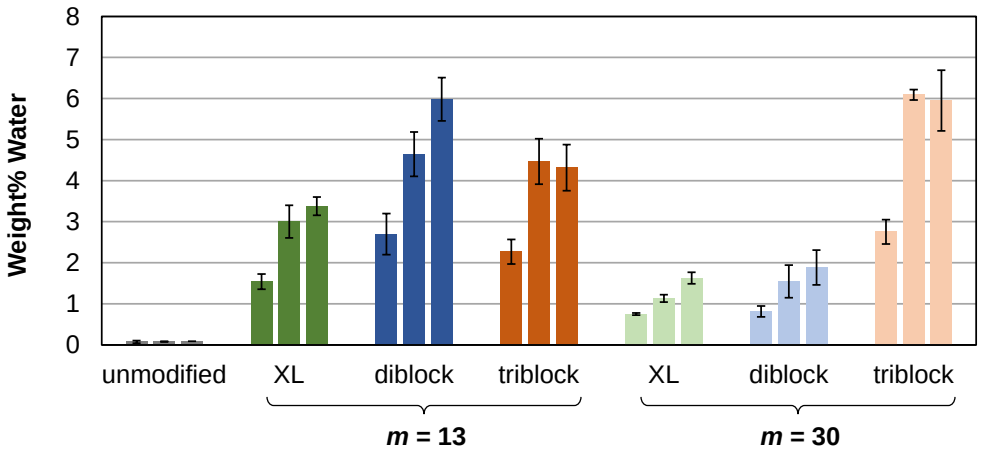

Figure 4.7. Percent water composition by weight of bulk-modified silicone films soaked in water for two weeks. For each film, bars are organized as the time underwater prior to measurement from left to right as follows: 24 h, 1 week, and 2 weeks. (XL: 'crosslinked' PEO-silane amphiphile)

Confirmation of water uptake explains the reversible changes in water-driven surface restructuring that were observed on all bulk-modified silicones during water conditioning. However, there is no apparent correlation between the amount of water uptake and the final water-driven surface restructuring behavior. It is possible that swelling and changing mechanical properties caused by water uptake would be undesirable for medical device materials. Significant swelling of films is likely to exacerbate SMA leaching. Water uptake is also undesirable for any elastomer crosslinked by condensation reactions (*i.e.* MED-1137) which are reversible in the presence of water. Based on these results, the *m* = 30 PEO-silane and diblock amphiphiles would be best suited for medical silicones due to their relatively low water

uptake. If even lower water content is desired, smaller quantities of SMA may be used to reduce water uptake without impairing protein resistance (Chapter III).

4.5 Conclusions

Silicones used for implantable medical devices are often compromised by their poor resistance to protein adsorption which causes thrombus formation and infection. When incorporated into a medical-grade silicone elastomer, PEO-silane amphiphiles act as SMAs that undergo water-driven surface restructuring when the silicone is exposed to aqueous/biological conditions. A particular formulation of PEO-silane amphiphile (m = 13, n = 8) had previously been shown to effectively reduce protein adsorption on silicone [266]. In this work, the same PEO-silane amphiphile was evaluated in terms of its ability to overcome the limitations typically associated with SMAs (*i.e.* leaching and poor abrasion recovery). To reduce leaching, PEO-silane amphiphiles have been synthesized with TEOS which is meant to covalently crosslink with the silicone network. When compared to an analogous diblock amphiphile without TEOS, it was found that the crosslinking group reduced leaching of bulk-modified silicone films. However, it was determined that leaching could be reduced more effectively by increasing the size of ODMS to m = 30, at which length the presence of TEOS became almost inconsequential. Sol content following extraction with DCM was found to increase for silicones prepared with SMAs, even those based on TEOS crosslinkable groups. Furthermore, the TEOS did not appear to significantly affect water uptake with m = 30 amphiphiles. Analogous triblock amphiphiles (m = 13 & 30), representative of traditional SMAs, were prepared

and similarly evaluated for comparison. They underwent similar restructuring to the diblock structures and best-resisted leaching at the longer ODMS length, but were more prone to water uptake. For all of the tested SMAs, bulk-modified silicone films exhibited little to no change in their water-driven surface restructuring behavior following surface abrasion. In conclusion, the m = 30 PEO-silane and diblock amphiphiles are similarly well-suited as silicone SMAs. Presumably, because the diblock amphiphile is significantly simpler to synthesize, it would be preferable in future work. As crosslinking does not appear to be necessary, non-crosslinkable diblock SMAs may also be suitable for any medical-grade silicone elastomer, regardless of curing chemistry.

CHAPTER V

CONCLUSIONS

5.1 Conclusions

Surface-induced thrombosis is a major limitation of silicone usage in blood-contacting medical devices. Due to its hydrophobic nature, silicone adsorbs high levels of plasma proteins which subsequently initiate thrombus formation. Antithrombotic drugs are commonly used to address this, but they are associated with bleeding complications, comorbidities, and limited efficacy. Representing a safer alternative is modification of silicone with poly(ethylene oxide) (PEO), which prevents thrombosis by effectively inhibiting protein adsorption. This hydrophilic polymer is highly effective when present at the material-biological interface at sufficient concentrations. Unfortunately, efforts to render polymeric materials thromboresistant with PEO have been met with disappointing and inconsistent results [169-171]. It is hypothesized that conventional PEO-silanes, when used as bulk-modifying additives (SMAs) for silicone, are unable to undergo efficient water-driven migration to the surface-biological interface which results in poor protein resistance.

In this work, PEO-silane amphiphiles ($\alpha(EtO)_3Si$-$(CH_2)_2$-oligodimethyl-siloxane$_{13}$-*block*-poly(ethylene oxide)$_n$-OCH_3) (n = 3, 8, and 16) were prepared as SMAs to effectively improve PEO-enrichment at the surface-water interface, and hence protein resistance, of silicone. The hydrophobic, flexible oligodimethylsiloxane (ODMS) tether served to enhance the solubility and mobility of PEO within the silicone network while

the triethoxysilane (TEOS) group formed chemical crosslinks with the network to reduce leaching.

In Chapter II, PEO-silane amphiphiles with three different PEO-segment lengths (n = 3, 8, and 16) were evaluated and compared to analogous PEO-silanes having no ODMS tether (*i.e.* PEO-controls). When grafted onto a model substrate absent of surface restructuring effects, the inherent protein resistance of PEO-silane amphiphiles was reduced versus the PEO-controls. It was confirmed with water contact angle analysis that the siloxane tether increased the relative hydrophobicity of the grafted PEO-silane amphiphiles which explained the increase in protein adsorption. When incorporated into a medical-grade silicone, the PEO-silane amphiphiles exhibited rapid, water-driven surface migration but the PEO-controls did not. PEO-silane amphiphiles n = 8 and 16 produced the greatest enhancement in water-induced surface hydrophilicity and protein resistance. Thus, these results demonstrated that the efficacy of PEO-silanes as SMAs for silicones could be dramatically improved via incorporation of an ODMS tether and tailoring the PEO-segment length. Furthermore, they revealed potential limitations with using model substrates to evaluate the protein resistance of PEO-silanes intended for polymeric materials.

The main purpose of Chapter III was to determine the efficacy of PEO-silane amphiphiles (n = 3, 8, and 16), in terms of the minimum required molar concentration in silicone, to form a PEO-enriched surface and resist protein adsorption. The significance of PEO-segment length was also examined. Each PEO-silane amphiphile was blended into silicone at five different molar concentrations (5, 10, 25, 50, and 100 μmol per 1 g

silicone). For each PEO-segment length, the extent of water-driven restructuring and resulting hydrophilicity increased with increasing molar concentrations. For n = 3, restructuring occurred quickly, but produced a relatively small change in silicone hydrophilicity due to its short PEO length. In contrast, n = 8 and n = 16 both led to rapid, water-driven surface restructuring but n = 8 did so more efficiently, requiring only 10 µmol (1.68 wt%) versus 25 µmol (4.90 wt%). Protein adsorption results correlated well with water-driven surface restructuring in that only n = 8 and 16 (at the minimum molar concentrations) were able to significantly reduce protein adsorption. When compared on the basis of "wt% PEO," it was determined that PEO length did influence surface restructuring and protein resistance and that n = 8 was the most effective. The efficacy of n = 8 to induce water-driven surface migration of PEO and subsequent protein resistance may be attributed to the balance of steric effects and solubility in the silicone matrix. It was therefore concluded that the PEO-segment length of n = 8 was optimal for PEO-silane amphiphiles (m = 13) as a silicone SMAs.

In Chapter 4, the efficacy of PEO-silane amphiphiles were evaluated in terms of their ability to minimize leaching from the silicone and maintain surface hydrophilicity after abrasion or extended exposure to water. Specifically, a diblock versus triblock architecture was examined as well as the presence or absence of a crosslinkable silane end group. While few are reported specifically for silicones, conventional SMAs possess a triblock architecture, lack crosslinkability, and are higher in molecular weight. Analogous to PEO-silane amphiphiles, diblock amphiphiles were prepared without TEOS (PEO_n-$ODMS_m$) to determine the efficacy of the crosslinker in preventing

leaching. Both the PEO-silane and diblock amphiphiles were prepared with a single PEO length (n = 8) and two ODMS tether lengths (m = 13 and 30). It was hypothesized that the longer tether could prevent leaching by simultaneously decreasing the amphiphile's solubility in water and increasing its affinity for the base polymer. Analogous triblock amphiphiles (PEO_8-$ODMS_m$-PEO_8) were also prepared which were representative of conventional SMAs for comparison. All amphiphiles were incorporated into the condensation-cure silicone elastomer at the same molar concentration (50 μmol per 1 g silicone) and were found to undergo excellent water-driven surface restructuring. This restructuring was not reduced with surface abrasion for any samples. Of all the SMAs tested, the m = 30 PEO-silane and diblock amphiphiles were the most resistant to leaching in water over a two-week period. This indicated that the m = 30, n = 8 PEO-silane and diblock amphiphiles were most ideal as silicone SMAs because they addressed both of the SMA-associated limitations (*i.e.* abrasion recovery and leaching). It was also determined that PEO-silane amphiphiles were not well-crosslinked to the silicone elastomer. Therefore, TEOS does not appear to be effective nor necessary as a crosslinking group for preventing aqueous leaching of PEO-silane amphiphiles, provided the ODMS segment is sufficiently long. In conclusion, the diblock amphiphile would be preferable for future work as it performs similarly to the PEO-silane amphiphile as a SMA, but is considerably easier to synthesize.

5.2 Future Directions

The curing mechanism of the silicone elastomer tested in this work was based on condensation chemistry; however, other chemistries are also used to crosslink room-temperature-vulcanizing (RTV) silicones. Common strategies for silicone curing employ addition (hydrosilylation, Pt-cure) and free-radical ([meth]acrylate polymerization, UV-cure) chemistries. Therefore, the finding that chemical crosslinking may not be necessary to prevent SMA leaching has important implications. The diblock amphiphile (m = 30, n = 8) that restructured effectively could potentially be incorporated into any silicone elastomer, regardless of curing chemistry, without concern for leaching. Without a crosslinking group, the amphiphile synthesis is simplified considerably as a second hydrosilylation reaction is not required. In future studies, the same PEO-silane and diblock amphiphiles tested in Chapter IV will be evaluated in Pt- and UV-cure silicone elastomers (**Figure 5.1**). The effects of crosslinking will again be examined. The diblock amphiphile is expected to covalently crosslink into Pt-cure silicone by nature of the hydrosilane-terminated ODMS tether. For that elastomer, PEO-silane amphiphiles can serve as the uncrosslinkable diblock amphiphile control. To crosslink with UV-cure silicones, an analogous methacrylate-functionalized diblock amphiphile has been prepared (see Appendix). It is possible that the lengths of the PEO and ODMS segments that were found to be optimal in this work may not be so within different silicone elastomers due to differences beyond curing chemistry (*e.g.* crosslinking density and filler content). Fortunately, this work lays out a basis for methodologies to optimize SMA concentration and formulation and can be reemployed in future studies if

necessary. In future work, it will also be important to confirm that each of the modified silicones is specifically resistant to thrombus formation with whole blood studies.

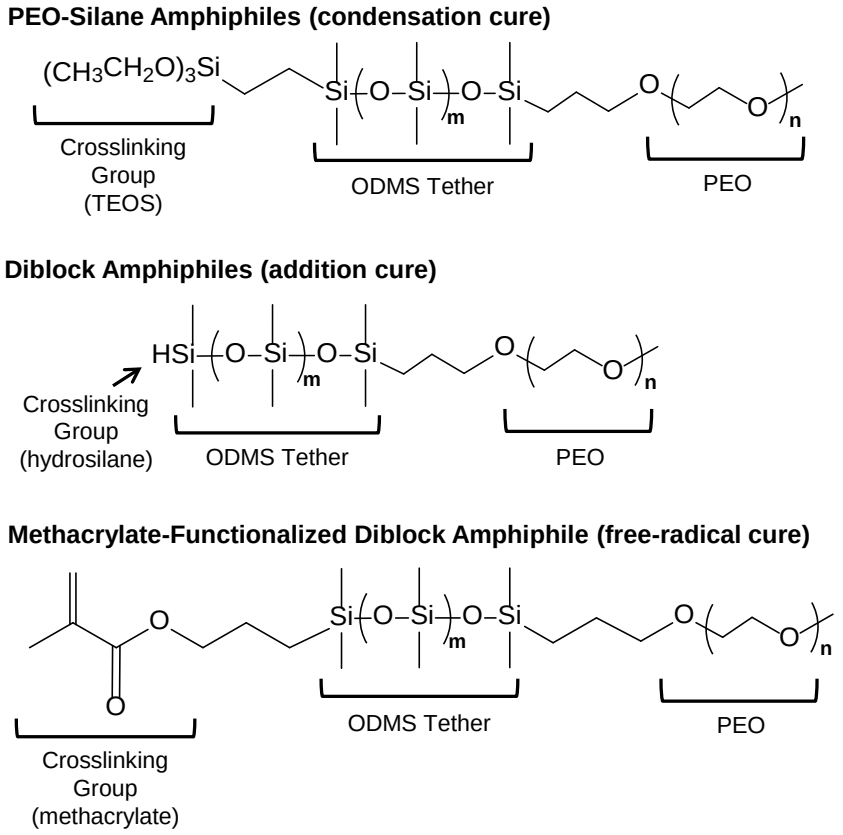

Figure 5.1. Derivatives of PEO-silane amphiphiles for crosslinking into silicone elastomers with different curing chemistries.

The main objective of this dissertation has been to develop a silicone elastomer for implantable medical devices that resists protein adsorption and subsequent thrombotic complications. However, there are other applications for which fouling-resistant silicones are desirable, particularly in the maritime industry. On ship hulls and other marine structures, the adhesion of marine organisms such as diatom slimes, algae, and barnacles (*i.e.* biofilms) is considered problematic. Biofilm formation creates

hydrodynamic drag as vessels move through water which increases fuel consumption rates [270]. The increased fuel consumption, as well as hull cleaning and repainting, represent significant financial burdens [270]. Silicone elastomers are commonly applied to hulls as foul-release (FR) coatings [227]. These coatings weaken the adhesion strength of biofouling organisms which facilitates their removal [227, 271, 272], but silicone's hydrophobicity increases the amount of fouling that occurs [229]. Modification with PEO could therefore improve the performance of marine silicones by enhancing surface wettability. In recent work by Hawkins and coworkers [247], silicone modified with the m = 13 and n = 8 PEO-silane amphiphile was found to resist marine bacterial and diatom biofilm formation. Additionally, the modified silicone was coated onto fiberglass panels and left in the Atlantic Ocean for 6 weeks and effectively prevented slime formation. These early results are promising and the use of PEO-silane amphiphiles in marine silicone coatings will continue to be explored.

With a methacrylate crosslinking group (**Figure 5.1**), these SMAs could also be incorporated into UV-cure hydrogel materials for a variety of potential benefits, including protein resistance. Tear protein accumulation is considered a major reason for soft contact lens discontinuation as it causes discomfort and reduced visual acuity [273-280]. Protein deposits additionally provide sites for bacterial attachment [281, 282] and are believed to cause giant papillary conjunctivitis [283, 284]. There is also a demand for contact lenses with enhanced oxygen permeability which can be accomplished by incorporation of silicone [285]. Unfortunately, it is difficult to incorporate silicone into hydrogels without increasing protein adsorption due to its hydrophobicity [285, 286]. As

the diblock amphiphiles contain silicone (ODMS) complexed with PEO, it may possible to incorporate them into contact lens hydrogels to simultaneously enhance both protein resistance and oxygen permeability. Furthermore, the presence of the free-end chains throughout the hydrogel bulk would resemble a loosely crosslinked second network and may therefore impart similar benefits to the bulk mechanical properties [287]. For this work, model contact lens hydrogel materials will be prepared with and without methacrylate-functionalized diblock amphiphiles and evaluated for protein resistance, oxygen permeability, and mechanical strength.

REFERENCES

1. Ratner, B.D., *Surface Properties and Surface Characterization of Materials*, in *Biomaterials Science: An Introduction to Materials in Medicine*, B.D. Ratner, et al., Editors. 2004, Elsevier Academic Press: New York. p. 40-59.

2. Horbett, T.A., *The Role of Adsorbed Proteins in Tissue Response to Biomaterials*, in *Biomaterials Science: An Introduction to Materials in Medicine*, B.D. Ratner, et al., Editors. 2004, Elsevier Academic Press: New York. p. 237-246.

3. Gordon, M. and P.G. Bullough, *Synovial and osseous inflammation in failed silicone-rubber prostheses.* J Bone Joint Surg Am, 1982. **64**(4): p. 574-580.

4. Chenoweth, D.E., *Complement activation in extracorporeal circuits.* Ann NY Acad Sci, 1987. **516**(1): p. 306-313.

5. Tang, L. and J.W. Eaton, *Inflammatory responses to biomaterials.* Am J Clin Pathol, 1995. **103**(4): p. 466-471.

6. Andersson, J., et al., *C3 adsorbed to a polymer surface can form an initiating alternative pathway convertase.* J Immunol, 2002. **168**(11): p. 5786-5791.

7. Henson, P.M., *The immunologic release of constituents from neutrophil leukocytes: I. The role of antibody and complement on nonphagocytosable surfaces or phagocytosable particles.* J Immunol, 1971. **107**(6): p. 1535-1546.

8. Henson, P.M., *The immunologic release of constituents from neutrophil leukocytes: II. Mechanisms of release during phagocytosis, and adherence to nonphagocytosable surfaces.* J Immunol, 1971. **107**(6): p. 1547-1557.

9. Pfeiffer, E.F., *The glucose sensor: The missing link in diabetes therapy.* Horm Metab Res Supp Ser, 1990. **24**(154).

10. Anderson, J.M., *Inflammation, Wound Healing, and the Foreign-Body Response*, in *Biomaterials Science: An Introduction to Materials in Medicine*, B.D. Ratner, et al., Editors. 2004, Elsevier Academic Press: New York. p. 296-304.

11. Anderson, J.M., A. Rodriguez, and D.T. Chang, *Foreign body reaction to biomaterials.* Semin Immunol, 2008. **20**(2): p. 86-100.

12. Hanson, S.R., *Blood-Coagulation and Blood-Materials Interactions*, in *Biomaterials Science: An Introduction to Materials in Medicine*, B.D. Ratner, et al., Editors. 2004, Elsevier Academic Press: New York. p. 332-338.

13. Anderson, J.M., *Biological responses to materials.* Ann Rev Mater Res, 2001. **31**: p. 81-110.

14. Pitt, W.G., K. Park, and S.L. Cooper, *Sequential protein adsorption and thrombus deposition on polymeric biomaterials.* J Colloid Interf Sci, 1986. **111**(2): p. 343-362.

15. Tang, L. and J.W. Eaton, *Fibrin(ogen) mediates acute inflammatory responses to biomaterials.* J Exp Med, 1993. **178**(6): p. 2147-2156.

16. Tsai, W.-B., J.M. Grunkemeier, and T.A. Horbett, *Human plasma fibrinogen adsorption and platelet adhesion to polystyrene.* J Biomed Mater Res, 1999. **44**(2): p. 130-139.

17. Wu, Y., et al., *The role of adsorbed fibrinogen in platelet adhesion to polyurethane surfaces: A comparison of surface hydrophobicity, protein adsorption, monoclonal antibody binding, and platelet adhesion.* J Biomed Mater Res A, 2005. **74A**(4): p. 722-738.

18. Wei, Q., et al., *Protein interactions with polymer coatings and biomaterials.* Angew Chem Int Ed, 2014. **53**(31): p. 8004-8031.

19. Hu, W.-J., et al., *Molecular basis of biomaterial-mediated foreign body reactions.* Blood, 2001. **98**(4): p. 1231-1238.

20. Gorbet, M.B. and M.V. Sefton, *Biomaterial-associated thrombosis: roles of coagulation factors, complement, platelets and leukocytes.* Biomaterials, 2004. **25**(26): p. 5681-5703.

21. Evans-Nguyen, K.M., et al., *Changes in adsorbed fibrinogen upon conversion to fibrin.* Langmuir, 2006. **22**(11): p. 5115-5121.

22. Lu, D.R. and K. Park, *Effect of surface hydrophobicity on the conformational changes of adsorbed fibrinogen.* J Colloid Interf Sci, 1991. **144**(1): p. 271-281.

23. Vroman, L. and A.L. Adams, *Findings with the recording ellipsometer suggesting rapid exchange of specific plasma proteins at liquid/solid interfaces.* Surf Sci, 1969. **16**: p. 438-446.

24. Lassen, B. and M. Malmsten, *Competitive protein adsorption at plasma polymer surfaces.* J Colloid Interf Sci, 1997. **186**(1): p. 9-16.

25. Hanson, S.R. and B.D. Ratner, *Evaluation of Blood-Materials Interactions*, in *Biomaterials Science: An Introduction to Materials in Medicine*, B.D. Ratner, et al., Editors. 2004, Elsevier Academic Press: New York. p. 367-379.

26. Lloyd, D.A., et al., *Does the fibrin coat around a central venous catheter influence catheter-related sepsis?* J Pediatr Surg, 1993. **28**(3): p. 345-349.

27. Raad, I.I., et al., *The relationship between the thrombotic and infectious complications of central venous catheters.* JAMA, 1994. **271**(13): p. 1014-1016.

28. Fux, C.A., et al., *Dynamics of hemodialysis catheter colonization by coagulase-negative staphylococci.* Infect Cont Hosp Ep, 2005. **26**(06): p. 567-574.

29. Kumar, V., et al., *Preventing Biofilm Formation on Biomedical Surfaces*, in *Plasma Technology for Hyperfunctional Surfaces: Food, Biomedical, and Textile Applications*, H. Rauscher, M. Perucca, and G. Buyle, Editors. 2010, Wiley-VCH Verlag GmbH & Co. KGaA: Weinheim. p. 183-223.

30. Schömig, A., et al., *A randomized comparison of antiplatelet and anticoagulant therapy after the placement of coronary-artery stents.* New Engl J Med, 1996. **334**(17): p. 1084-1089.

31. Bertrand, M.E., et al., *Randomized multicenter comparison of conventional anticoagulation versus antiplatelet therapy in unplanned and elective coronary stenting : The full anticoagulation versus aspirin and ticlopidine (FANTASTIC) study.* Circulation, 1998. **98**(16): p. 1597-1603.

32. Leon, M.B., et al., *A clinical trial comparing three antithrombotic-drug regimens after coronary-artery stenting.* New Engl J Med, 1998. **339**(23): p. 1665-1671.

33. Stein, P.D., et al., *Antithrombotic therapy in patients with mechanical and biological prosthetic heart valves.* Chest, 2001. **119**(1 suppl): p. 220S-227S.

34. Zellweger, M., et al., *Systemic anticoagulation and prevention of hemodialysis catheter malfunction.* ASAIO J, 2005. **51**(4): p. 360-365.

35. Colì, L., et al., *Anticoagulation therapy for the prevention of hemodialysis tunneled cuffed catheters (TCC) thrombosis.* J Vasc Access, 2006. **7**(3): p. 118-122.

36. Willms, L. and L.M. Vercaigne, *Does warfarin safely prevent clotting of hemodialysis catheters?* Semin Dial, 2008. **21**(1): p. 71-77.

37. Levine, M.N., et al., *Hemorrhagic complications of anticoagulant treatment.* Chest, 2004. **126**(3 suppl): p. 287S-310S.

38. Rogacka, R., et al., *Dual antiplatelet therapy after percutaneous coronary intervention with stent implantation in patients taking chronic oral anticoagulation.* J Am Coll Cardiol Intv, 2008. **1**(1): p. 56-61.

39. Guerrouij, M., et al., *The clinical impact of bleeding during oral anticoagulant therapy.* J Thromb Thrombolys, 2011. **31**(4): p. 419-423.

40. Stulak, J.M., et al., *Gastrointestinal bleeding and subsequent risk of thromboembolic events during support with a left ventricular assist device.* J Heart Lung Transpl, 2014. **33**(1): p. 60-64.

41. Palareti, G., et al., *Bleeding complications of oral anticoagulant treatment: an inception-cohort, prospective collaborative study (ISCOAT).* Lancet, 1996. **348**(9025): p. 423-428.

42. Torn, M., et al., *Risks of oral anticoagulant therapy with increasing age.* Arch Intern Med, 2005. **165**(13): p. 1527-1532.

43. Warkentin, T.E., *Heparin-Induced Thrombocytopenia*, in *Critical Decisions in Thrombosis and Hemostasis*, J. Ginsberg, C. Kearon, and J. Hirsh, Editors. 1998, B.C. Decker Inc.: Hamilton, Ontario. p. 100-108.

44. Foley, R.N., P.S. Parfrey, and M.J. Samak, *Clinical epidemiology of cardiovascular disease in chronic renal disease.* Am J Kidney Dis, 1998. **32**(5): p. S112-S119.

45. Dua, A., et al., *The impact of warfarin on patients with end stage renal disease.* Adv Vasc Med, 2014. **2014**: p. 4.

46. Moe, S.M. and N.X. Chen, *Pathophysiology of vascular calcification in chronic kidney disease.* Circ Res, 2004. **95**(6): p. 560-567.

47. Danziger, J., *Vitamin K-dependent proteins, warfarin, and vascular calcification.* Clin J Am Soc Nephrol, 2008. **3**(5): p. 1504-1510.

48. Popov, A.F., et al., *Clinical experience with HeartWare left ventricular assist device in patients with end-stage heart failure.* Ann Thorac Surg, 2012. **93**(3): p. 810-815.

49. Park, S.J., et al., *Outcomes in advanced heart failure patients with left ventricular assist devices for destination therapy.* Circ Heart Fail, 2012. **5**(2): p. 241-248.

50. Kirklin, J.K., et al., *Interagency Registry for Mechanically Assisted Circulatory Support (INTERMACS) analysis of pump thrombosis in the HeartMate II left ventricular assist device.* J Heart Lung Transpl, 2014. **33**(1): p. 12-22.

51. Palmerini, T., et al., *Stent thrombosis with drug-eluting and bare-metal stents: evidence from a comprehensive network meta-analysis.* Lancet, 2012. **379**(9824): p. 1393-1402.

52. Mauri, L., et al., *Stent thrombosis in randomized clinical trials of drug-eluting stents.* New Engl J Med, 2007. **356**(10): p. 1020-1029.

53. Armstrong, E.J., et al., *Clinical presentation, management, and outcomes of angiographically documented early, late, and very late stent thrombosis.* JACC Cardiovasc Interv, 2012. **5**(2): p. 131-140.

54. Sarno, G., et al., *Lower risk of stent thrombosis and restenosis with unrestricted use of 'new-generation' drug-eluting stents: A report from the nationwide Swedish Coronary Angiography and Angioplasty Registry (SCAAR).* Eur Heart J, 2012. **33**(5): p. 606-613.

55. Urban, P., et al., *Stent thrombosis and bleeding complications after implantation of sirolimus-eluting coronary stents in an unselected worldwide population: A report from the e-SELECT (Multi-Center Post-Market Surveillance) registry.* J Am Coll Cardiol, 2011. **57**(13): p. 1445-1454.

56. Joner, M., et al., *Pathology of drug-eluting stents in humans: Delayed healing and late thrombotic risk.* J Am Coll Cardiol, 2006. **48**(1): p. 193-202.

57. Bavry, A.A., et al., *Late thrombosis of drug-eluting stents: A meta-analysis of randomized clinical trials.* Am J Med, 2006. **119**(12): p. 1056-1061.

58. Cook, S., et al., *Incomplete stent apposition and very late stent thrombosis after drug-eluting stent implantation.* Circulation, 2007. **115**(18): p. 2426-2434.

59. Daemen, J., et al., *Early and late coronary stent thrombosis of sirolimus-eluting and paclitaxel-eluting stents in routine clinical practice: data from a large two-institutional cohort study.* Lancet, 2007. **369**(9562): p. 667-678.

60. Nakazawa, G., et al., *Delayed arterial healing and increased late stent thrombosis at culprit sites after drug-eluting stent placement for acute myocardial infarction patients: An autopsy study.* Circulation, 2008. **118**(11): p. 1138-1145.

61. Cook, S., et al., *Correlation of intravascular ultrasound findings with histopathological analysis of thrombus aspirates in patients with very late drug-eluting stent thrombosis.* Circulation, 2009. **120**(5): p. 391-399.

62. Hassan, A.K.M., et al., *Late stent malapposition risk is higher after drug-eluting stent compared with bare-metal stent implantation and associates with late stent thrombosis.* Eur Heart J, 2010. **31**(10): p. 1172-1180.

63. Iakovou, I., et al., *Incidence, predictors, and outcome of thrombosis after successful implantation of drug-eluting stents.* JAMA, 2005. **293**(17): p. 2126-2130.

64. Kuchulakanti, P.K., et al., *Correlates and long-term outcomes of angiographically proven stent thrombosis with sirolimus- and paclitaxel-eluting stents.* Circulation, 2006. **113**(8): p. 1108-1113.

65. Finn, A.V., et al., *Pathological correlates of late drug-eluting stent thrombosis: Strut coverage as a marker of endothelialization.* Circulation, 2007. **115**(18): p. 2435-2441.

66. van Werkum, J.W., et al., *Long-term clinical outcome after a first angiographically confirmed coronary stent thrombosis: An analysis of 431 cases.* Circulation, 2009. **119**(6): p. 828-834.

67. Kimura, T., et al., *Comparisons of baseline demographics, clinical presentation, and long-term outcome among patients with early, late, and very late stent thrombosis of sirolimus-eluting stents: Observations from the Registry of Stent Thrombosis for Review and Reevaluation (RESTART).* Circulation, 2010. **122**(1): p. 52-61.

68. Palmerini, T., et al., *Predictors and implications of stent thrombosis in non–ST-segment elevation acute coronary syndromes: The ACUITY trial.* Circ Cardiovasc Interv, 2011. **4**(6): p. 577-584.

69. Räber, L., et al., *Very late coronary stent thrombosis of a newer-generation everolimus-eluting stent compared with early-generation drug-eluting stents: A prospective cohort study.* Circulation, 2012. **125**(9): p. 1110-1121.

70. *2014 USRDS annual data report: An overview of the epidemiology of kidney disease in the United States*. 2014, National Institutes of Health, National Institute of Diabetes and Digestive and Kidney Diseases: Bethesda, MD.

71. Geerts, W., *Central venous catheter–related thrombosis.* ASH Education Program Book, 2014. **2014**(1): p. 306-311.

72. McGee, D.C. and M.K. Gould, *Preventing complications of central venous catheterization.* New Engl J Med, 2003. **348**(12): p. 1123-1133.

73. Ethier, J., et al., *Vascular access use and outcomes: an international perspective from the dialysis outcomes and practice patterns study.* Nephrol Dial Transplant, 2008. **23**(10): p. 3219-3226.

74. Besarab, A. and R. Pandey, *Catheter management in hemodialysis patients: Delivering adequate flow.* Clin J Am Soc Nephrol, 2011. **6**(1): p. 227-234.

75. Napalkov, P., et al., *Incidence of catheter-related complications in patients with central venous or hemodialysis catheters: a health care claims database analysis.* BMC Cardiovasc Disord, 2013. **13**(1): p. 86.

76. Whitman, E.D., *Complications associated with the use of central venous access devices.* Curr Prob Surg, 1996. **33**(4): p. 309-378.

77. *National Kidney Foundation. KDOQI Clinical practice guidelines and clinical practice recommendations for 2006 updates: Hemodialysis adequacy, peritoneal dialysis adequacy and vascular access.* Am J Kidney Dis, 2006. **48**(Suppl. 1): p. S1-S322.

78. Sehgal, A.R., A. Dor, and A.C. Tsai, *Morbidity and cost implications of inadequate hemodialysis.* Am J Kidney Dis, 2001. **37**(6): p. 1223-1231.

79. Diebold, J. and U. Löhrs, *Venous thrombosis and pulmonary embolism: A study of 5039 autopsies.* Pathol Res Pract, 1991. **187**(2–3): p. 260-266.

80. Willicombe, M.K., K. Vernon, and A. Davenport, *Embolic complications from central venous hemodialysis catheters used with hypertonic citrate locking solution.* Am J Kidney Dis, 2010. **55**(2): p. 348-351.

81. Sarnak, M.J. and B.L. Jaber, *Mortality caused by sepsis in patients with end-stage renal disease compared with the general population.* Kidney Int, 2000. **58**(4): p. 1758-1764.

82. Peters, W.R., et al., *The development of fibrin sheath on indwelling venous catheters.* Surg Gynecol Obstet, 1973. **137**(1): p. 43-7.

83. Forauer, A.R., C.G.A. Theoharis, and N.L. Dasika, *Jugular vein catheter placement: Histologic features and development of catheter-related (fibrin) sheaths in a swine model.* Radiology, 2006. **240**(2): p. 427-434.

84. Xiang, D.Z., et al., *Composition and formation of the sleeve enveloping a central venous catheter.* J Vasc Surg, 1998. **28**(2): p. 260-271.

85. Nifong, T.P. and T.J. McDevitt, *THe effect of catheter to vein ratio on blood flow rates in a simulated model of peripherally inserted central venous catheters.* Chest, 2011. **140**(1): p. 48-53.

86. Heaton, D.C., D.Y. Han, and A. Inder, *Minidose (1 mg) warfarin as prophylaxis for central vein catheter thrombosis.* Internal Med J, 2002. **32**(3): p. 84-88.

87. Couban, S., et al., *Randomized placebo-controlled study of low-dose warfarin for the prevention of central venous catheter–associated thrombosis in patients with cancer.* J Clin Oncol, 2005. **23**(18): p. 4063-4069.

88. Young, A.M., et al., *Warfarin thromboprophylaxis in cancer patients with central venous catheters (WARP): An open-label randomised trial.* Lancet. **373**(9663): p. 567-574.

89. Lamontagne, F., et al., *Nonleg venous thrombosis in critically ill adults: A nested prospective cohort study.* JAMA Intern Med, 2014. **174**(5): p. 689-696.

90. Thomas, C.M., et al., *Concentration of heparin-locking solution and risk of central venous hemodialysis catheter malfunction.* ASAIO J, 2007. **53**(4): p. 485-488.

91. Brzosko, S., et al., *Femoral localization and higher ultrafiltration rate but not concentration of heparin used for canal locking of hemodialysis catheter are negative predictors for its malfunction.* Am J Nephrol, 2008. **28**: p. 298-303.

92. Moran, J., et al., *A randomized trial comparing gentamicin/citrate and heparin locks for central venous catheters in maintenance hemodialysis patients.* Am J Kidney Dis, 2012. **59**(1): p. 102-107.

93. Vorweg, M., et al., *The 'heparin lock': Cause for iatrogenic coagulopathy.* Eur J Anaesthesiol, 2006. **23**(1): p. 50-53.

94. Sungur, M., et al., *Exit of catheter lock solutions from double lumen acute haemodialysis catheters: An in vitro study.* Nephrol Dial Transplant, 2007. **22**(12): p. 3533-3537.

95. Pepper, R.J., et al., *Inadvertent postdialysis anticoagulation due to heparin line locks.* Hemodial Int, 2007. **11**(4): p. 430-434.

96. Karaaslan, H., et al., *Risk of heparin lock-related bleeding when using indwelling venous catheter in haemodialysis.* Nephrol Dial Transplant, 2001. **16**(10): p. 2072-2074.

97. Moritz, M.L., A. Vats, and D. Ellis, *Systemic anticoagulation and bleeding in children with hemodialysis catheters.* Pediatr Nephrol, 2003. **18**(1): p. 68-70.

98. Yevzlin, A.S., et al., *Concentrated heparin lock is associated with major bleeding complications after tunneled hemodialysis catheter placement.* Semin Dial, 2007. **20**(4): p. 351-354.

99. Weijmer, M.C., et al., *Randomized, clinical trial comparison of trisodium citrate 30% and heparin as catheter-locking solution in hemodialysis patients.* J Am Soc Nephrol, 2005. **16**(9): p. 2769-2777.

100. Hendrickx, L., et al., *A comparative prospective study on the use of low concentrate citrate lock versus heparin lock in permanent dialysis catheters.* Int J Artif Organs, 2001. **24**(4): p. 208-211.

101. Power, A., et al., *Sodium citrate versus heparin catheter locks for cuffed central venous catheters: A single-center randomized controlled trial.* Am J Kidney Dis, 2009. **53**(6): p. 1034-1041.

102. Niyyar, V.D. and M.R. Chan, *Interventional nephrology: Catheter dysfunction—Prevention and troubleshooting.* Clin J Am Soc Nephrol, 2013. **8**(7): p. 1234-1243.

103. Brown, J.M., *Polyurethane and silicone: Myths and misconceptions.* J Intraven Nurs, 1995. **18**(3): p. 120-123.

104. Tal, M.G. and N. Ni, *Selecting optimal hemodialysis catheters: Material, design, advanced features, and preferences.* Tech Vasc Interv Radiol, 2008. **11**(3): p. 186-191.

105. Xu, L.-C., J.W. Bauer, and C.A. Siedlecki, *Proteins, platelets, and blood coagulation at biomaterial interfaces.* Colloid Surface B, 2014. **124**: p. 49-68.

106. Boudot, C., et al., *Protein Adsorption and Adhesion of Blood Platelets on Silicone Rubber under Static and Dynamic Flow Conditions*, in *6th European Conference of the International Federation for Medical and Biological Engineering*, I. Lacković and D. Vasic, Editors. 2015, Springer International Publishing. p. 541-544.

107. Ratner, B.D. and A.S. Hoffman, *Physicochemical Surface Modification of Materials Used in Medicine*, in *Biomaterials Science: An Introduction to Materials in Medicine*, B.D. Ratner, et al., Editors. 2004, Elsevier Academic Press: New York. p. 201-218.

108. Tanzi, M.C., *Bioactive technologies for hemocompatibility.* Expert Rev Med Dev, 2005. **2**(4): p. 473-492.

109. Wendel, H.P. and G. Ziemer, *Coating-techniques to improve the hemocompatibility of artificial devices used for extracorporeal circulation.* Eur J Cardio-Thorac, 1999. **16**(3): p. 342-350.

110. Chen, H., et al., *Biocompatible polymer materials: Role of protein–surface interactions.* Prog Polym Sci, 2008. **33**(11): p. 1059-1087.

111. *US Food and Drug Administration. Medical Devices and Diagnostic Products that May Contain or Be Coated with Heparin*. [web page] 2013 Sept 24 [cited 2015 Mar 31]; Available from: http://www.fda.gov/medicaldevices/safety/alertsandnotices/ucm135347.htm.

112. Du, Y.J., et al., *Protein adsorption on polyurethane catheters modified with a novel antithrombin-heparin covalent complex.* J Biomed Mater Res A, 2007. **80A**(1): p. 216-225.

113. Park, K.D., et al., *Blood compatibility of SPUU-PEO-heparin graft copolymers.* J Biomed Mater Res, 1992. **26**(6): p. 739-756.

114. Shah, P.S. and N. Shah, *Heparin-bonded catheters for prolonging the patency of central venous catheters in children.* Cochrane Dat Syst Rev, 2014. **2**.

115. Jain, G., et al., *Does heparin coating improve patency or reduce infection of tunneled dialysis catheters?* Clin J Am Soc Nephrol, 2009. **4**(11): p. 1787-1790.

116. Clark, T., et al., *Comparison of heparin-coated and conventional split-tip hemodialysis catheters.* Cardiovasc Inter Rad, 2009. **32**(4): p. 703-706.

117. Kakkos, S.K., J. Kournoian, and G.K. Haddad, *A comparative study of the Sapphire and Equistream hemodialysis tunneled cuffed catheters.* JAVA, 2013. **18**(1): p. 37-44.

118. Laster, J. and D. Silver, *Heparin-coated catheters and heparin-induced thrombocytopenia.* J Vasc Surg, 1988. **7**(5): p. 667-672.

119. Laster, J.L., W.K. Nichols, and D. Silver, *Thrombocytopenia associated with heparin-coated catheters in patients with heparin-associated antiplatelet antibodies.* Arch Intern Med, 1989. **149**(10): p. 2285-2287.

120. Bittl, J.A., *Heparin-coated stent and heparin-induced thrombocytopenia: True, true, and conceivably related.* Catheter Cardio Inte, 2003. **58**(1): p. 84-85.

121. Sefton, M.V. and C.H. Gemmel, *Nonthrombogenic Treatments and Strategies*, in *Biomaterials Science: An Introduction to Materials in Medicine*, B.D. Ratner, et al., Editors. 2004, Elsevier Academic Press: New York. p. 456-470.

122. Andrade, J.D. and V. Hlady, *Protein adsorption and materials biocompatibility: A tutorial review and suggested hypotheses.* Adv Polymer Sci, 1986. **79**: p. 1-63.

123. Chang, T.M.S., *Platelet–surface interaction: Effect of albumin coating or heparin complexing on thrombogenic surfaces.* Can J Physiol Pharm, 1974. **52**(2): p. 275-285.

124. Matsuda, T., et al., *The blood interface with segmented polyurethanes: Multilayered protein passivation mechanism.* ASAIO J, 1984. **30**(1): p. 353-358.

125. Geelhood, S.J., et al., *Passivating protein coatings for implantable glucose sensors: Evaluation of protein retention.* J Biomed Mater Res Part B Appl Biomater, 2007. **81B**(1): p. 251-260.

126. Nakanishi, K., T. Sakiyama, and K. Imamura, *On the adsorption of proteins on solid surfaces, a common but very complicated phenomenon.* J Biosci Bioeng, 2001. **91**(3): p. 233-244.

127. Rabe, M., D. Verdes, and S. Seeger, *Understanding protein adsorption phenomena at solid surfaces.* Adv Colloid Interfac, 2011. **162**(1–2): p. 87-106.

128. Andrade, J.D., et al., *Water as a biomaterial.* ASAIO J, 1973. **19**(1): p. 1-7.

129. Hoffman, A.S., T.A. Horbett, and B.D. Ratner, *Interactions of blood and blood components at hydrogel interfaces.* Ann NY Acad Sci, 1977. **283**(1): p. 372-382.

130. Seifert, L.M. and R.T. Greer, *Evaluation of in vivo adsorption of blood elements onto hydrogel-coated silicone rubber by scanning electron microscopy and fourier transform infrared spectroscopy.* J Biomed Mater Res, 1985. **19**(9): p. 1043-1071.

131. Hanson, S.R., et al., *In vivo evaluation of artificial surfaces with a nonhuman primate model of arterial thrombosis.* J Lab Clin Med, 1980. **95**(2): p. 289-304.

132. Ratner, B.D., et al., *Blood-compatibility-water-content relationships for radiation-grafted hydrogels.* J Polym Sci Pol Sym, 1979. **66**(1): p. 363-375.

133. Amiji, M. and K. Park, *Prevention of protein adsorption and platelet adhesion on surfaces by PEO/PPO/PEO triblock copolymers.* Biomaterials, 1992. **13**(10): p. 682-692.

134. Tan, J.S., et al., *Surface modification of nanoparticles by PEO/PPO block copolymers to minimize interactions with blood components and prolong blood circulation in rats.* Biomaterials, 1993. **14**(11): p. 823-833.

135. Higuchi, A., et al., *Serum protein adsorption and platelet adhesion on pluronic™-adsorbed polysulfone membranes.* Biomaterials, 2003. **24**(19): p. 3235-3245.

136. Nonckreman, C.J., et al., *Competitive adsorption of fibrinogen and albumin and blood platelet adhesion on surfaces modified with nanoparticles and/or PEO.* Colloid Surface B, 2010. **77**(2): p. 139-149.

137. Nejadnik, M.R., et al., *Adsorption of Pluronic F-127 on surfaces with different hydrophobicities probed by quartz crystal microbalance with dissipation.* Langmuir, 2009. **25**(11): p. 6245-6249.

138. Lee, S. and J. Vörös, *An aqueous-based surface modification of poly(dimethylsiloxane) with poly(ethylene glycol) to prevent biofouling.* Langmuir, 2005. **21**(25): p. 11957-11962.

139. Gombotz, W.R., W. Guanghui, and A.S. Hoffman, *Immobilization of poly(ethylene oxide) on poly(ethylene terephthalate) using a plasma polymerization process.* J Appl Polym Sci, 1989. **37**(1): p. 91-107.

140. Pale-Grosdemange, C., et al., *Formation of self-assembled monolayers by chemisorption of derivatives of oligo(ethylene glycol) of structure* $HS(CH_2)_{11}(OCH_2CH_2)_mOH$ *on gold.* J Am Chem Soc, 1991. **113**(1): p. 12-20.

141. Feldman, K., et al., *Probing resistance to protein adsorption of oligo(ethylene glycol)-terminated self-assembled monolayers by scanning force microscopy.* J Am Chem Soc, 1999. **121**(43): p. 10134-10141.

142. Prime, K.L. and G.M. Whitesides, *Adsorption of proteins onto surfaces containing end-attached oligo(ethylene oxide): a model system using self-assembled monolayers.* J Am Chem Soc, 1993. **115**(23): p. 10714-10721.

143. Tseng, Y.C. and K. Park, *Synthesis of photoreactive poly(ethylene glycol) and its application to the prevention of surface-induced platelet activation.* J Biomed Mater Res, 1992. **26**(3): p. 373-391.

144. Sofia, S.J., V. Premnath, and E.W. Merrill, *Poly(ethylene oxide) grafted to silicon surfaces: grafting density and protein adsorption.* Macromolecules, 1998. **31**(15): p. 5059-5070.

145. Lee, S.-W. and P.E. Laibinis, *Protein-resistant coatings for glass and metal oxide surfaces derived from oligo(ethylene glycol)-terminated alkyltrichlorosilanes.* Biomaterials, 1998. **19**(18): p. 1669-1675.

146. Jo, S. and K. Park, *Surface modification using silanated poly(ethylene glycol)s.* Biomaterials, 2000. **21**(6): p. 605-616.

147. Chen, H., et al., *Protein repellant silicone surfaces by covalent immobilization of poly(ethylene oxide).* Biomaterials, 2005. **26**(15): p. 2391-2399.

148. Papra, A., et al., *Microfluidic networks made of poly(dimethylsiloxane), Si, and Au coated with polyethylene glycol for patterning proteins onto surfaces.* Langmuir, 2001. **17**(13): p. 4090-4095.

149. Desai, N.P. and J.A. Hubbell, *Biological responses to polyethylene oxide modified polyethylene terephthalate surfaces.* J Biomed Mater Res, 1991. **25**(7): p. 829-843.

150. Bergström, K., et al., *Reduction of fibrinogen adsorption on PEG-coated polystyrene surfaces.* J Biomed Mater Res, 1992. **26**(6): p. 779-790.

151. Zhang, M., T. Desai, and M. Ferrari, *Proteins and cells on PEG immobilized silicon surfaces.* Biomaterials, 1998. **19**(10): p. 953-960.

152. Papra, A., N. Gadegaard, and N.B. Larsen, *Characterization of ultrathin poly(ethylene glycol) monolayers on silicon substrates.* Langmuir, 2001. **17**(5): p. 1457-1460.

153. Zhang, M. and M. Ferrari, *Hemocompatible polyethylene glycol films on silicon.* Biomed Microdevices, 1998. **1**(1): p. 81-89.

154. Knoll, D. and J. Hermans, *Polymer-protein interactions: Comparison of experiment and excluded volume theory.* J Biol Chem, 1983. **258**(9): p. 5710-5715.

155. Jeon, S.I., et al., *Protein-surface interactions in the presence of polyethylene oxide: I. Simplified theory.* J Colloid Interface Sci, 1991. **142**(1): p. 149-158.

156. Jeon, S.I. and J.D. Andrade, *Protein-surface interactions in the presence of polyethylene oxide: II. Effect of protein size.* J Colloid Interface Sci, 1991. **142**(1): p. 159-166.

157. Lee, J.H., H.B. Lee, and J.D. Andrade, *Blood compatibility of polyethylene oxide surfaces.* Prog Polym Sci, 1995. **20**(6): p. 1043-1079.

158. Szleifer, I., *Protein adsorption on surfaces with grafted polymers: A theoretical approach.* Biophys J, 1997. **72**(2 Pt 1): p. 595-612.

159. Chen, S., et al., *Surface hydration: Principles and applications toward low-fouling/nonfouling biomaterials.* Polymer, 2010. **51**(23): p. 5283-5293.

160. Rufin, M.A. and M.A. Grunlan, *Surface-Grafted Polymer Coatings: Preparation, Characterization, and Anti-Fouling Behavior*, in *Functional Polymer Coatings: Principles, Methods, and Applications*, L. Wu and J. Baghdachi, Editors. 2015, John Wiley & Sons, Ltd. p. 218-238.

161. Chaikof, E.L., et al., *PEO enhancement of platelet deposition, fibrinogen deposition, and complement C3 activation.* J Biomed Mater Res, 1992. **26**(9): p. 1163-1168.

162. Desai, N.P. and J.A. Hubbell, *Solution technique to incorporate polyethylene oxide and other water-soluble polymers into surfaces of polymeric biomaterials.* Biomaterials, 1991. **12**(2): p. 144-153.

163. Nagaoka, S., et al., *Interaction Between Blood Components and Hydrogels With Poly(Oxyethylene) Chains*, in *Polymers as Biomaterials*, S. Shalaby, et al., Editors. 1984, Springer US. p. 361-374.

164. Malmsten, M., K. Emoto, and J.M. Van Alstine, *Effect of chain density on inhibition of protein adsorption by poly(ethylene glycol) based coatings.* J Colloid Interface Sci, 1998. **202**(2): p. 507-517.

165. Kingshott, P., H. Thissen, and H.J. Griesser, *Effects of cloud-point grafting, chain length, and density of PEG layers on competitive adsorption of ocular proteins.* Biomaterials, 2002. **23**(9): p. 2043-2056.

166. Li, L., et al., *Protein adsorption on oligo(ethylene glycol)-terminated alkanethiolate self-assembled monolayers: The molecular basis for nonfouling behavior.* J Phys Chem B, 2005. **109**(7): p. 2934-2941.

167. Zheng, J., et al., *Strong repulsive forces between protein and oligo (ethylene glycol) self-assembled monolayers: A molecular simulation study.* Biophys J, 2005. **89**(1): p. 158-166.

168. Zheng, J., et al., *Molecular simulation study of water interactions with oligo (ethylene glycol)-terminated alkanethiol self-assembled monolayers.* Langmuir, 2004. **20**(20): p. 8931-8938.

169. Park, K., et al., *In vitro and in vivo studies of PEO-grafted blood-contacting cardiovascular prostheses.* J Biomat Sci Polym Ed, 2000. **11**(11): p. 1121-1134.

170. Du, Y.J., et al., *In vivo rabbit acute model tests of polyurethane catheters coated with a novel antithrombin-heparin covalent complex.* Thromb Haemostasis, 2005. **94**(8): p. 366-372.

171. Hunt, J.A., G. Meijs, and D.F. Williams, *Hydrophilicity of polymers and soft tissue responses: A quantitative analysis.* J Biomed Mater Res, 1997. **36**(4): p. 542-549.

172. Ostuni, E., et al., *A survey of structure-property relationships of surfaces that resist the adsorption of protein.* Langmuir, 2001. **17**(18): p. 5605-5620.

173. Zhang, L., et al., *Zwitterionic hydrogels implanted in mice resist the foreign-body reaction.* Nat Biotech, 2013. **31**(6): p. 553-556.

174. Jiang, S. and Z. Cao, *Ultralow-fouling, functionalizable, and hydrolyzable zwitterionic materials and their derivatives for biological applications.* Adv Mater, 2010. **22**(9): p. 920-932.

175. Sin, M.-C., S.-H. Chen, and Y. Chang, *Hemocompatibility of zwitterionic interfaces and membranes.* Polym J, 2014. **46**(8): p. 436-443.

176. Liu, X., et al., *Blood compatible materials: state of the art.* J Mater Chem B, 2014. **2**(35): p. 5718-5738.

177. Browning, M.B., et al., *Determination of the in vivo degradation mechanism of PEGDA hydrogels.* J Biomed Mater Res A, 2014. **102**(12): p. 4244-4251.

178. Tsai, W.-B., et al., *Platelet adhesion to polystyrene-based surfaces preadsorbed with plasmas selectively depleted in fibrinogen, fibronectin, vitronectin, or von Willebrand's factor.* J Biomed Mater Res, 2002. **60**(3): p. 348-359.

179. Delamarche, E., et al., *Microcontact printing using poly(dimethylsiloxane) stamps hydrophilized by poly(ethylene oxide) silanes.* Langmuir, 2003. **19**(21): p. 8749-8758.

180. Yianni, Y., *Biocompatible Surfaces Based Upon Biomembrane Mimicry*, in *Structural and Dynamic Properties of Lipids and Membranes*, P. Quinn and R. Cherry, Editors. 1992, Portland Press Ltd: London. p. 182-217.

181. Ishihara, K., et al., *Effects of phospholipid adsorption on nonthrombogenicity of polymer with phospholipid polar group.* J Biomed Mater Res, 1993. **27**(10): p. 1309-1314.

182. Ishihara, K., *New polymeric biomaterials — phospholipid polymers with a biocompatible surface.* Front Med Biol Eng, 2000. **10**(2): p. 83-95.

183. Xu, J., et al., *Ozone-induced grafting phosphorylcholine polymer onto silicone film grafting 2-methacryloyloxyethyl phosphorylcholine onto silicone film to improve hemocompatibility.* Colloid Surface B, 2003. **30**(3): p. 215-223.

184. West, S.L., et al., *The biocompatibility of crosslinkable copolymer coatings containing sulfobetaines and phosphobetaines.* Biomaterials, 2004. **25**(7–8): p. 1195-1204.

185. Zhou, J., et al., *Platelet adhesion and protein adsorption on silicone rubber surface by ozone-induced grafted polymerization with carboxybetaine monomer.* Colloid Surface B, 2005. **41**(1): p. 55-62.

186. Chen, S., L. Liu, and S. Jiang, *Strong resistance of oligo(phosphorylcholine) self-assembled monolayers to protein adsorption.* Langmuir, 2006. **22**(6): p. 2418-2421.

187. Zhang, Z., et al., *Blood compatibility of surfaces with superlow protein adsorption.* Biomaterials, 2008. **29**(32): p. 4285-4291.

188. Li, G., et al., *Ultra low fouling zwitterionic polymers with a biomimetic adhesive group.* Biomaterials, 2008. **29**(35): p. 4592-4597.

189. Tanaka, M., et al., *Synthesis of phosphorylcholine–oligoethylene glycol–alkane thiols and their suppressive effect on non-specific adsorption of proteins.* Tetrahedron Lett, 2009. **50**(28): p. 4092-4095.

190. Gao, C., et al., *Functionalizable and ultra-low fouling zwitterionic surfaces via adhesive mussel mimetic linkages.* Biomaterials, 2010. **31**(7): p. 1486-1492.

191. Chen, S., et al., *Strong resistance of phosphorylcholine self-assembled monolayers to protein adsorption: Insights into nonfouling properties of zwitterionic materials.* J Am Chem Soc, 2005. **127**(41): p. 14473-14478.

192. Liu, Q., A. Singh, and L. Liu, *Amino acid-based zwitterionic poly(serine methacrylate) as an antifouling material.* Biomacromolecules, 2012. **14**(1): p. 226-231.

193. Liu, P., et al., *Facile surface modification of silicone rubber with zwitterionic polymers for improving blood compatibility.* Mat Sci Eng C, 2013. **33**(7): p. 3865-3874.

194. Feng, W., J.L. Brash, and S. Zhu, *Non-biofouling materials prepared by atom transfer radical polymerization grafting of 2-methacryloloxyethyl phosphorylcholine: Separate effects of graft density and chain length on protein repulsion.* Biomaterials, 2006. **27**(6): p. 847-855.

195. Feng, W., et al., *Protein resistant surfaces: Comparison of acrylate graft polymers bearing oligo-ethylene oxide and phosphorylcholine side chains.* Biointerphases, 2006. **1**(1): p. 50-60.

196. Feng, W., et al., *Methacrylate polymer layers bearing poly(ethylene oxide) and phosphorylcholine side chains as non-fouling surfaces: In vitro interactions with plasma proteins and platelets.* Acta Biomaterialia, 2011. **7**(10): p. 3692-3699.

197. Keefe, A.J., N.D. Brault, and S. Jiang, *Suppressing surface reconstruction of superhydrophobic PDMS using a superhydrophilic zwitterionic polymer.* Biomacromolecules, 2012. **13**(5): p. 1683-1687.

198. He, Y., et al., *Molecular simulation studies of protein interactions with zwitterionic phosphorylcholine self-assembled monolayers in the presence of water.* Langmuir, 2008. **24**(18): p. 10358-10364.

199. Harding, J.L. and M.M. Reynolds, *Combating medical device fouling.* Trends Biotechnol, 2014. **32**(3): p. 140-146.

200. Chen, C., et al., *Phosphorylcholine coating of ePTFE reduces platelet deposition and neointimal hyperplasia in arteriovenous grafts.* J Surg Res, 1998. **77**(2): p. 119-125.

201. Chen, H., M.A. Brook, and H. Sheardown, *Silicone elastomers for reduced protein adsorption.* Biomaterials, 2004. **25**(12): p. 2273-2282.

202. Chen, H., et al., *Surface properties of PEO–silicone composites: reducing protein adsorption.* J Biomat Sci Polym E, 2005. **16**(4): p. 531-548.

203. Merrill, E.W., et al., *Platelet-compatible hydrophilic segmented polyurethanes from polyethylene glycols and cyclohexane diisocyanate.* ASAIO J, 1982. **28**(1): p. 482-487.

204. Shu Qin, L., Y. Ito, and Y. Imanishi, *Synthesis and non-thrombogenicity of polyurethanes with poly(oxyethylene) side chains in soft segment regions.* J Biomat Sci Polym E, 1989. **1**(2): p. 111-122.

205. Okkema, A.Z., et al., *Bulk, surface, and blood-contacting properties of polyetherurethanes modified with polyethylene oxide.* J Biomat Sci Polym E, 1989. **1**(1): p. 43-62.

206. Lee, J.H., et al., *Platelet adhesion onto segmented polyurethane surfaces modified by PEO- and sulfonated PEO-containing block copolymer additives.* J Biomed Mater Res, 1998. **40**(2): p. 314-323.

207. Mao, C., et al., *Modification of polyethylene with Pluronics F127 for improvement of blood compatibility.* Colloid Surface B, 2009. **74**(1): p. 362-365.

208. Lee, J.H., Y.M. Ju, and D.M. Kim, *Platelet adhesion onto segmented polyurethane film surfaces modified by addition and crosslinking of PEO-containing block copolymers.* Biomaterials, 2000. **21**(7): p. 683-691.

209. Tan, J. and J.L. Brash, *Nonfouling biomaterials based on polyethylene oxide-containing amphiphilic triblock copolymers as surface modifying additives: Adsorption of proteins from human plasma to copolymer/polyurethane blends.* J Biomed Mater Res A, 2009. **90A**(1): p. 196-204.

210. Ward, R., K. White, and C. Hu, *Use of Surface-Modifying Additives in the Development of a New Biomedical Polyurethaneurea*, in *Polyurethanes in Biomedical Engineering, Elsevier, Amsterdam*, H. Plank, G. Egbers, and I. Syre, Editors. 1984, Elsevier: New York. p. 181-200.

211. Tsai, C.-C., et al., *Surface modifying additives for improved device-blood compatibility.* ASAIO J, 1994. **40**(3): p. M619-M624.

212. Ye, S.H., et al., *Novel cellulose acetate membrane blended with phospholipid polymer for hemocompatible filtration system.* J Membr Sci, 2002. **210**(2): p. 411-421.

213. Hong, Y., et al., *A small diameter, fibrous vascular conduit generated from a poly(ester urethane)urea and phospholipid polymer blend.* Biomaterials, 2009. **30**(13): p. 2457-2467.

214. Lopez-Donaire, M.L. and J.P. Santerre, *Surface modifying oligomers used to functionalize polymeric surfaces: Consideration of blood contact applications.* J Appl Polym Sci, 2014. **131**(14).

215. Baumann, M., et al., *Prolonged catheter survival in intermittent hemodialysis using a less thrombogenic micropatterned polymer modification.* ASAIO J, 2003. **49**(6): p. 708-712.

216. Meier, P., et al., *Prolonged catheter survival in patients with acute kidney injury on continuous renal replacement therapy using a less thrombogenic micropatterned polymer modification.* Nephrol Dial Transplant, 2010.

217. Kakkos, S.K., et al., *Long-term complication and patency rates of Vectra and IMPRA Carboflo Vascular Access Grafts with aggressive monitoring, surveillance and endovascular management.* Vascular, 2011. **19**(1): p. 21-28.

218. Gu, Y.J., et al., *Cardiopulmonary bypass circuit treated with surface-modifying additives: A clinical evaluation of blood compatibility.* Ann Thorac Surg, 1998. **65**(5): p. 1342-1347.

219. Defraigne, J.-O., et al., *SMA circuits reduce platelet consumption and platelet factor release during cardiac surgery.* Ann Thorac Surg, 2000. **70**(6): p. 2075-2081.

220. Murthy, R., et al., *Protein-resistant silicones: Incorporation of poly(ethylene oxide) via siloxane tethers.* Biomacromolecules, 2007. **8**(10): p. 3244-3252.

221. Hawkins, M.L. and M.A. Grunlan, *The protein resistance of silicones prepared with a PEO-silane amphiphile.* J Mater Chem, 2012. **22**(37): p. 19540-19546.

222. Hawkins, M.L., et al., *Direct observation of the nanocomplex surface reorganization of antifouling silicones containing a highly mobile PEO-silane amphiphile.* J Mater Chem B, 2014. **2**: p. 5689-5697.

223. Hawkins, M.L., *Antifouling Silicone Coatings Prepared with PEO-Silane Amphiphiles*, in *Biomedical Engineering*. 2014, Texas A&M University: College Station. p. 141.

224. Curtis, J. and A. Colas, *Medical Applications of Silicones*, in *Biomaterials Science: An Introduction to Materials in Medicine*, B.D. Ratner, et al., Editors. 2004, Elsevier Academic Press: New York. p. 697-707.

225. Van Dyke, M.E., S.J. Clarson, and R. Arshady, *Silicone Biomaterials*, in *An Introduction to Polymeric Biomaterials*, R. Arshady, Editor. 2003, Citrus Books: London. p. 109-135.

226. El-Zaim, H.S. and J.P. Heggers, *Silicones for Pharmaceutical and Biomedical Applications*, in *Polymeric Biomaterials*, S. Dumitriu, Editor. 2001, Marcel Dekker: New York. p. 79-90.

227. Lejars, M., A. Margaillan, and C. Bressy, *Fouling release coatings: A nontoxic alternative to biocidal antifouling coatings.* Chem Rev, 2012. **112**(8): p. 4347-4390.

228. Brash, J.L., *Hydrophobic polymer surfaces and their interactions with blood.* Ann NY Acad Sci, 1977. **283**(1): p. 356-371.

229. Krishnan, S., C.J. Weinman, and C.K. Ober, *Advances in polymers for anti-biofouling surfaces.* J Mater Chem, 2008. **18**(29): p. 3405-3413.

230. Hron, P., *Hydrophilisation of silicone rubber for medical applications.* Polym Int, 2003. **52**(9): p. 1531-1539.

231. Abbasi, F., H. Mirzadeh, and A.-A. Katbab, *Modification of polysiloxane polymers for biomedical applications: a review.* Polym Int, 2001. **50**(12): p. 1279-1287.

232. Bodas, D. and C. Khan-Malek, *Formation of more stable hydrophilic surfaces of PDMS by plasma and chemical treatments.* Microelectron Eng, 2006. **83**(4–9): p. 1277-1279.

233. Yao, K., et al., *Improvement of the surface biocompatibility of silicone intraocular lens by the plasma-induced tethering of phospholipid moieties.* J Biomed Mater Res A, 2006. **78A**(4): p. 684-692.

234. Zhang, H., et al., *Nitric oxide releasing silicone rubbers with improved blood compatibility: Preparation, characterization, and in vivo evaluation.* Biomaterials, 2002. **23**(6): p. 1485-1494.

235. Morra, M., E. Occhiello, and F. Garbassi, *Surface modification of blood contacting polymers by poly(ethyleneoxide).* Clin Mater, 1993. **14**(3): p. 255-265.

236. Archambault, J.G. and J.L. Brash, *Protein resistant polyurethane surfaces by chemical grafting of PEO: amino-terminated PEO as grafting reagent.* Colloid Surface B, 2004. **39**(1–2): p. 9-16.

237. Balakrishnan, B., et al., *Chemical modification of poly(vinyl chloride) resin using poly(ethylene glycol) to improve blood compatibility.* Biomaterials, 2005. **26**(17): p. 3495-3502.

238. Banerjee, I., R.C. Pangule, and R.S. Kane, *Antifouling coatings: Recent developments in the design of surfaces that prevent fouling by proteins, bacteria, and marine organisms.* Adv Mater, 2011. **23**(6): p. 690-718.

239. Harris, J.M., ed. *Poly(Ethylene Glycol) Chemistry: Biotechnical and Biomedical Applications*. 1992, Plenum Press: New York.

240. Yasuda, H., A.K. Sharma, and T. Yasuda, *Effect of orientation and mobility of polymer molecules at surfaces on contact angle and its hysteresis.* J Polym Sci Pol Phys, 1981. **19**(9): p. 1285-1291.

241. Owen, M.J. and P.J. Smith, *Plasma treatment of polydimethylsiloxane.* J Adhes Sci Technol, 1994. **8**(10): p. 1063-1075.

242. Owen, M.J., *Siloxane Surface Activity*, in *Silicon-Based Polymer Science: A Comprehensive Resource*, J.M. Zeigler and F.W.G. Fearon, Editors. 1990, American Chemical Society: Washington, D.C. p. 705-739.

243. Owen, M.J., *Surface Chemistry and Applications*, in *Siloxane Polymers*, S.J. Clarson and J.A. Semlyen, Editors. 1993, Prentice Hall: Englewood Cliffs. p. 309.

244. Mark, J.E., *Silicon-Containing Polymers*, in *Silicon-Based Polymer Science: A Comprehensive Review*, J.M. Zeigler and F.W.G. Fearon, Editors. 1990, American Chemical Society: Washington, D.C. p. 47-68.

245. Lane, T.H. and S.A. Burns, *Silica, Silicon and Silicones... Unraveling the Mystery*, in *Immunology of Silicones*, M. Potter and N.R. Rose, Editors. 1996, Springer: Berlin. p. 3-12.

246. Thompson, D.B., A.S. Fawcett, and M.A. Brook, *Simple Strategies to Manipulate Hydrophilic Domains in Silicones*, in *Silicon Based Polymers*, F. Ganachaud, S. Boileau, and B. Boury, Editors. 2008, Springer. p. 29-38.

247. Hawkins, M.L., et al., *Bacteria and diatom resistance of silicones modified with PEO-silane amphiphiles.* Biofouling, 2014. **30**(2): p. 247-258.

248. Murthy, R., C.E. Shell, and M.A. Grunlan, *The influence of poly(ethylene oxide) grafting via siloxane tethers on protein adsorption.* Biomaterials, 2009. **30**(13): p. 2433-2439.

249. Murthy, R., et al., *Amphiphilic silicones prepared from branched PEO-silanes with siloxane tethers.* J Polym Sci Pol Chem, 2010. **48**(18): p. 4108-4119.

250. Hooper, R., et al., *Highly conductive siloxane polymers.* Macromolecules, 2001. **34**(4): p. 931-936.

251. Chang, Y., et al., *Amphiphilic linear PEO−dendritic carbosilane block copolymers.* Macromolecules, 2000. **33**(12): p. 4496-4500.

252. Unsworth, L.D., et al., *Chemisorption of thiolated poly(ethylene oxide) to gold: surface chain densities measured by ellipsometry and neutron reflectometry.* J Colloid Interface Sci, 2005. **281**(1): p. 112-121.

253. Moreau, O., et al., *Adhesion of polyethylene glycol and quaternary ammonium salt-grafted silicon surfaces: Influences of physicochemical properties.* Surf Coat Technol, 2007. **201**: p. 5994-6004.

254. Cole, M.A., et al., *A new approach to the immobilisation of poly(ethylene oxide) for the reduction of non-specific protein adsorption on conductive substrates.* Surf Sci, 2007. **601**: p. 1716-1725.

255. Sharma, S., R.W. Johnson, and T.A. Desai, *Ultrathin poly(ethylene glycol) films for silicon-based microdevices.* Appl Surf Sci, 2003. **206**(1–4): p. 218-229.

256. Zdyrko, B., V. Klep, and I. Luzinov, *Synthesis and surface morphology of high-density poly(ethylene glycol) grafted layers.* Langmuir, 2003. **19**(24): p. 10179-10187.

257. Harder, P., et al., *Molecular conformation in oligo(ethylene glycol)-terminated self-assembled monolayers on gold and silver surfaces determines their ability to resist protein adsorption.* J Phys Chem B, 1998. **102**(2): p. 426-436.

258. Soong, R. and P.M. Macdonald, *PEG molecular weight and lateral diffusion of PEG-ylated lipids in magnetically aligned bicelles.* BBA Biomembr, 2007. **1768**(7): p. 1805-1814.

259. Allen, C., et al., *Controlling the physical behavior and biological performance of liposome formulations through use of surface grafted poly(ethylene glycol).* Biosience Rep, 2002. **22**(2): p. 225-250.

260. Sangermano, M., et al., *Fluorinated epoxides as surface modifying agents of UV-curable systems.* J Appl Polym Sci, 2003. **89**(6): p. 1524-1529.

261. Hemmersam, A.G., et al., *Adsorption of fibrinogen on tantalum oxide, titanium oxide and gold studied by the QCM-D technique.* Colloid Surface B, 2005. **43**(3–4): p. 208-215.

262. Luan, Y., et al., *125I-Radiolabeling, Surface Plasmon Resonance, and Quartz Crystal Microbalance with Dissipation: Three Tools to Compare Protein Adsorption on Surfaces of Different Wettability.* Langmuir, 2014. **30**(4): p. 1029-1035.

263. Lord, M.S., et al., *Lysozyme interaction with poly(HEMA)-based hydrogel.* Biomaterials, 2006. **27**(8): p. 1341-1345.

264. Tanaka, M., et al., *In situ studies on protein adsorption onto a poly(2-methoxyethylacrylate) surface by a quartz crystal microbalance.* Colloid Surf A, 2001. **193**(1–3): p. 145-152.

265. Cooper, M.A. and V.T. Singleton, *A survey of the 2001 to 2005 quartz crystal microbalance biosensor literature: applications of acoustic physics to the analysis of biomolecular interactions.* J Mol Recognit, 2007. **20**(3): p. 154-184.

266. Rufin, M.A., et al., *Enhancing the protein resistance of silicone via surface-restructuring PEO-silane amphiphiles with variable PEO length.* J Mater Chem B, 2015. **3**(14): p. 2816-2825.

267. Tan, J., W.G. McClung, and J.L. Brash, *Nonfouling biomaterials based on polyethylene oxide-containing amphiphilic triblock copolymers as surface modifying additives: Protein adsorption on PEO-copolymer/polyurethane blends.* J Biomed Mater Res A, 2008. **85A**(4): p. 873-880.

268. van Oeveren, W., et al., *Comparison of coagulation activity tests in vitro for selected biomaterials.* Artif Organs, 2002. **26**(6): p. 506-511.

269. Ruzette, A.-V. and L. Leibler, *Block copolymers in tomorrow's plastics.* Nat Mater, 2005. **4**(1): p. 19-31.

270. Callow, M.E. and J.E. Callow, *Marine biofouling: A sticky problem.* Biologist, 2002. **49**(1): p. 1-5.

271. Brady, R.F., *Fouling-release coatings for warships.* Def Sci J, 2005. **55**(1): p. 75-81.

272. Krishnan, S., *Marine Bioadhesion on Polymer Surfaces and Strategies for Its Prevention*, in *Polymer Adhesion, Friction, and Lubrication*, H. Zeng, Editor. 2013, John Wiley & Sons, Inc. p. 227-281.

273. Nichols, J.J., *Contact lenses 2010.* Contact Lens Spectrum, 2011. **26**(1).

274. Baines, M.G., F. Cai, and H.A. Backman, *Adsorption and removal of protein bound to hydrogel contact lenses.* Optometry Vision Sci, 1990. **67**(11): p. 807-810.

275. Bohnert, J.L., et al., *Adsorption of proteins from artificial tear solutions to contact lens materials.* Invest Ophth Vis Sci, 1988. **29**(3): p. 362-73.

276. Minno, G.E., et al., *Quantitative analysis of protein deposits on hydrophilic soft contact lenses: I. Comparison to visual methods of analysis. II. Deposit variation among FDA lens material groups.* Optometry Vision Sci, 1991. **68**(11): p. 865-872.

277. Gellatly, K.W., N.A. Brennan, and N. Efron, *Visual decrement with deposit accumulation of HEMA contact lenses.* Am J Optom Phys Opt, 1988. **65**(12): p. 937-941.

278. Bleshoy, H., M. Guillon, and D. Shah, *Influence of contact lens material surface characteristics on replacement frequency.* Int Contact Lens Clin, 1994. **21**(5–6): p. 82-95.

279. Pritchard, N., D. Fonn, and K. Weed, *Ocular and subjective responses to frequent replacement of daily wear soft contact lenses.* Eye Contact Lens, 1996. **22**(1): p. 53-60.

280. Dumbleton, K., et al., *The impact of contemporary contact lenses on contact lens discontinuation.* Eye Contact Lens, 2013. **39**(1): p. 93-99 10.1097/ICL.0b013e318271caf4.

281. Patrinely, J.R., et al., *Bacterial keratitis associated with extended wear soft contact lenses.* Eye Contact Lens, 1985. **11**(3): p. 234-236.

282. Willcox, M.D.P., et al., *Bacterial interactions with contact lenses; effects of lens material, lens wear and microbial physiology.* Biomaterials, 2001. **22**(24): p. 3235-3247.

283. Refojo, M.F. and F.J. Holly, *Tear protein adsorption on hydrogels: A possible cause of contact lens allergy.* Eye Contact Lens, 1977. **3**(1): p. 23-36.

284. Donshik, P.C., *Contact lens chemistry and giant papillary conjunctivitis.* Eye Contact Lens, 2003. **29**(1 Suppl): p. S37-9; discussion S57-9, S192-4.

285. Santos, L., et al., *The influence of surface treatment on hydrophobicity, protein adsorption and microbial colonisation of silicone hydrogel contact lenses.* Contact Lens Anterior Eye, 2007. **30**(3): p. 183-188.

286. Lloyd, A.W., R.G.A. Faragher, and S.P. Denyer, *Ocular biomaterials and implants.* Biomaterials, 2001. **22**(8): p. 769-785.

287. Gong, J.P., et al., *Double-network hydrogels with extremely high mechanical strength.* Adv Mater, 2003. **15**(14): p. 1155-1158.

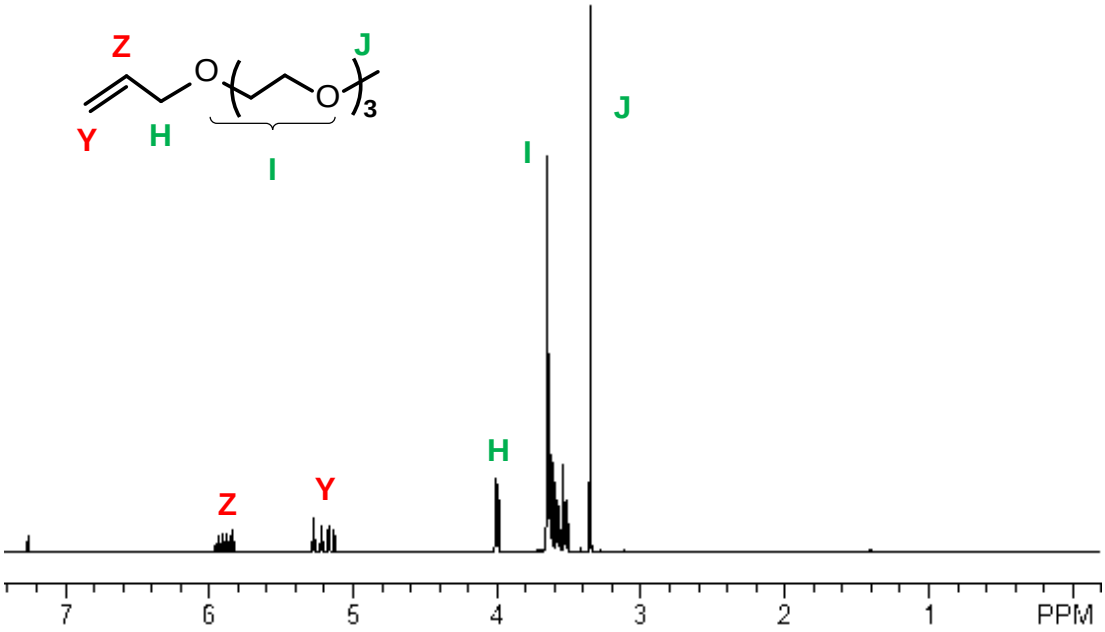

^{1}H NMR of tri(ethylene oxide) allyl methyl ether (**allyl methyl PEO$_3$**) [From Chapter II]

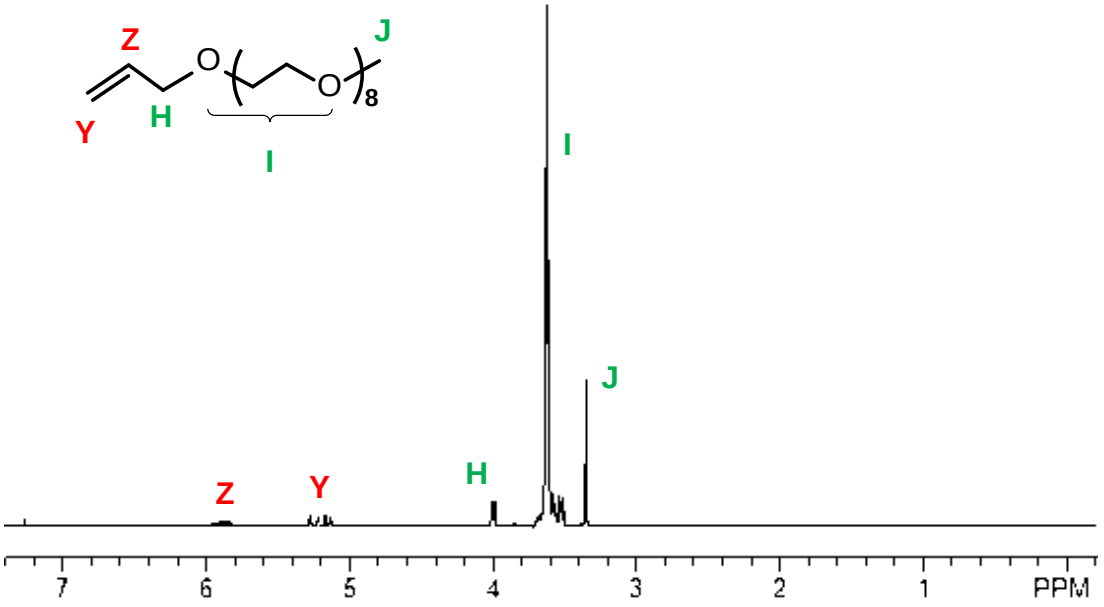

^{1}H NMR of poly(ethylene oxide)$_8$ allyl methyl ether (**allyl methyl PEO$_8$**) [From Chapter II]

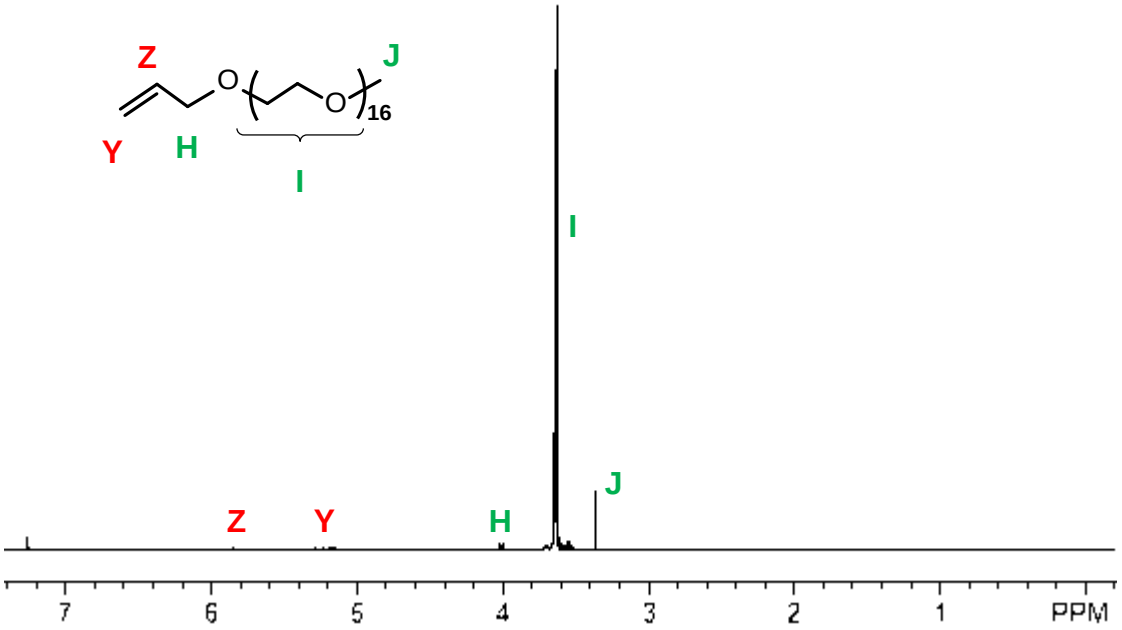

^{1}H NMR of poly(ethylene oxide)$_{16}$ allyl methyl ether (**allyl methyl PEO$_{16}$**) [From Chapter II]

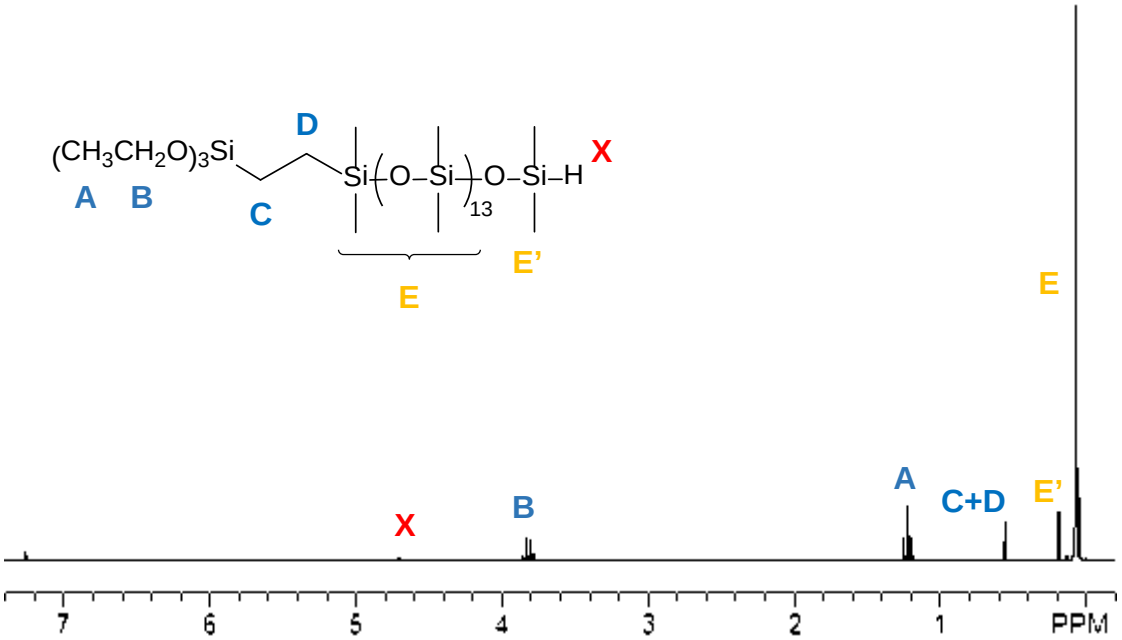

^{1}H NMR of triethoxysilylethyl-polydimethylsiloxane$_{13}$ (**siloxane-control**) [From Chapter II]

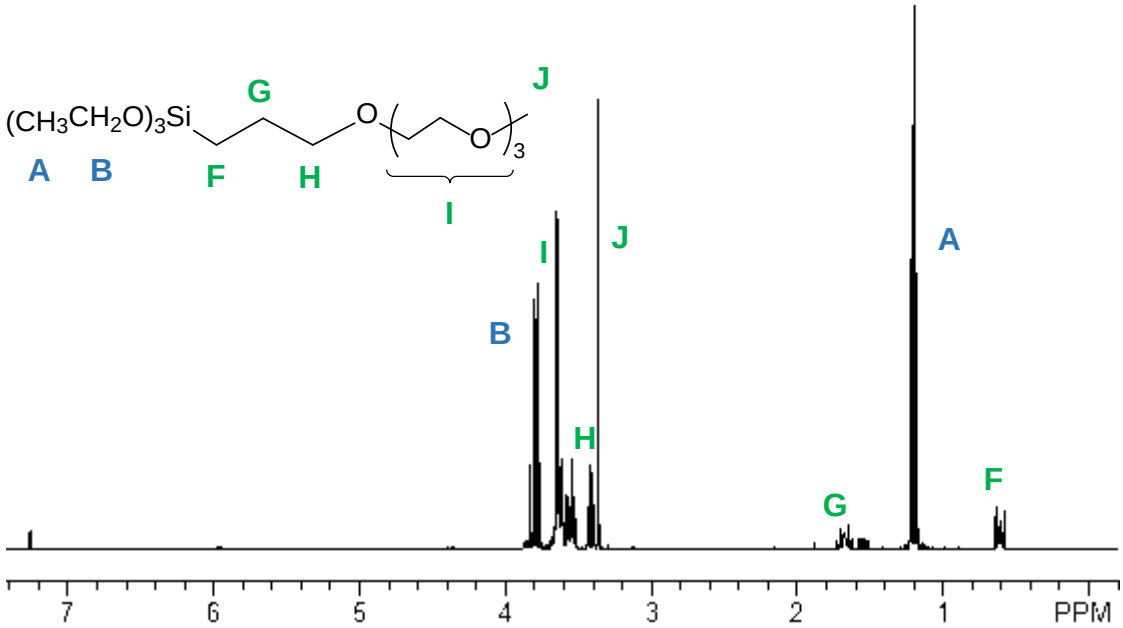

^{1}H NMR of triethoxysilylpropyl-PEO$_3$ (***n* = 3 PEO-control**) [From Chapter II]

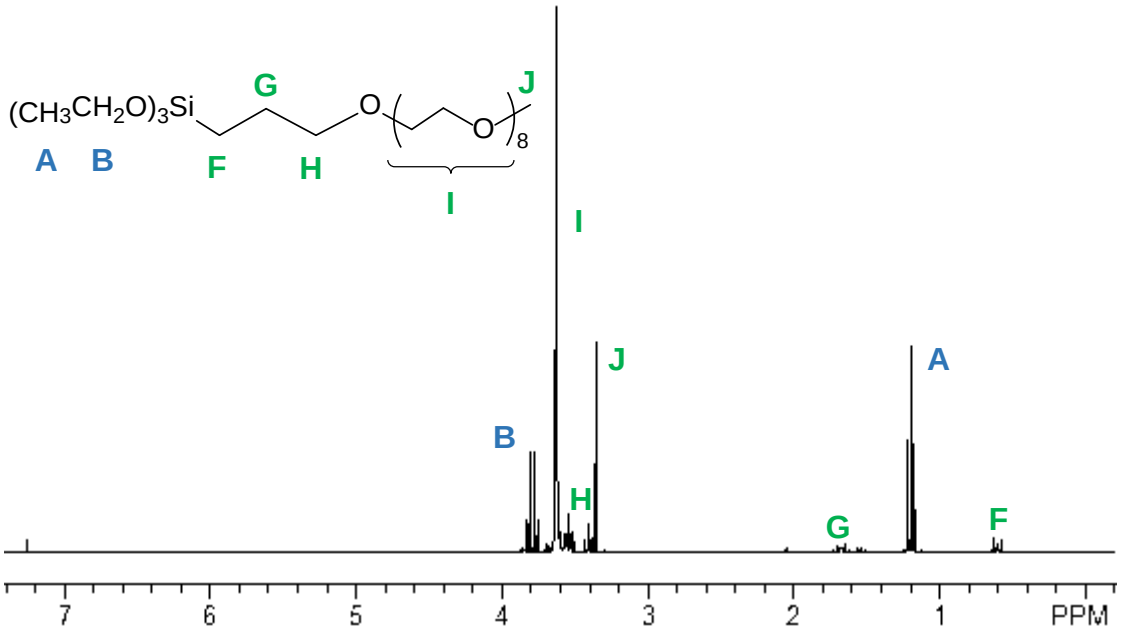

^{1}H NMR of triethoxysilylpropyl-PEO$_8$ (***n* = 8 PEO-control**) [From Chapter II]

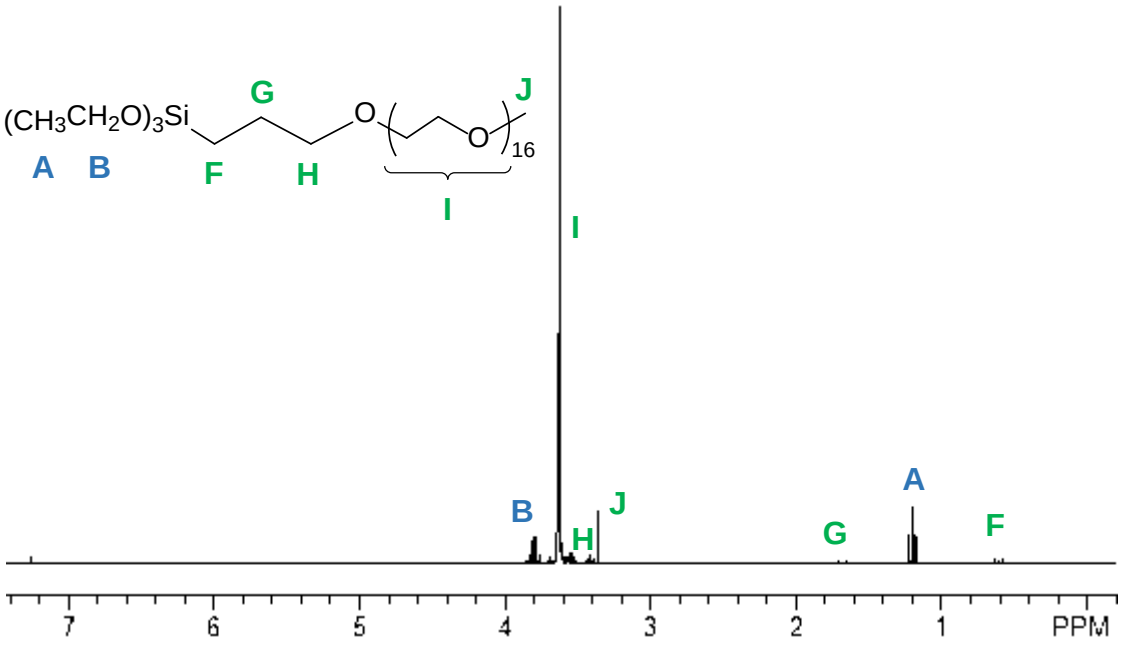

^{1}H NMR of triethoxysilylpropyl-PEO$_{16}$ (***n* = 16 PEO-control**) [From Chapter II]

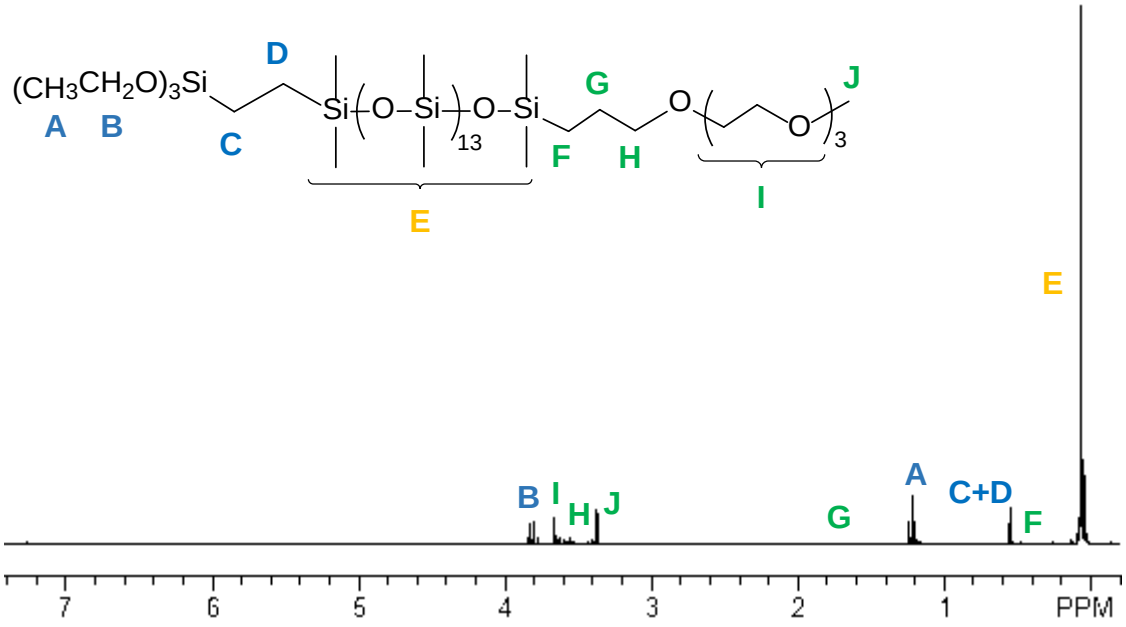

^{1}H NMR of triethoxysilylethyl-polydimethylsiloxane$_{13}$-*block*-PEO$_{3}$ (***n* = 3 PEO-silane amphiphile**) [From Chapter II and III]

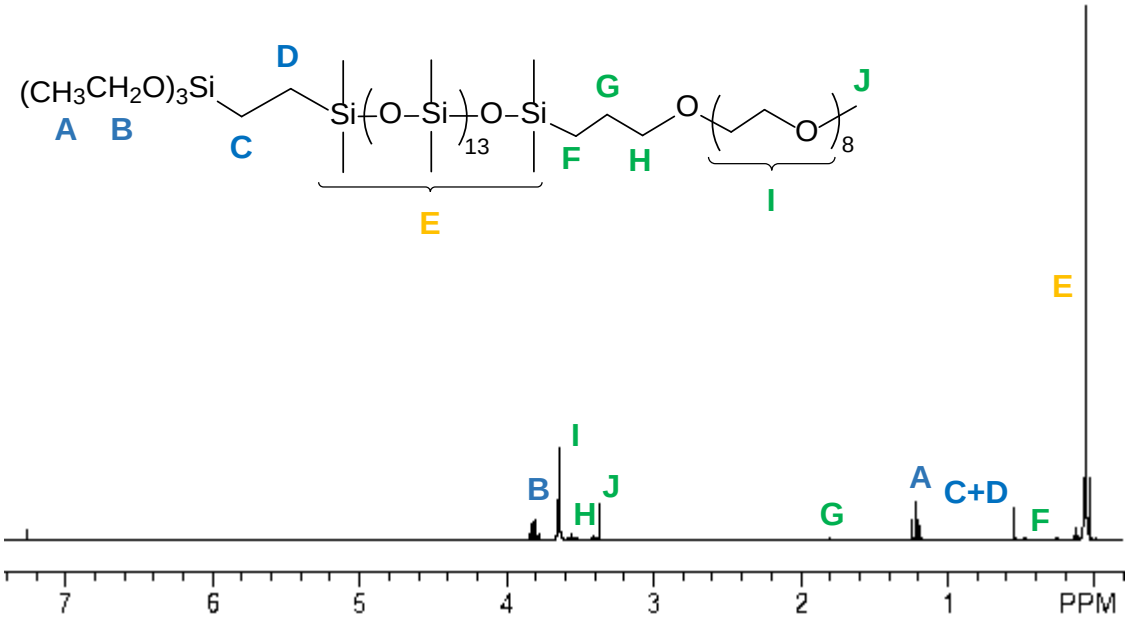

^{1}H NMR of triethoxysilylethyl-polydimethylsiloxane$_{13}$-*block*-PEO$_{8}$ (***n* = 8, *m* = 13 PEO-silane amphiphile**) [From Chapter II, III and IV]

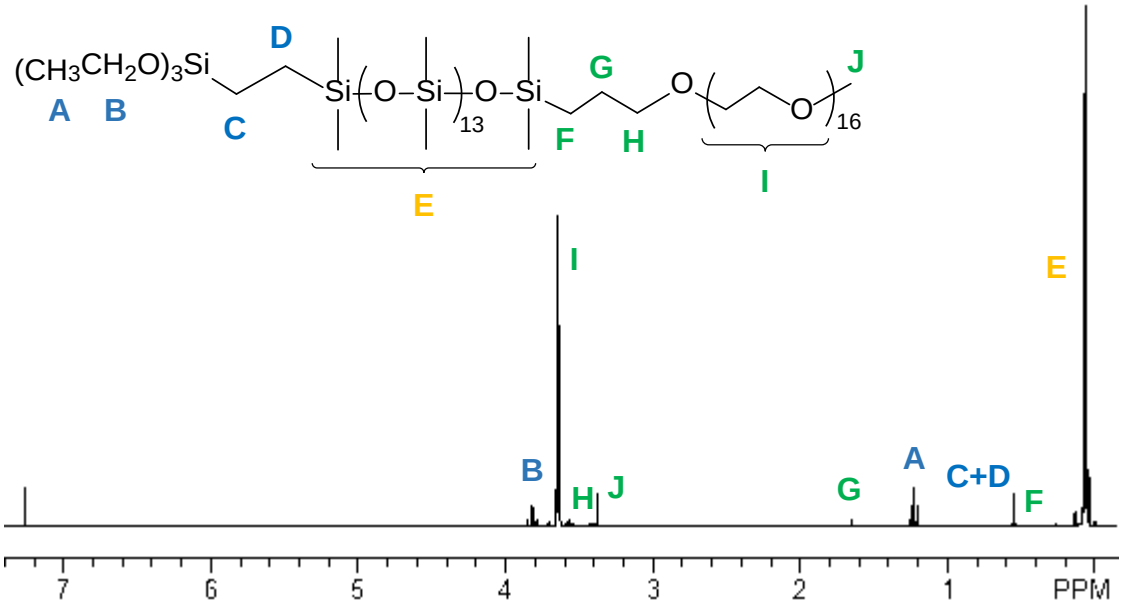

^{1}H NMR of triethoxysilylethyl-polydimethylsiloxane$_{13}$-*block*-PEO$_{16}$ (***n* = 16 PEO-silane amphiphile**) [From Chapter II and III]

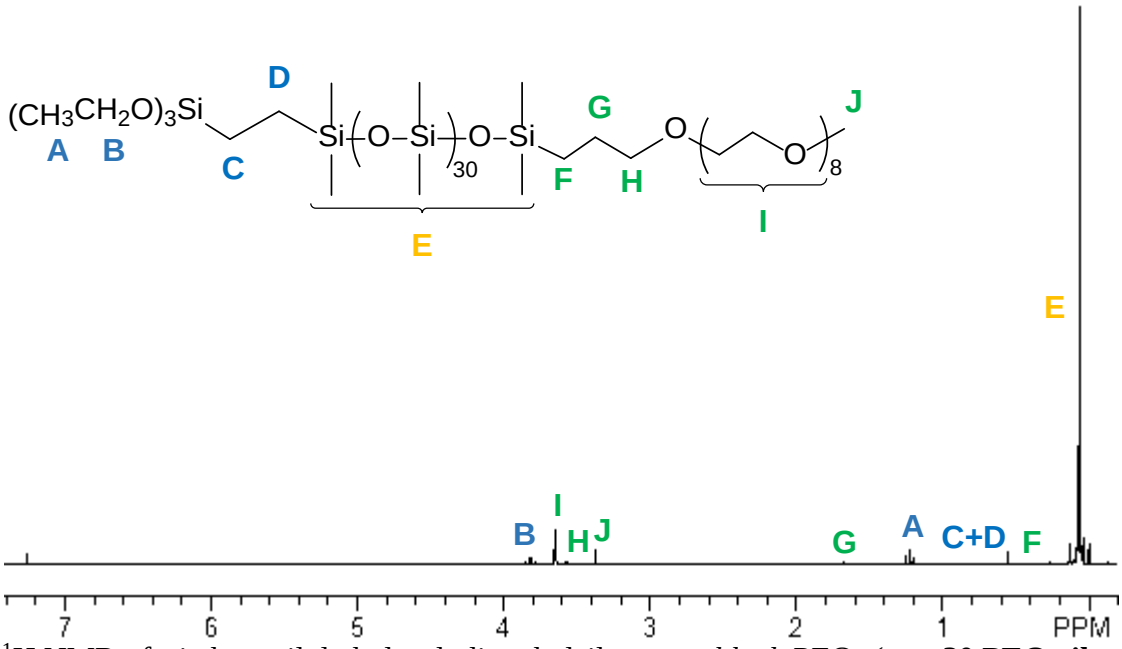

^{1}H NMR of triethoxysilylethyl-polydimethylsiloxane$_{30}$-*block*-PEO$_{8}$ (***m* = 30 PEO-silane amphiphile**) [From Chapter IV]

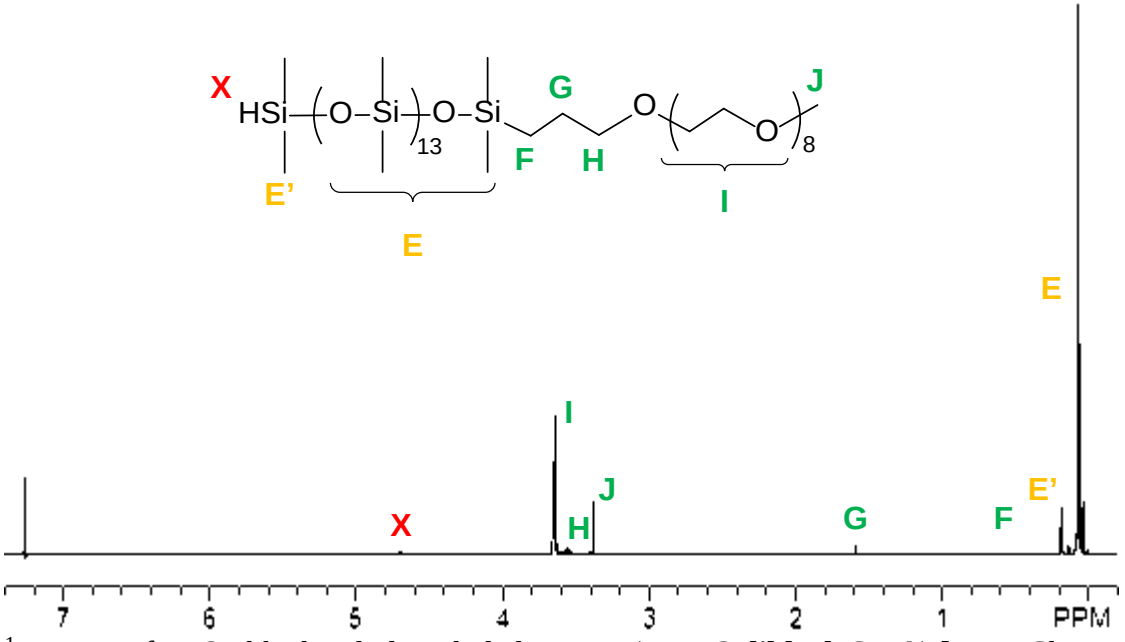

^{1}H NMR of PEO$_{8}$-*block*-polydimethylsiloxane$_{13}$ (***m* = 13 diblock SMA**) [From Chapter IV]

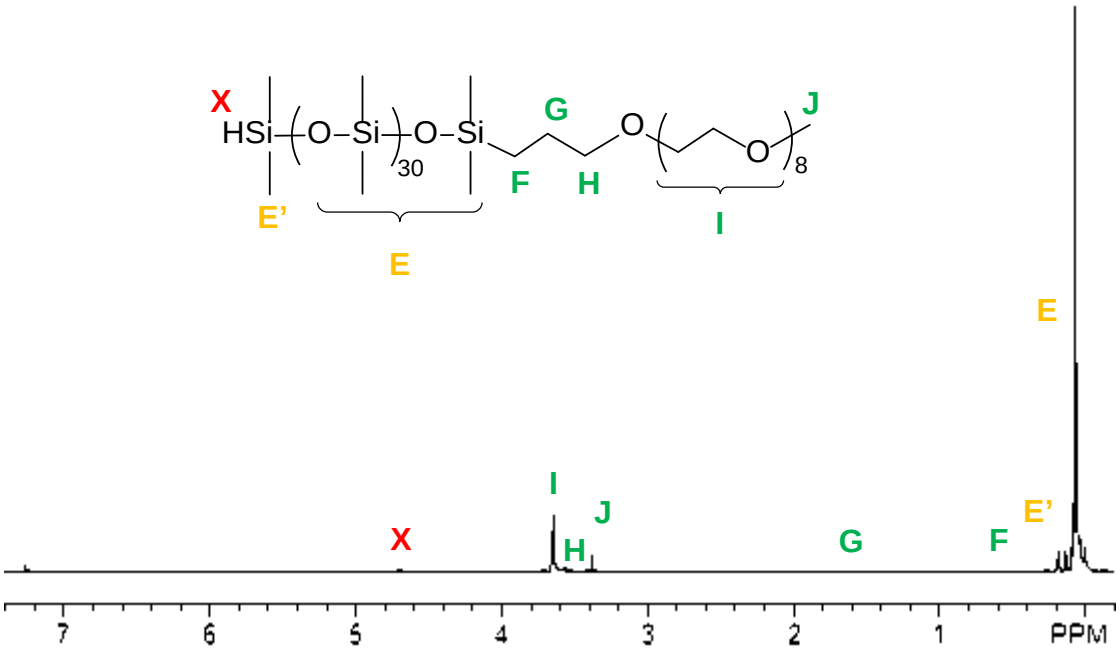

^{1}H NMR of PEO_8-*block*-polydimethylsiloxane$_{30}$ (***m* = 30 diblock SMA**) [From Chapter IV]

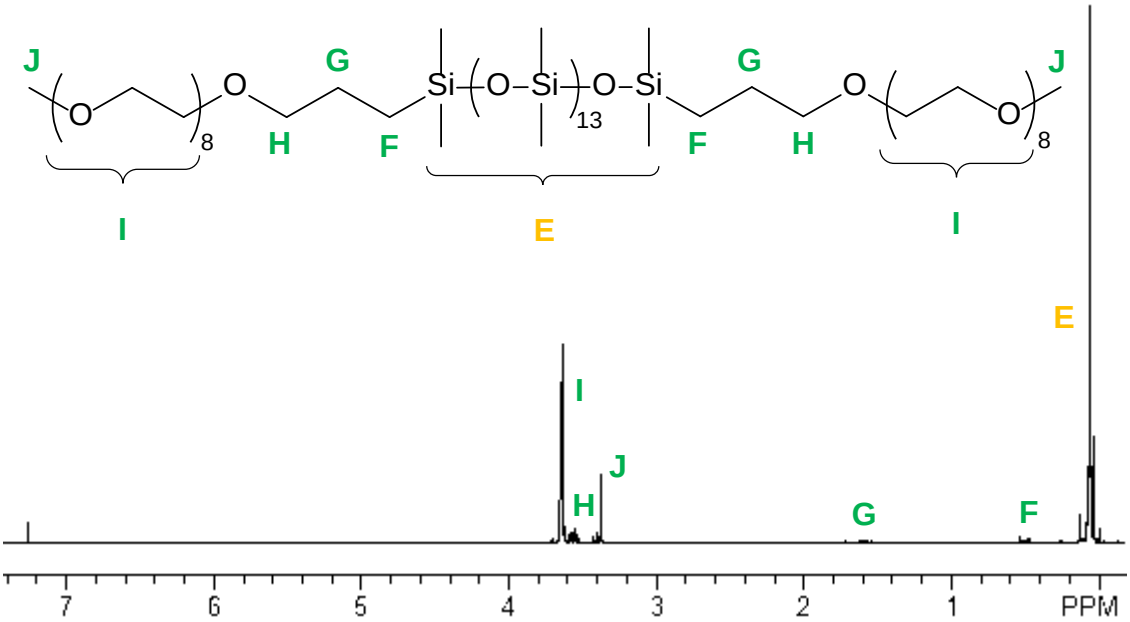

^{1}H NMR of PEO_8-*block*-polydimethylsiloxane$_{13}$-*block*-PEO_8 (***m* = 13 triblock SMA**) [From Chapter IV]

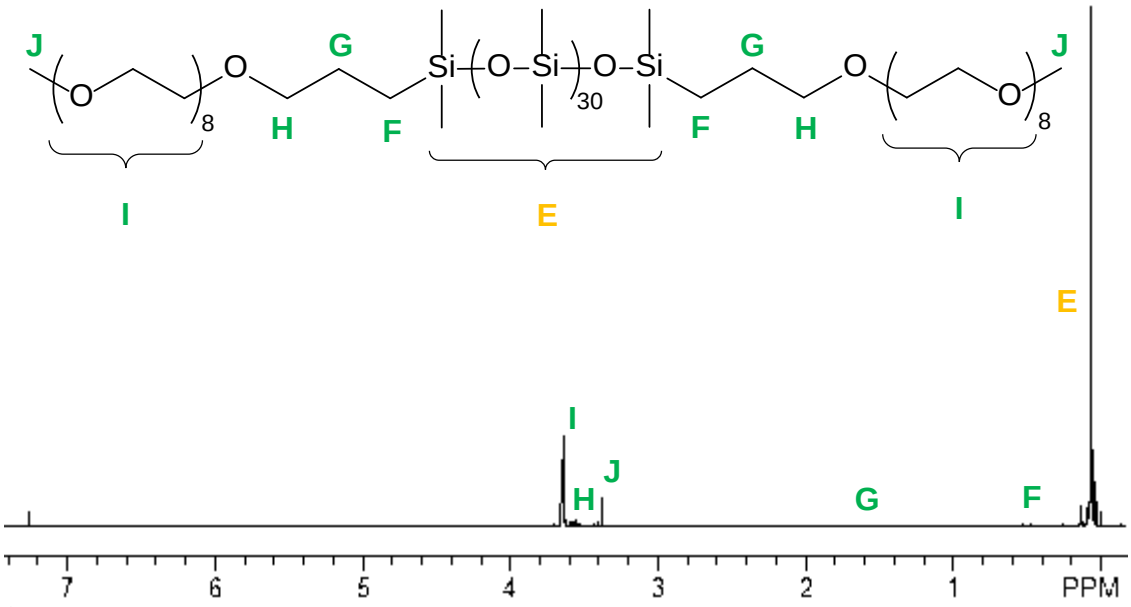

^{1}H NMR of PEO$_{8}$-*block*-polydimethylsiloxane$_{30}$-*block*-PEO$_{8}$ (***m* = 30 triblock SMA**) [From Chapter IV]

Synthesis of Methacrylate-Functionalized PDMS-*block*-PEO

PEO-*block*-PDMS copolymers were functionalized by addition of allyl methacrylate using Karstedt's-catalyzed hydrosilylation. Diblock SMA (*m* = 13, from Chapter IV) (5.00 g, 3.29 mmol) and allyl methacrylate (0.84 g, 6.67 mmol) (1:2 molar ratio), hydroquinone (0.01 g), and Karstedt's catalyst (10 µL) were reacted in a 25 mL pressure tube with 6 mL dry toluene. A Teflon-coated stir bar was added to agitate the mixture and the tube was purged with N_2 gas before sealing and heating in an oil bath set to 60 °C. After 6 h, the reaction was removed from heat and volatiles removed under reduced pressure. Chemical structure was confirmed with NMR spectroscopy using a Mercury 300 MHz spectrometer operating in the Fourier transform mode and using $CDCl_3$ as the standard. ^{1}H NMR (δ, ppm): -0.01–0.12 (m, 90H, SiCH_3), 0.47–0.60 (m,

4H, SiCH_2), 1.52–1.76 (m, 4H, $CH_2CH_2CH_2$), 1.90–1.97 (m, 3H, CCH_3), 3.38 (s, 3H, OCH_3), 3.41 (t, J = 7.1 Hz, 2H, $SiCH_2CH_2CH_2OCH_2$), 3.52–3.73 (m, 32H, OCH_2CH_2O), 4.10 (t, J = 6.9 Hz, 2H, $SiCH_2CH_2CH_2OC$), 5.52–5.68 (m, 1H, CCH_2), and 6.09–6.21 (m, 1H, CCH_2).

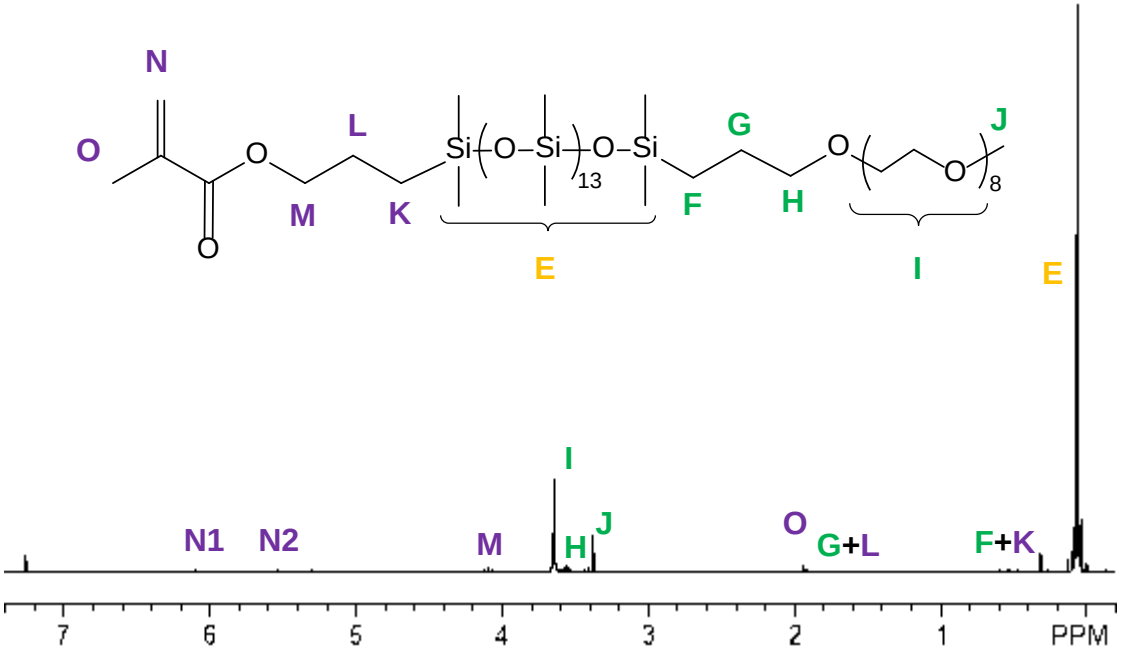

^{1}H NMR of PEO_8-*block*-polydimethylsiloxane$_{30}$-propylmethacrylate [From Chapter V]